

5-2007

Modification of Semi-metal Oxide and Metal Oxide Powders by Atomic Layer Deposition of Thin Films

Mark Q. Snyder

Follow this and additional works at: <http://digitalcommons.library.umaine.edu/etd>

 Part of the [Chemical Engineering Commons](#), and the [Inorganic Chemistry Commons](#)

Recommended Citation

Snyder, Mark Q., "Modification of Semi-metal Oxide and Metal Oxide Powders by Atomic Layer Deposition of Thin Films" (2007).
Electronic Theses and Dissertations. 228.
<http://digitalcommons.library.umaine.edu/etd/228>

This Open-Access Dissertation is brought to you for free and open access by DigitalCommons@UMaine. It has been accepted for inclusion in Electronic Theses and Dissertations by an authorized administrator of DigitalCommons@UMaine.

**MODIFICATION OF SEMI-METAL OXIDE AND METAL OXIDE POWDERS
BY ATOMIC LAYER DEPOSITION OF THIN FILMS**

By

Mark Q. Snyder

B.S. Georgia Institute of Technology, 1998

M.S. Institute of Paper Science & Technology, 2001

A THESIS

Submitted in Partial Fulfillment of the

Requirements for the Degree of

Doctor of Philosophy

(in Chemical Engineering)

The Graduate School

The University of Maine

May, 2007

Advisory Committee:

William J. DeSisto, Associate Professor of Chemical Engineering,
Advisor

Doug Bousfield, Professor of Chemical Engineering

M. Clayton Wheeler, Assistant Professor of Chemical Engineering

Carl P. Tripp, Professor of Chemistry

Joe DiCarlo, Yardney Technical Products

LIBRARY RIGHTS STATEMENT

In presenting this thesis in partial fulfillment of the requirements for an advanced degree at The University of Maine, I agree that the Library shall make it freely available for inspection. I further agree that permission for “fair use” copying this thesis for scholarly purposes may be granted by the Librarian. It is understood that any copying or publication of this thesis for financial gain shall not be allowed without my written permission.

Signature:

Date:

**MODIFICATION OF SEMI-METAL OXIDE AND METAL OXIDE POWDERS
BY ATOMIC LAYER DEPOSITION OF THIN FILMS**

By Mark Q. Snyder

Thesis Advisor: Dr. William J. DeSisto

An Abstract of the Thesis Presented
In Partial Fulfillment of the Requirements for the
Degree of Doctor of Philosophy
(in Chemical Engineering)
May, 2007

This work describes two methods of modifying, and the subsequent characterizing of, oxide nanopowders. The first method, atomic layer deposition, or ALD, is a series of surface-limited reactions that are repeated to deposit a thin, inorganic film on the surface of the nanopowder. Deposition of a thin film is a useful method to alter the surface properties of a material while retaining its bulk properties.

Part of this thesis concerns the understanding of the growth mechanism of thin film titanium nitride (a material known for thermal and chemical stability as well as electronic conductivity) on silica through the ALD process. In situ IR spectroscopy was used to observe the changes that occur to the surface in each ALD half-cycle. Previous research has dealt with titanium nitride growth on planar silica substrates, but this was the first time that such growth was studied on a silica nanopowder. Silica is a commonly-used thin film substrate because it can be easily monitored with infrared (IR) spectroscopy.

The surface of another nanopowder, lithium titanate spinel (LTS), was studied to determine its suitability as a substrate for thin film growth. Interest exists in LTS for its use as a lithium-ion battery anode. However, a potential disadvantage of this material is its poor electrical contact with the anodic current collector. Several hundred layers of a titanium nitride thin film were deposited on LTS to determine if this would improve the material's performance as a lithium-ion battery anode. The material was fabricated into a test cell and evaluated against an unmodified LTS cell for comparison.

Another modification technique is to use supercritical carbon dioxide (sc-CO₂) to dissolve reactants and deposit them on a surface. This technique can be used at temperatures considerably lower than those for ALD. By first depositing a nonvolatile base dissolved in sc-CO₂, organosilanes may be catalytically attached to a substrate otherwise not possible at low temperatures.

1 INTRODUCTION

Understanding the surface properties of a substrate is important, because these properties will strongly influence the chemical reactions that occur at the surface, and, ultimately, how the substrate will interact with other reactive species. If the substrate has a high surface area, such as a powder, then a large interfacial region for chemical reaction can exist in a relatively small volume. By coating this powder surface with a thin film (thickness $< 1 \mu\text{m}$), the surface properties of the film will be distributed across the high surface area of the substrate. This can be especially advantageous when the thin film material is not available with a high surface area morphology, or if the pairing of the bulk material with the thin film material has desirable properties.

Using this concept, the research detailed in this thesis describes the modification of a nanoparticulate (diameter $< 100 \text{ nm}$) material by a process called atomic layer deposition. Atomic layer deposition (ALD) coats a substrate with one monolayer of atoms (or molecules) at a time allowing for precise control of film thickness. This technique was used to synthesize a thin film of titanium nitride on lithium titanate spinel ($\text{Li}_4\text{Ti}_5\text{O}_{12}$, LTS) a nanoparticulate material used as an anode in lithium-ion batteries. By nature, LTS is a poor electrical conductor. The purpose of this work was to examine the effects a thin film on the performance of a lithium-ion coin cell including whether or not the electrical conductivity can be improved by the addition of a conductive thin film.

Prior to this, preliminary work was performed in two related areas. The first was determining the ALD growth mechanism of TiN on a nanoparticulate surface. The second area was the study and characterization of the surface of LTS. No prior research, to the author's knowledge, has been conducted about the surface chemistry of LTS.

Results from the surface study of LTS indicated that it was, indeed, amenable to ALD. Modification and subsequent testing of the LTS powder with a TiN ALD coating showed that the modified powder produced more consistent voltage profiles and a higher specific charge capacity than unmodified LTS powder when fabricated into a lithium-ion test cell.

A method of surface modification similar to ALD is the use supercritical CO₂ (sc-CO₂) as a solvent to attach reactants to a surface. In this work, the use of sc-CO₂ to transport reactants with low volatility, bases in particular, to catalyze reactions between organochlorosilanes with a porous SiO₂ surface was examined. Without base catalysis, organochlorosilanes may polymerize or fail to covalently bond to the substrate.

1.1 Titanium Nitride

Titanium nitride has received considerable attention because of its excellent thermal stability [1-6] chemical stability [1-3], wear resistance [7-9], high electrical conductivity [5, 7, 8, 10] and resistance to chemical etching [5, 11]. When TiN is deposited as a thin film, it has been used as a hard coating on cutting tools [3, 12, 13], a diffusion barrier in microelectronic devices [7, 8, 12, 14-23], an optical coating [7, 8], a jewelry surface coating [7, 8, 13], solar films [3, 8, 13], and as an adhesion layer in microelectronic devices [8, 24]. The unique bonding characteristics of TiN are responsible in part for its properties. Titanium nitride has covalently bonded *p* and *d* hybridized orbital electrons as well as metallic bonding through *d* electrons. Thus, its electrical and thermal properties resemble that of a metal [25].

1.2 Thin Film Deposition Methods

In one thin film application, semiconductor devices require diffusion barriers to prevent metal atoms from interconnects from migrating to other regions of the device. An inorganic metal-like thin film, TiN, is often used for this purpose [23, 26, 27]. However, shrinking device dimensions of micro-electronic components require more precise deposition processes, especially in high-aspect ratio contact holes and vias [26].

Numerous methods for coating surfaces exist. Among them are sol-gel [28, 29], physical vapor deposition [9, 22], electrochemical oxidation [7], molecular beam epitaxy [14], chemical vapor deposition [2, 9, 13, 16, 22, 30, 31], and atomic layer deposition [32-35]. Most of these methods, however, are effective for thin film synthesis on planar substrates. For surfaces with high-aspect ratio features, vapor deposition reactions are more effective [2, 16, 36]. The gas-phase methods are described below.

1.2.1 Chemical Vapor Deposition

Researchers have also deposited TiN using chemical vapor deposition (CVD) [3, 9, 12, 13, 22, 30]. Advantages of CVD are a high deposition rate, good surface coverage, good adhesion and simple equipment [37]. A significant step in lowering CVD reaction temperatures was achieved by Musher and Gordon by using preheated ammonia instead of nitrogen. The reaction



was carried out at 500 °C instead of the previous temperature range of 900-1200 °C [5].

Several authors report improved step coverage with CVD compared to PVD [2, 12].

However, most CVD reaction temperatures were higher than could be tolerated for low-k polymer components in devices such as integrated circuits [38]. Prior research shows that

CVD films perform better as diffusion barriers than those prepared by PVD [39].

Drawbacks of CVD include Cl⁻ contamination from chlorine-containing precursors and reliability problems caused by carbon residue from organometallic precursors used in metalorganic CVD [40].

1.2.2 Atomic Layer Deposition

A variant of CVD that has received growing attention over the last two decades is atomic layer deposition (ALD) [14], also referred to as atomic layer epitaxy [14, 41, 42] and atomic layer processing [43] amongst other names [44], for its potential to deposit thin, conformal inorganic films [15, 19, 45-47]. Regardless of the name, the technique became popular with the developing need for a new way to manufacture thin film electroluminescent displays [14, 33] and dynamic random access memory components [47]. Atomic layer deposition can deposit as little as a fraction of a monolayer on a substrate using sequential, self-terminating surface reactions [44]. Precise thickness control [24, 33, 48-51] of ALD films can be used for amorphous [17, 18, 33, 38, 52], high-surface area [41, 42, 53, 54], single crystal [21, 40], nanorod [55], and polycrystalline substrates [33]. Agglomeration and uneven coating, problematic in CVD reactors, does not occur in the ALD process [48].

1.2.2.1 The ALD Process

Atomic layer deposition film growth occurs through the following steps:

1. Self-limiting reaction through exposure of the substrate to the first gas-phase precursor [17, 19, 38, 43, 47, 48, 56-59].
2. Purge of the reactor with an inert gas to remove byproducts and unreacted precursor [12, 17, 24, 38, 51].

3. Self-limiting reaction through exposure of the substrate to a second gas-phase precursor [17, 19, 38, 43, 47, 48, 56-59] or to prepare the surface for the first reactant [19, 44, 60]
4. Purge of the reactor with an inert gas to remove byproducts and unreacted precursor [12, 17, 24, 38, 51].

The sequence listed above comprises one ALD cycle, referred to as “binary sequence reaction chemistry” by George, et al. [43], while steps 1 and 3 individually represent a half-reaction [43, 44]. A typical ALD exposure might last from 0.5 to several seconds [14] and deposit films with a thickness of 0.08 [61] to 3 Å per cycle [14]. The above binary reaction sequence chemistry can be used to deposit a single-element film if the precursor in step 3 is a “stripping” material [19, 60].

The term “self-terminating reaction” means that the precursor chemisorbs [24, 41, 47, 49, 56-58] on to and saturates [49] the surface in an irreversible, surface controlled reaction [62] leading to growth of uniform, conformal films [44]. Once the surface has been saturated, and all reactive functional groups converted to those of the most recently deposited precursor [43], no further reactions can occur [14, 43]. Advantages of such reactions are

- Control of film thickness through dependence upon the number of deposition cycles [14, 24, 33, 43, 44, 49-51]
- Less dependence on a constant precursor flux for suitable conformality and reproducibility [14, 59]
- Usage of solid precursors through a relaxed demand for high evaporation rates because of self-limiting growth [14]

- A decrease in the likelihood of gas-phase reactions (or CVD-like reactions) [14, 38, 51, 59]
- Possibility of depositing multi-layer structures[49, 51, 63]
- Conformal coating of high-aspect ratio structures and porous materials [15, 19, 45-47]
- Lower temperatures than for comparable CVD reactions [8, 38]

Other variables such as reactants, substrates, and temperature have a lesser influence on the reaction [44, 64]. Selection of ALD reaction parameters can be challenging, though, because each half-reaction may be optimized at a different pressure and temperature.

Also, effectively evacuating or purging the ALD reactor area is crucial, because lingering precursors may lead to CVD-like growth, impede growth per cycle measurements, and interfere with the self-terminating reaction [43].

1.2.2.2 ALD Thin Film Growth

Molecules can adsorb on to a surface through one of two methods. The first method, physical adsorption, often referred to as physisorption, occurs by forming weak bonds and multiple layers on a substrate. Little change occurs to the gas-phase reactant [44]. The second method is chemical adsorption, or chemisorption. Chemisorption requires that chemical bonds be made [65] and broken between the adsorbent (surface) and the adsorbate (adsorbed molecule) [44]. This type of reaction stipulates that one reactive site can bond with only one precursor molecule leading to monolayer formation [44]. Three assumptions commonly made when discussing chemisorption coverage are 1) the maximum amount of adsorbed species is assumed to be a monolayer, 2) all adsorption sites are considered equal, and 3) neighboring adsorption sites do not interact with each

other [44, 65, 66]. From this point on, a monolayer will refer to the quantity of adsorbed molecules on the surface, regardless of whether or not all surface sites are occupied [49]. Fumed SiO₂ will have approximately 1.5×10^{14} reaction sites at 400 °C [67], the temperature at which reactions were performed during this research.

Puurunen suggests three mechanisms of chemisorption in ALD shown in Figure 1.1. The first is ligand exchange (Figure 1.1a), where a reactant molecule, ML_n (where M represents a metal atom, and L, the ligand molecule), is split when reacting with the surface. A ligand, L, reacts with a surface group, denoted aZ, and forms a volatile compound that is released as a byproduct, aL. The remainder of the reactant molecule, ML_{n-1}, adsorbs onto the surface. The reactant molecule may occupy more than one surface site if $n > 1$ [35, 68]. The dissociation model (Figure 1b) predicts that the ML_n molecule will split when it reacts with a surface M'-Z group. The result is the formation of M'-L and Z-ML_{n-1} groups [35, 68]. The third model (Figure 1.1c) is association in which a coordinative bond is formed at the reaction site and chemisorption occurs without the release of a ligand [69].

The size of the precursor molecule [14] and resulting steric hindrance [8, 43] can play a significant role in the surface formation of a monolayer. Puurunen states that the shielding of reaction sites caused by steric hindrance [68, 70, 71] and the number of reaction sites present on a surface have the greatest impact on monolayer formation [42, 54]. Hence, three models of thin film growth have been discussed in the literature as well.

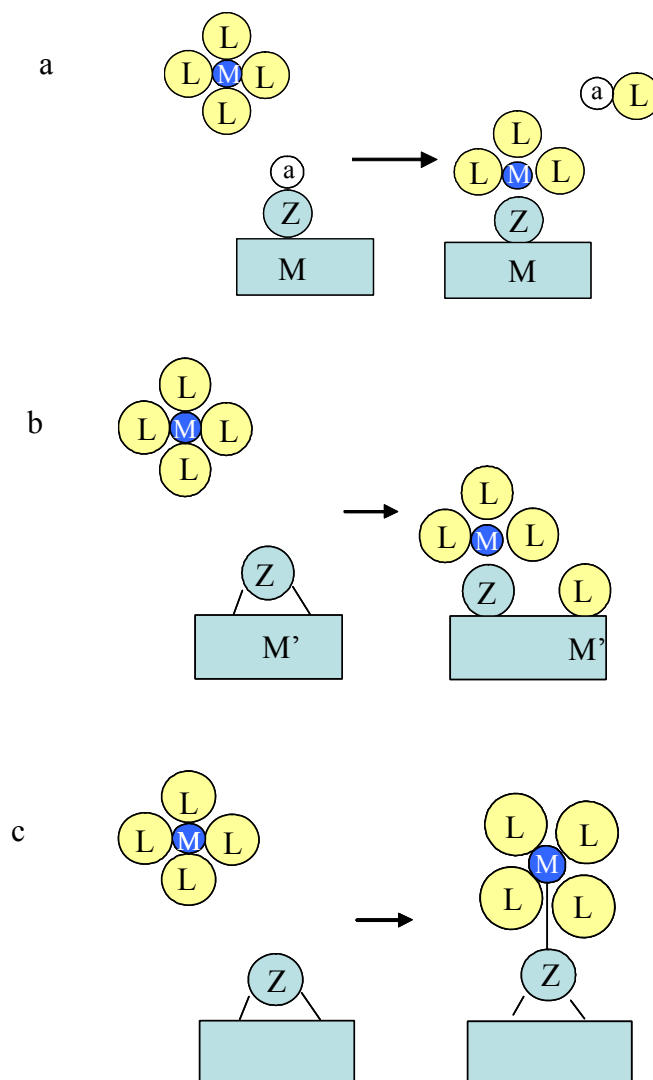


Figure 1.1 Mechanisms of ALD chemisorption on a surface by (a) ligand exchange between a precursor, ML_n and a surface group Za (hydroxyl, $-OH^*$), producing $-Z-ML_{n-1}^*$ and aL ; (b) dissociation forming $-Z-ML_{n-1}^*$ and $M'-L^*$; and (c) association of ML_n onto the surface to form $-Z-ML_n^*$.

The first, referred to as Model I (Figure 1.2a), was developed by Ritala, et al. [72, 73] and Morozov, et al. [74] and is based on the size of the reactant, ML_n . The effective size of the reactant is a result of its density and the area it covers when a close-packed monolayer is assumed. This model replicates a physisorbed layer and maximum

achievable growth per cycle. Model II (Figure 1.2b), developed by Ylilammi [64], takes the size and geometry of the adsorbed reactant, ML_z , into account. The size, bond lengths and bond angles of M and L must be known. This model predicts that the growth per cycle will increase as the size of ML_z decreases. Model III (Figure 1.2c), developed simultaneously by Puurunen and Siimon and Aarik [75], predicts a maximum growth per cycle based on the size and number of adsorbed ligands based on a close-packed monolayer. The model simulates a physisorbed monolayer of ligands. Using the L/M ratio from the ML_z adsorbate, the amount of metal can be calculated. Puurunen states that if a TiO_2 monolayer were to be deposited from $TiCl_4$ on an $-OH$ terminated surface [44], Model I predicts 28% of a TiO_2 monolayer [72, 73]; Model II, 19% [64]; and Model III, 33% [76].

An advantage of using ALD for thin film deposition is that the number of deposition cycles performed is purportedly related to the thickness of the resulting film [8, 14, 43, 62]. This assumes that the number of reaction sites remains constant throughout the reaction. Not all ALD reactions exhibit the same outcome based on the number of cycles, though. Three types of effects of growth per cycle behavior have been observed: a) linear growth in which the growth from the first to the last cycle is the same [57, 77] (Figure 1.3a), b) substrate enhanced growth occurs when the number of reactive sites is greater than the number of reactive sites on the ALD-grown material [78, 79] (Figure 1.3b), and c) substrate-inhibited growth where the growth per cycle is lower on the substrate than on the ALD-grown material in the steady regime. Substrate-inhibited growth can be divided further into two sub-groups. The growth pattern just described is known as Type 1 [56, 71, 80-82] (Figure 1.3c). Type 2 (Figure 1.3d) growth reaches a

maximum then settles to a steady value. Island growth is often seen in this regime as well. Some work has been performed suggesting that TiN ALD does not exhibit linear growth and falls under the substrate-inhibited growth model instead [23, 56, 83, 84]. The research reported in this thesis will attempt to elucidate the growth mechanism of TiN on a SiO_2 substrate and provide reasons for the non-linear growth regime.

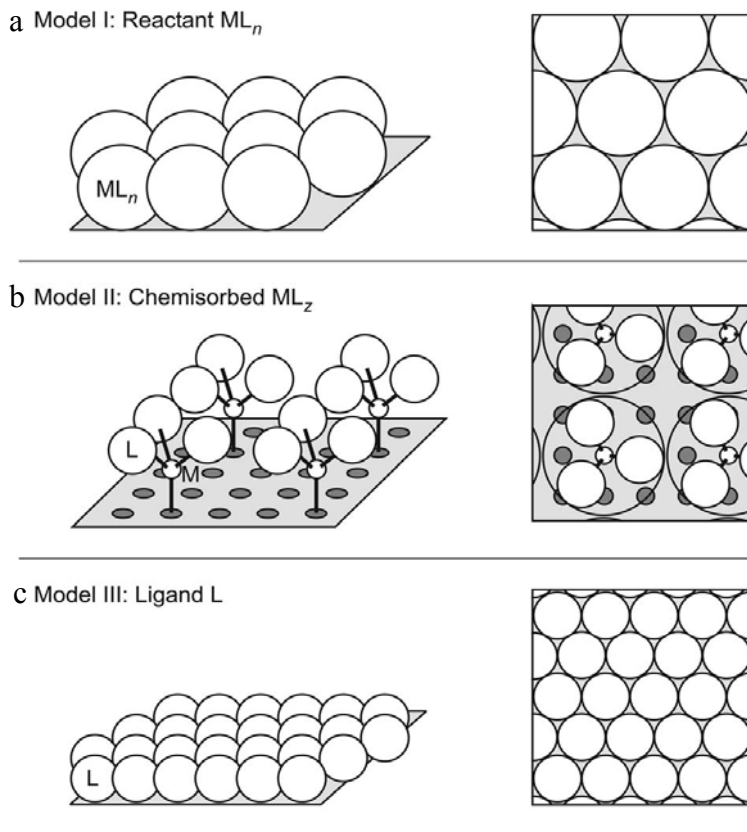


Figure 1.2 Three theoretical models of monolayer formation are (a) Model I which is based on the size of the reactant, ML_n , (b) Model II, determined by the size and geometry of the chemisorbed reactant, ML_z , and (c) Model III, which assumes a close-packed monolayer of ligands. Figure taken from Puurunen [44].

As the monolayers are deposited on the substrate, three different growth models have been observed: layer-by-layer growth, island growth, and random deposition. The first growth model, layer-by-layer growth, also called Frank-van der Merwe growth [57, 85, 86]. In this model, deposited material settles in the lowest unfilled area on the surface and a monolayer of deposited material covers the surface completely. When the ALD material shows a preference for the material previously deposited over the substrate, island growth occurs [57, 85-87]. Material that shows layer growth and then demonstrates a change to island growth regime grows by random deposition, or Stranski-Krastanov growth [44].

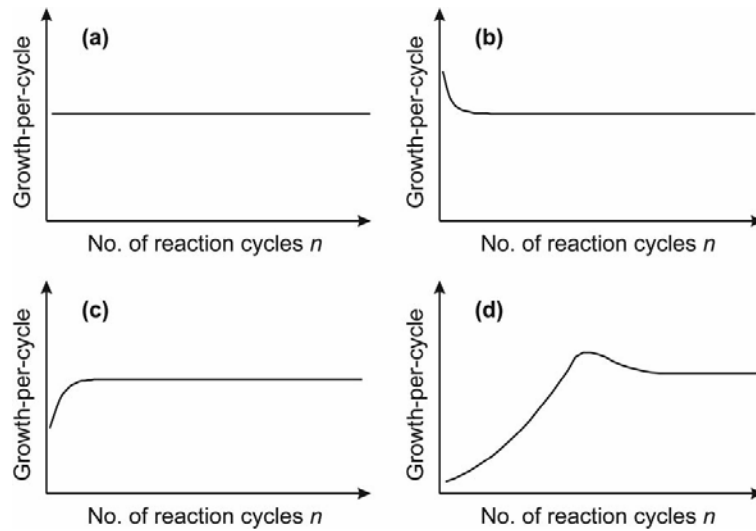


Figure 1.3 The effect of ALD growth per cycle illustrated by three different growth models: (a) linear growth, (b) substrate-enhanced growth and substrate inhibited growth, which is further divided into (c) Type I growth and (d) Type II growth. Figure taken from Puurunen [44].

1.2.2.3 ALD Precursors

Atomic layer deposition has been used to grow semi-metal and metal oxides, nitrides, sulfides, tellurides, pure elements, and others [44]. Oxides and nitrides are some of the most commonly formed. Water is typically used as the oxidant [33, 35, 42, 45, 88], though O₂ [89], and O₃ [90-92] have been used as well in oxide formation. Elements such as W have been deposited as elements with Si₂H₆ as a stripping agent [19, 60]. Nitrides are often formed from NH₃ [8, 17, 18, 24, 26, 52, 56, 93, 94], H₂/NH₃ plasma [46], or an alkylamide [21, 50, 95]. Numerous researchers have studied TiN thin film deposition by ALD [15, 17, 18, 26, 27, 38, 40, 46, 49, 50, 56, 57, 62, 84, 93, 96-98]. The precursors most frequently used are TiCl₄ and NH₃ [18, 49, 56, 59, 62, 93, 97]. However, work has been reported on the use of tetrakisdimethylamidotitanium (TDMAT) [26, 83], tetrakisethylmethylaminotitanium (TEMAT) [98] and N₂ with H₂ [46].

Atomic layer deposition precursors must be either a gas, volatile liquid, or solid and have a high enough vapor pressure for mass transport to occur and the material to be deposited [14, 44, 99]. Furthermore, precursors must be thermally stable at reaction temperature because decomposition counteracts self-limiting growth [14, 44]. All substrates used throughout the research presented in this thesis are semi-metal or metal oxides that bind with ALD precursors through covalent bonding with surface hydroxyl groups or the surface terminated by the previous precursor [14, 41-43, 54].

Metal ALD precursors can be described as either inorganic or metalorganic. The most common examples of inorganic precursors are metal halides [12, 42, 81, 94, 96, 100, 101]. Halides are much more volatile than previously-used elemental precursors and have increased in use since the 1960s [34]. Halides are thermally stable and highly

reactive while their ligands are small. Unfortunately, their growth per cycle is usually a small fraction of a monolayer and their byproducts are undesirable and may become incorporated in the deposited film, blocking adsorption sites. One halide, TiCl_4 , can form particles within at temperatures below $200\text{ }^\circ\text{C}$ with water or [53, 54] NH_3 [102].

Metalorganic precursors, compounds that can be classified as either those that form direct metal-carbon bonds or those with no direct carbon-metal bonds [44]. Compounds that form carbon-metal bonds are called organometallic compounds. Alkyls are common organometallic precursors. Alkyls were first used in the 1980s as ALD reactants and can be used to grow a variety of thin films [103, 104]. The advantages of alkyls include their high reactivity, small ligands, and high growth per cycle. However, they are not available in a wide range of metals. Also, they tend to decompose at high temperatures and form residues that can contaminate the film [44].

Other metalorganic ALD metal precursors are alkoxides [73] and alkylamides [26, 98, 105]. Alkoxides have been in use since the 1990s, but have only seen use in oxide deposition. This may be caused by the difficulty of breaking the M-O bond. Alkoxides may decompose at temperatures as low as $200\text{ }^\circ\text{C}$ —even lower than those of alkyls—and negatively affect film conformality. Like alkyls, carbon and hydrogen residue also can interfere with film performance [26, 43].

Alkylamides have also been used as ALD precursors increasingly over the last decade [21, 50, 95]. They may be used in oxide, nitride and selenide film formation. As with other metalorganic precursors, they decompose at low temperatures [26] and contaminate films with carbon and hydrogen. Another observation was greater-than-monolayer growth attributed to readsorption and precursor decomposition [50, 83, 84, 98].

1.2.2.4 TiN ALD

Problems with film contamination and the prevention of self-terminating reactions were mentioned previously in this section. In using TDMAT as a reactant, Elam et al., found that a porous film resulted that facilitated oxidation [26]. The use of TDMAT as an ALD precursor only accentuated the problems of TiN film oxidation. Oxidation of TiN films has received attention in the past [4, 23, 59, 106]. Oxygen may be incorporated into the film through three methods: 1) by residual O₂ in the reactor system, NH₃ or carrier gas; 2) cooling after the reaction 3) exposure to air after deposition and cooling. The size of the film grains may play a role as well, because the thinnest films (which have the smallest grains) were found to have the highest oxygen content suggesting that the oxygen is able to easily diffuse into them. Exposure to air indicated the film contained approximately 15% oxygen [8].

Disadvantages exist for the usage of TiCl₄ with NH₃ as well. Ammonia has a low reactivity with TiCl₄ [96]. Ritala et al., found that when growing a TiN thin film, the surface Ti atom density was 1.0 Ti/nm² and a growth per cycle of 0.19 Å, while a TiO₂ thin film deposited with TiCl₄ had a density of 1.4 Ti/nm². In a separate result, AlCl₃ and NH₃ were used to deposit an AlN film with average growth of 1.0 Å/cycle [8]. Reasons

proposed for this low growth per cycle are dissociation during chemisorption, blocking of other sites and preferential bonding to NH_x sites [8]. Zinc pulses were added between the TiCl_4 and NH_3 pulses to act as an additional reducing agent to enhance growth, but improvements were minimal. A decrease in resistivity and more developed grain structure was observed however [8]. Other difficulties with the aforementioned reactants are the formation of chloride residue in the film and the generation of HCl [96] that can etch interconnects [26]. The formation of NH_4Cl salt has also been observed [26, 93] but other evidence shows that at reaction temperatures (greater than $400\text{ }^\circ\text{C}$) this salt will sublime [96].

The cleanness of the reaction and less-porous nature of the film are of particular importance as TiN ALD thin films are being considered for use as a conducting and passivating film for lithium-ion battery electrodes. In spite of the drawbacks of HCl byproducts and low growth per cycle mentioned in relation to using TiCl_4 and NH_3 as ALD precursors, the availability, thermal stability and relative lack of film contamination of TiCl_4 relative to alkylamides made it the precursor of choice for the following experiments in this thesis. On the other hand, the pervasiveness of oxygen in the film is a reality that must be accepted for the time being. Presently, the aim of the research presented here is to first evaluate whether or not the deposition of a thin film is detrimental to the performance of the electrode in the lithium-ion cell. Process optimization is not an issue at the present.

1.3 Lithium-Ion Batteries

The development and advancement of battery systems often drives the demands of portable power applications. With the continual miniaturization of electronic devices, the challenges of powering the devices are great [107, 108]. Devices must utilize the full potential of the power source [109]. Oftentimes, the battery weight accounts for half of the weight of the device [107]. To this end, lithium has the lightest weight, highest voltage and the greatest energy density of any metal [107, 109] (Figure 1.4). Lithium ion batteries have a greater capacity than nickel cadmium, nickel metal hydride and other types of rechargeable batteries [110].

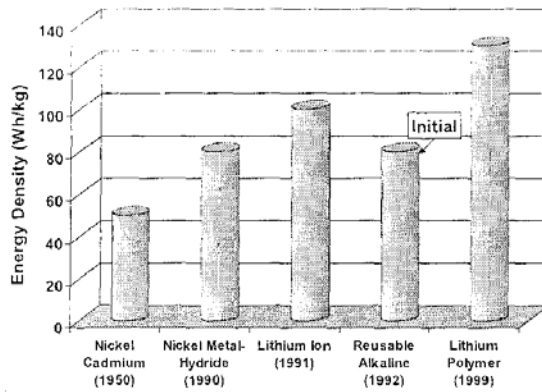
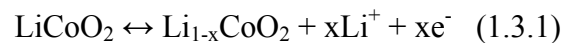


Figure 1.4 Energy density for a variety of battery metals and the first year of their commercial deployment [108].

The output of a lithium-ion battery is 3.7 V, or approximately three times greater than rechargeable Ni-Cd and Ni-MH batteries [111, 112]. Their operating range is between 2.8 and 4.2 V [109]. Unlike nickel-based batteries, lithium-ion batteries do not need to be charged and discharged periodically to maintain capacity, a phenomenon known as the “memory” effect [109, 112]. The longer lifetimes of lithium-ion batteries have made them prevalent in notebook computers, personal digital assistants and cellular phones [111].

Batteries convert chemical energy into electrical energy through oxidation-reduction reactions between its active materials [109, 112]. A battery, in general, consists of an anode (negative electrode), a cathode (positive electrode) and an electrolyte [108, 113] while the electrolyte acts as a separator and serves as a conduit for charge transfer [108]. The reaction causes electrons to flow from one electrode to another through an electric circuit [109].

A lithium ion battery is a cell composed of lithium intercalation compounds (compounds that can incorporate lithium ions into its lattice structure) used as its cathode and anode. The most common cathode material is lithium cobalt oxide (LiCoO_2). The cathode is attached to a current collector, often aluminum foil. The reaction at the cathode is described below.



The anode is often composed of graphite, because of its high specific capacity on the copper current foil collector [109]. In a lithium-ion battery (Li-ion), the lithium ions carry energy from the anode, through the electrolyte, and on to the cathode during discharge (Figure 1.5). The opposite path is followed during charging [113]. At the point when the lattice structure is fully lithiated, the transition metal is fully reduced. Subsequently, it is fully oxidized when all lithium ions are extracted [107].

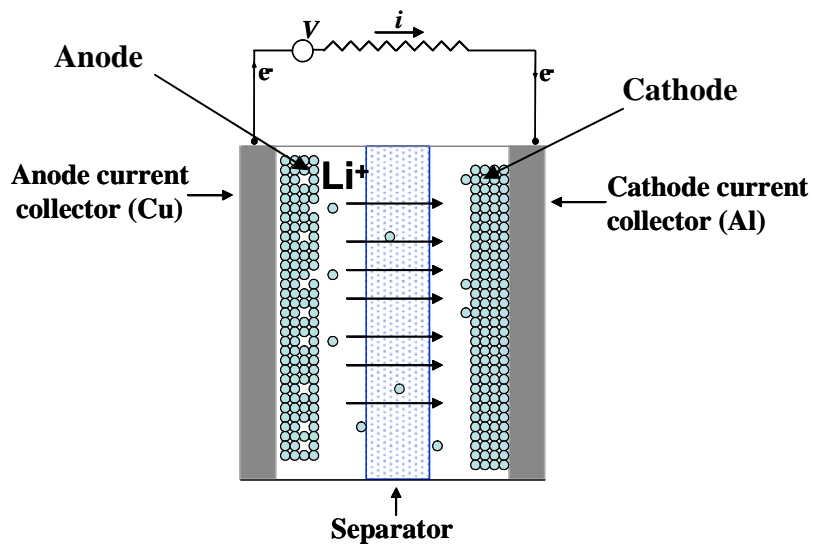


Figure 1.5 Schematic of a Li-ion battery. Arrows within the figure indicate Li-ion discharge.

In this research, however, lithium titanate spinel ($\text{Li}_4\text{Ti}_5\text{O}_{12}$) will be used as the anode material. Advantages of using this material will be discussed later in this thesis. Research on conduction in solids has demonstrated that alkali metals (lithium, in this case) move well in electronically conducting transition metal lattices [107].

The electrolyte is usually a liquid gel or polymer and must be able to conduct lithium ions while being an electrical insulator. Many of the drawbacks of Li-ion batteries, such as power fade, capacity loss, and poor cyclability are caused by the interactions between the electrode and the electrolyte at the interface of the two components [113].

During the initial stages of charging (potentials $< \sim 1.0$ V), the electrolyte solution will decompose and form a secondary electrolyte interface (SEI) because no electrolytes are thermodynamically stable in this range [113]. The SEI film is Li-ion conducting and electrically insulating [114-116]. The lithium salt species forms as a thin layer [113, 117] ranging between 15 and 900 Å [113]. Once formed, the SEI fulfills two roles: 1) suppress cointercalation of solvent molecules from the electrode basal and edge planes and 2) prevent solvent decomposition over the whole surface [113, 116].

When using highly ordered pyrolytic graphite as an anode at potentials less than 1.0 V, expansion of the electrode volume has reached 150% of its original size because of the solvent (ethylene carbonate, in this case) intercalating as well as Li-ions. Once incorporated into the graphite, the electrolyte becomes an immobile compound stuck between the graphene sheets and inhibits further intercalation [116, 118, 119] (Figure 1.6).

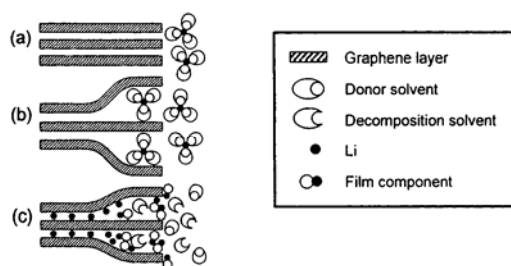


Figure 1.6 Solvent intercalation in a graphene anode [116].

Formation of the SEI inhibits further electrolyte decomposition and enhances safety and cyclability [113, 116], but causes irreversible charge consumption, and, hence, capacity loss [116]. Constant dissolution of the anode material causes breakdown of the surface films which are then repaired. However, this can lead to non-uniform surface films that lead to non-uniform secondary current distribution, and eventually, to a non-uniform electrochemical process [117].

Li-ion battery anodes have been made out of Li, carbon-based materials, and Li alloys. An electrode, or Li-insertion compound must conduct Li-ions and electrons as well as possess either a network or layered structure. The most common type of Li-ion battery anode is carbon (in a variety of forms) because of the relatively low volume expansion of approximately 10 % that it undergoes upon intercalation of lithium ions [113]. Furthermore, surface instability, inefficient passivation, and irreversible charge consumption from surface reactions between the alloy and solution can result from a change in volume of the Li-ion host. These volume changes can ultimately lead to the deactivation of the active mass and bulk changes to the alloy [117]. A good electrode host material has the following properties:

- mixed ionic-electronic conductor
- retention of overall structure upon removal of alkali metal
- an acceptable potential difference exists between the lithiated and partially lithiated structure relative to lithium
- insertion and removal of lithium has minimal change on the dimensions of the structure
- a voltage range similar to that of the electrolyte [107].

Lithium titanate spinel ($\text{Li}_4\text{Ti}_5\text{O}_{12}$, or LTS) has potential as a lithium ion battery electrode because it is a “zero-strain” insertion material meaning that lithium ions can be inserted and extracted with minimal change to its lattice dimensions. At a potential of 1.55 V, each mole of $\text{Li}_4\text{Ti}_5\text{O}_{12}$ can reversibly react with three moles of Li [112]. Although LTS has many properties that make it a promising alternative to carbonaceous anodes, it has the disadvantage of being a poor electrical conductor ($\sim 1 \times 10^{-7} \text{ S cm}^{-1}$ at 140 °C) [120]. Conductive diluents are included in the electrode composite to overcome this problem. Still, more interparticle electrical contact is necessary. One way to achieve more interparticle contact is to modify the surface chemistry of LTS. It has been shown that uniform, conformal coatings could be achieved using ALD[121, 122]. Specifically, using ALD to conformally coat LTS with TiN could improve performance by acting as a passivating layer and as a metallic conductor[8, 11, 26].

1.4 Supercritical Carbon Dioxide as a Solvent

A coated, high surface-area powder capitalizes on the characteristics of the thin film distributed over its increased reaction area. However, several drawbacks exist to using high surface area materials. Packing of submicron-sized particles and exposure to gas can reduce the surface area by 10^6 times because of agglomeration [123]. Furthermore, since such a high surface area is required, not all surfaces are reacted evenly.

Employing supercritical CO₂ (sc-CO₂) as a solvent for surface modification may be a solution to problems such as agglomeration, sintering and diffusion limitations of a powder packed bed. The solvent properties of sc-CO₂ are a combination of those of a liquid and a gas [124, 125]. The high density of sc-CO₂ means that it has solvating properties more similar to those of a liquid than a gas and is a suitable solvating agent [126], and it removes the constraints of using precursors with volatility requirements thus expanding the variety of materials that may be used including those with environmentally friendly ligands [127]. Supercritical CO₂ has a low viscosity, high diffusivity [128], and no surface tension [124, 127]. This absence of surface tension means tortuous surfaces within a porous material may be wetted [127]. The ability of sc-CO₂ to remove all surface H₂O allows for improved metal-substrate binding and decreases growth rate variability and uncontrolled polymerization [129, 130].

Lower temperatures (60-200 °C) can be used when performing surface modification with supercritical fluids compared to 400-600 °C as is typical for ALD. An increase in film purity through higher ligand solubility relative to traditional CVD [127]

and ALD is also obtained. Advantages of using non-volatile precursors include easier handling, more benign byproducts, and potentially lower costs. Solid ALD precursors must also be vaporized, but this is unnecessary with sc-CO₂ as a carrier. The CO₂ solvent itself is much “greener” than organic solvents as well.

1.5 Infrared Spectroscopy

To truly understand how a surface is modified, in this case, through the deposition of a thin film, knowledge of how that surface changes as the reaction proceeds is crucial. Therefore, in situ measurements are an important part of surface chemistry. A variety of in situ measurements such as mass spectrometry [63], quartz crystal microbalance [15], x-ray photoelectron spectroscopy [59], and spectroscopic ellipsometry [46] have been used with atomic layer deposition to monitor the changing surface chemistry. Metal-oxide powders, like TiO₂, and semi-metal oxides, like SiO₂, typically form covalent bonds with both organic and inorganic reactants. Infrared spectroscopy is an effective technique because it measures the absorption of electromagnetic radiation of these covalent bonds in the infrared region of the electromagnetic spectrum. More specifically, the vibrational region of the infrared spectrum, ranging from 2.5 to 25 μm, is examined. Instead of referring to a vibration’s wavelength, its wavenumber, ν , is given to describe its location within the spectrum. The wavenumber is calculated by writing the wavelength in centimeters and taking its inverse. The advantage of this is that the wavenumber is directly proportional to energy. In terms of wavenumbers, the vibrational IR spectrum spans from 400 to 4000 cm⁻¹ [131].

For infrared absorption to occur, the molecule must have a dipole moment that changes as a function of time as the infrared radiation changes sinusoidally. The molecule will then only absorb radiation at a frequency that corresponds to its vibrational frequencies. Absorbed radiation heightens the vibrational amplitude of the molecule by increasing its stretching and bending motions [131].

Infrared spectra provide structural information about a molecule [131]. For example, the IR spectrum of a metal oxide powder will usually show absorption bands that represent surface hydroxyl groups, adsorbed water and various bulk metal oxide modes. Fourier transform infrared (FTIR) spectroscopy (a particular method to determine the intensity of a certain frequency in a frequency-domain spectrum from a time-domain spectrum) is a convenient method for bulk and surface characterization because it is one of the few methods that do not require high-vacuum conditions [41, 43]. One requirement is that the material being examined has a high surface area because of the small cross-section of IR vibration transitions. A material such as SiO₂ can be monitored with in situ FTIR because all of its surface species possess IR-active vibrational modes [43].

When examining an ALD reaction in situ, the use of a difference spectrum can highlight changes to the surface as they occur in each half-reaction and throughout the film deposition process. A difference spectrum is collected by scanning the unmodified material and saving it as a reference. A reference spectrum is collected to serve as a background for the material and any CO₂ and water vapor present in the atmosphere or

reaction cell. After a surface-modifying reaction has occurred, an IR spectrum is collected using the previously-taken reference. Any positive absorption bands present in the difference spectrum represent groups that have been added to the surface. Likewise, any negative bands represent groups removed from the surface [26, 43, 45, 88, 93].

When spectra are collected in situ during reactions with sc-CO₂, the SiOH region becomes opaque because more-intense sc-CO₂ bands are present in the same region. Deuteration of the surface silanols with D₂O to form surface SiOD groups makes the silanols visible in the IR spectrum by shifting them to a lower wavenumber. Decreasing the pressure in the IR cell to 1 bar also permits the viewing of the SiOH region of the spectrum [129].

A Fourier transform IR spectrometer modulates the broadband infrared radiation creating an interferogram (Figure 1.6). The interferogram is a result of the passing the IR beam through a Michelson interferometer, and each IR wavelength is modulated at a different frequency. As the IR beam contacts the sample to be studied (finely ground and applied to a pressed salt disk), some of the light is absorbed while some is transmitted or reflected. The transmitted or reflected light is measured by a detector and the interferogram is Fourier-transformed by the computer resulting in a spectrum[132].

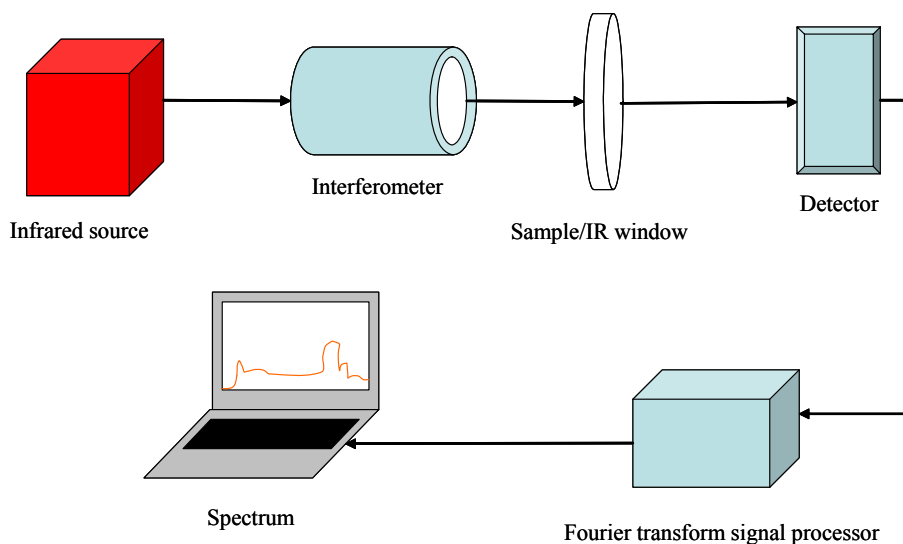


Figure 1.7 Schematic of an FTIR spectrometer.

1.6 Outline of this Dissertation

Chapter 2 of this dissertation discusses the initial stages of titanium nitride atomic layer deposition using sequential additions of TiCl_4 and NH_3 on fumed silica powder. This process was investigated using in situ FTIR spectroscopy techniques. After the first stage, it was found that the primary active surface species for the formation of TiN were determined to be TiCl_x and Ti_2NH . After six complete atomic layer deposition cycles, the infrared spectrum indicated a strong TiN band that was verified by diffuse reflectance infrared (DRIFT) spectroscopy recorded on pure TiN powder. Incomplete surface reactions were also observed during each cycle.

Chapter 3 examines the surface chemistry of lithium titanate spinel ($\text{Li}_4\text{Ti}_5\text{O}_{12}$, or LTS) because it is receiving consideration as a nanopowder anode material for use in lithium-ion batteries. While numerous studies are examining the performance of lithium titanate spinel (LTS) as a lithium-ion battery, little is known about the surface chemistry of it. Diffuse reflectance infrared Fourier transform spectroscopy was used to study the

type of surface groups present on LTS as a function of temperature. The surface was found to contain isolated and hydrogen-bonded TiOH groups and the dehydroxylation behavior with thermal treatment was similar to that of TiO₂. In addition, hexamethyldisilazane (HMDZ) and pyridine were used to probe the reactivity of surface hydroxyl groups and the presence of Lewis acid sites, respectively. The reaction of HMDZ occurred with both LiOH and TiOH groups to form Li-O-Si and Ti-O-Si. In addition, the reaction of gaseous CO₂ with the Li⁺ ions resulted in the formation of surface carbonate ions. The carbonate ions are removed by heating at 400 °C in air.

After confirming that TiN thin films can be deposited on a powder by ALD, and having gained a clearer understanding of the surface characteristics of LTS, *Chapter 4* describes how ALD was then used to coat LTS with TiN. Lithium titanate spinel has more positive working potential than traditional graphite anodes, and it does not react with electrolyte components. However, the main drawback of LTS powder is its poor interparticle electronic conductance that reduces the high-rate ability of the electrode. To improve this, the surface of LTS powder was coated with a titanium nitride layer by atomic layer deposition (ALD). In situ infrared spectroscopy studies were conducted to confirm the attachment of the titanium precursor. The nitrogen content of films was measured by total nitrogen content testing. TEM micrographs confirmed the formation of a thin titanium nitride film around LTS particles by ALD. Finally, lithium-ion cells with electrodes made of original and modified LTS nanopowders were assembled and tested.

While success has been achieved using ALD to coat particle surfaces, the high temperatures required for the reaction can damage the substrate. A precursor with a substantial vapor pressure is also necessary. *Chapter 5* discusses using supercritical CO₂

as a solvent that has the advantages of requiring a low reaction temperature and the capacity to dissolve non-volatile reactants. Specifically, the solvation of non-volatile bases in CO₂ and subsequent reaction with fumed silica as the first step in a base-catalyzed reaction with an alkylchlorosilane was examined. First, a separate experiment in which the base was added to silica dissolved in toluene followed by addition of an alkylchlorosilane was performed to verify that the base reacts with silica.

The dissertation concludes with *Chapter 6* which summarizes the findings from earlier chapters. Additional work for ALD coating of LTS to improve lithium-ion battery performance and deposition of non-volatile bases using sc-CO₂ is also suggested.

Note: Chapters 2-4 were prepared as manuscripts for publication. The chapter titles are the same as those of the publications. Chapter 2 was published in *Thin Solid Films*. Chapter 3 has been submitted to *Applied Surface Science*, while Chapter 4 appears in *Journal of Power Sources*. Therefore, there is some repetition with regard to references and background discussion.

2 AN INFRARED STUDY OF THE SURFACE CHEMISTRY OF TITANIUM NITRIDE ATOMIC LAYER DEPOSITION ON SILICA FROM TITANIUM TETRACHLORIDE AND AMMONIA

2.1 Introduction

Titanium nitride is a conducting, refractory material that has been studied for a variety of thin film applications. Titanium nitride thin films have been widely used as diffusion barriers for metal interconnects in ultra large-scale integrated circuit processing [2, 5, 22, 36], cutting tools, solar films for windows, and even for decorative purposes [3, 8, 31]. Traditionally, physical vapor deposition techniques have been used to synthesize TiN thin films. Though they are useful because of their low reaction temperatures, they offer poor step coverage [5, 8]. Chemical vapor deposition is often used to produce more conformal films for surfaces with features such as trenches [5, 9, 16, 22].

Atomic layer deposition (ALD) is an attractive method for synthesizing thin films. Conformality and step coverage of ALD films is much greater than those created by other deposition methods [8, 24, 49, 50]. In ALD, film deposition is achieved by repeated cycling of half-reactions (for a binary film) of individual precursors. These gaseous precursors are introduced individually followed by an inert gas purge of the reactor system. Ideally, each of the precursors saturates the substrate surface, thus allowing control of the thickness of the deposited film [8, 26, 97]. Ritala used TiCl_4 and NH_3 and introduced a reducing zinc pulse in between the two precursors to deposit a film on soda lime glass. The zinc led to a change in the appearance of the film and its electrical resistivity [8]. Kim et al. used TiCl_4 and NH_3 on p-type Si wafers (1 0 0) [97], while Lim et al. used tetrakis-dimethylamino titanium (TDMAT) and NH_3 on Si (1 0 0) to allow

lower reaction temperatures (60-240°C) and eliminate chlorine contamination and corrosion [26, 83]. Min et al. used tetrakis(ethylmethylamino) titanium (TEMAT) and NH_3 , also at lower reaction temperatures than those required for TiCl_4 [98].

Applications requiring a high surface area with specific surface properties may be realized by coating particles by ALD. ALD on high surface area materials has been described by Lindblad [133] and Haukka [105] and is preceded by the work of Aleskovskii et al. [32, 34, 134] plus numerous other examples cited by Puurunen [44]. Early work in ALD coating of powders was performed by Suntola, Haukka, Lakomaa and others [41, 42, 53, 54]. More recently, BN particles have been modified with coatings of SiO_2 [48, 135] and Al_2O_3 [136], and coatings of TiO_2 have been formed on SiO_2 [45, 88] and kaolin [88]. But, in general, most ALD work has been performed on traditional planar substrates with minimal focus on powder substrates. We are interested in using ALD to generate TiN coatings on high surface area particles. The high conductivity of TiN makes it an attractive candidate for passivating the surface of smaller electrode particles and thus could lead to the use of higher surface area electrode material in high-energy lithium-ion batteries.

Clearly, it is important to understand the fundamental surface chemistry in the ALD process and its relationship to film properties. In an ALD reaction, the number of deposition cycles determines the thickness of the film. In the case of TiN, there has been some examination of an initial transient region for TiN, particularly on SiO_2 , in which there is a non-linear relationship between number of deposition cycles and film growth [15, 50, 56]. However, little knowledge exists of the chemical reactions that occur on the substrate surface and how this is related to the growth rate of a TiN thin film. Ritala states

that steric hindrances alone cannot account for the low growth rate of 1.0 Ti atom/nm² that is deposited per cycle [8]. A fraction of a monolayer growth rate is observed for each ALD cycle. This low growth rate was attributed to possible dissociative chemisorption and the readsorption of the HCl byproduct [8], although other research has shown that HCl is chemisorbed at a surface density of $\ll 1$ molecule/10 nm² [137], or approximately 1% of a monolayer. Therefore, for HCl to inhibit growth, it would have to adsorb after the formation of at least one TiN monolayer. It has been postulated that during the initial 150 cycles, incoming molecules may react with exposed surface sites on the underlying substrate giving rise to a non-linear growth rate. At the same time, a partially formed layer could hinder the close packing of reactant precursors during the next cycle [50, 83]. Satta also reported that at temperatures of 400°C and above, 3-D growth of TiN solely on the deposited TiN occurs after only 25 complete cycles [56, 57]. They concluded that a non-linear growth rate during the initial cycles was due to preferential reaction at TiN “islands” [56, 57].

Studies of the formation of TiN on a SiO₂ surface have focused on aspects such as film composition [56], the effects of different SiO₂ substrates [57], and the kinetics of film growth [50, 83]. To gain a better understanding of the chemistry of TiN formation on a powder substrate we have used in situ Fourier transform infrared (FTIR) spectroscopy to study the surface species during the first six ALD cycles of TiCl₄/purge/NH₃/purge on a silica powder. While this approach has been used to elucidate the mechanism of TiO₂ growth on silica powder [45, 88], to the best of our knowledge, a similar study of the substrate-precursor interactions involved in forming TiN on SiO₂ has not been reported.

2.2 Experimental methods

Fumed silica (Degussa Aerosil A380), with a measured Brunauer-Emmett-Teller surface area of $358 \text{ m}^2/\text{g}$, was spread as a thin film on a standard CsI infrared transmission disk. A thin film of silica was used to gain access to the region below 1300 cm^{-1} where characteristic Si-O-Ti, Si-N, Ti-N and Ti-Cl modes lie. The region below 1300 cm^{-1} is opaque when using pressed disks of silica due to absorption by the Si-O bulk modes. The disk was inserted in a heatable, evacuable infrared cell fit with CsI windows [138]. The reference for the thin film of silica was recorded through the thin film just prior to addition of the reagents. All spectra were recorded at 400°C unless otherwise stated.

IR spectra were recorded on an ABB FTLA 2000 spectrometer equipped with a mercury cadmium telluride detector. The disk was placed inside an evacuable IR cell connected to a standard glass vacuum line. All spectra were recorded at 4 cm^{-1} resolution using 100 scans requiring approximately a two-minute collection time. TiN powder, used as obtained from Aldrich, was not amenable to transmission measurement as its large particle size led to scattering of the IR beam. IR spectra of the TiN powder were recorded in diffuse reflectance infrared (DRIFT) spectroscopy using a Praying Mantis diffuse reflectance apparatus from Harrick Scientific. KBr powder was used to record the reference for the DRIFT spectra. DRIFT spectra were also recorded at 4 cm^{-1} resolution. Where noted, the spectra were recorded as difference spectra, meaning that positive IR bands arose from addition of bonds to the reference sample and negative bands represent bonds that were removed from the reference sample.

Titanium (IV) tetrachloride from Aldrich (99.9%) and anhydrous ammonia from Matheson Tri-Gas (99.99%) were used as received. The precursors were transferred to evacuable glass flasks. Vapor from the reagents was introduced to the infrared cell using standard vacuum line methods. Precursor vapors were added in an A-B sequence. Approximately 0.4 torr of TiCl_4 was added at 400°C for 10 s followed by evacuation of the system to 10^{-5} torr for the A cycle. The B cycle consisted of two NH_3 exposures of approximately 0.5 torr over a three-minute span at 400°C followed by evacuation of the system to a pressure of 10^{-5} torr. Spectra were recorded after each evacuation for every half cycle. Six complete cycles were performed.

2.3 Results and discussion

2.3.1 Cycle 1

Figure 2.1 shows the spectrum of the silica substrate under vacuum at 400°C (Figure 2.1a) and the spectra from each half reaction in cycle 1 (Figures 2.1b and 2.1c, respectively). The reference for the spectrum of the silica substrate was recorded through the evacuated cell containing the CsI window. This spectrum is the absorbance spectrum of the thin film of silica. In this spectrum, the band at 3743 cm^{-1} is due to the -OH stretching mode of the isolated silanols and the three bands centered at 1095, 812 and 471 cm^{-1} are various Si-O-Si bulk modes.

Figure 2.1b is the difference spectrum obtained after exposure to TiCl_4 vapor for ten seconds at 400°C followed by evacuation. Note that the reference for this spectrum was recorded through the silica film just prior to addition of the gaseous TiCl_4 . The intensity of the negative band at 3743 cm^{-1} is equivalent in intensity to the positive peak at 3743 cm^{-1} in Figure 1a, and, thus, the reaction of TiCl_4 was rapid and complete as was

demonstrated by Lakomaa [42] and others [45, 88]. The positive bands at 995 and 909 cm^{-1} are assigned to the Si-O-Ti stretching modes of monodentate and bidentate $(\text{Si-O})_n\text{-TiCl}_{4-n}$ groups, (where $n = 1, 2$ for monodentate and bidentate peaks, respectively) [41, 42, 45, 54, 88]. Bands at 768 and 711 cm^{-1} are due to formation of multiply-bonded Ti-O species [139]. These bands could also be due to partial hydrolysis of the surface TiCl_x species with rogue water in the vacuum line.

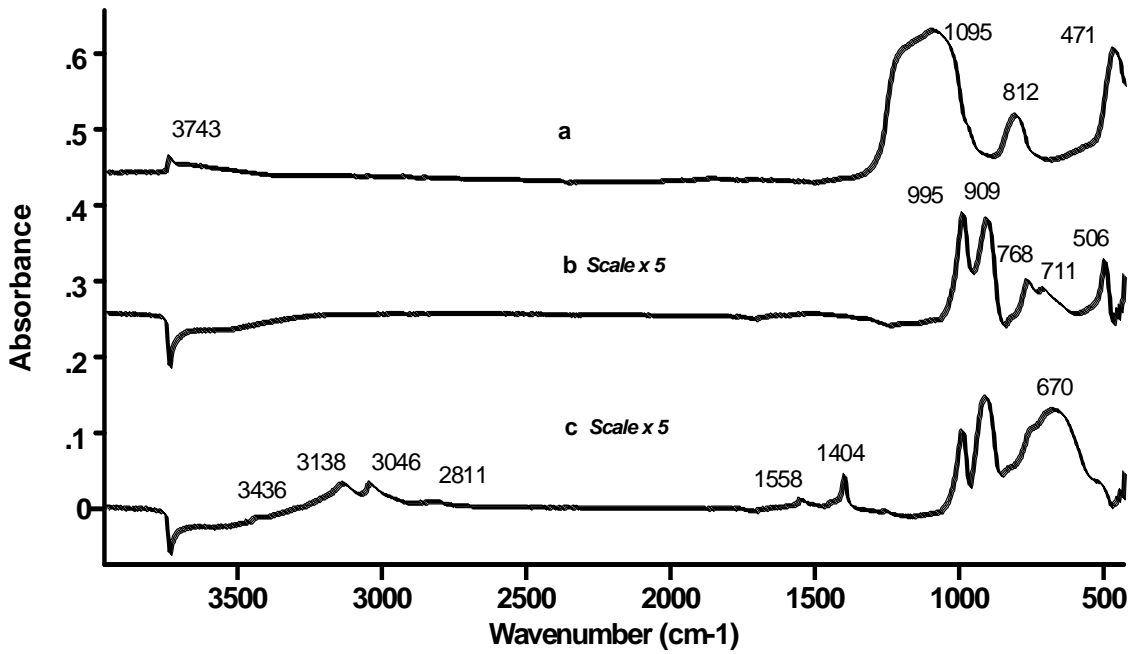
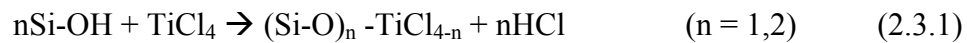


Figure 2.1 Thin film IR spectra of (a) silica substrate, (b) Cycle 1 first exposure of TiCl_4 , and (c) first exposure of NH_3 .

A band at 506 cm^{-1} indicates the presence of Ti-Cl_x surface species. The IR spectra obtained in the first half-cycle is in agreement with the results of others [8, 18, 45, 88] showing that the overall reaction is:



It has been shown that the relative amount of monodentate and bidentate species are reaction temperature-dependent. Blitz *et al.* showed that monodentate species are favored at higher reaction temperature [140] while Lakomaa *et al.* and Greer *et al.* state that bidentate species are favored at this reaction temperature [15, 42]. In our case, bands at 995 and 909 cm^{-1} show that both types of Si-O-Ti bonds appear after the first half cycle.

In the second half cycle, ammonia was added for approximately three minutes at 400°C, and the sample cell was then evacuated. The difference spectrum recorded is shown in Figure 2.1c. Positive bands appearing at 3435 and 1558 cm^{-1} are due to N-H stretching and bending modes, respectively. The frequency position of these bands are consistent with the formation of a surface $\text{M}_2\text{-NH}$ group with either two silicon atoms [141, 142], two titanium atoms or one of each. Evidence of primary amines (M-NH_2), which have bands between 3450-3490 and between 3530-3580 cm^{-1} , as stated by Peri [137] was not observed. The reaction with ammonia at the surface is accompanied by the removal of the Ti-Cl_x band at 506 cm^{-1} which shows that the reaction of ammonia occurs with the Ti-Cl_x groups and thus the most likely $\text{M}_2\text{-NH}$ species is $\text{Ti}_2\text{-NH}$. Furthermore, the reaction of ammonia with silica at temperatures greater than 300°C leads to the appearance of a secondary -NH peak at 3440 cm^{-1} [142]. The NH_4Cl is a byproduct of the reaction between NH_3 and HCl generated in the reaction as seen through the appearance of peaks at 3138, 3046, 2811, and 1404 cm^{-1} and corresponds well with Kiselev [142] and Hamann [143]. The salt sublimates from the silica surface between 400 and 600°C and forms -NH_2 groups on the surface [26, 137]. Elers states that NH_4Cl will decompose at temperatures greater than 370°C and may leave chlorine residue on the surface [96]. The absence of -NH_2 surface groups in the silica spectra verifies that the

observed NH_4Cl salt must have formed on the IR windows. In a controlled experiment, the CsI window with the SiO_2 was removed and a spectrum of the IR windows was taken and yielded an NH_4Cl spectrum of equal intensity to that observed during the *in situ* experiments. The sample window with the SiO_2 was then examined without the IR windows with no NH_4Cl peaks appearing on the surface. Tripp and Hair report that surface salt is removed from the spectrum under vacuum at 200°C [144].

We now address the question of whether TiN is formed. Figure 2.1c also shows a strong, broad mode at 670 cm^{-1} , and this band position is consistent with formation of Ti-N. However, this assignment could be debated as TiO_2 also produces a broad band in the same region. To resolve this question we refer to the data presented in Figure 2.2. Figure 2.2a is a replot of Figure 2.1c and is provided for comparative purposes. Figure 2.2b is the spectrum obtained in a separate experiment in which water vapor was added instead of ammonia in step B of cycle 1 [45]. The substitution of water vapor for ammonia leads to the growth of a TiO_2 layer on the surface [41, 42, 45]. In this case, there are clear differences between Figures 2.2a and 2.2b in the region where TiN and TiO_2 bands are expected. The growth of TiO_2 leads to a broad band centered at a slightly higher position (700 cm^{-1}) than the 670 cm^{-1} peak in Figure 2.2a and is accompanied by a second band near 374 cm^{-1} . This second band is not observed in Figure 2.2a. For comparison, Figures 2c and 2d are IR spectra of TiN and TiO_2 powder, respectively. TiO_2 powder, again, has a broad band near 700 cm^{-1} and a second band at 316 cm^{-1} whereas TiN has a single broad peak centered at 670 cm^{-1} . Also note a similar shape to the TiN

band at 670 cm^{-1} in both Figures 2.2a and 2.2c. For example, both spectra have shoulder bands located at 765 and 530 cm^{-1} . Therefore, the spectra in Figure 2.2 support an assignment of the 670 cm^{-1} peak to growth of TiN on the surface.

However, the reaction of ammonia in cycle 1 is more complicated than just reaction with the Ti-Cl_x groups leading to formation of Ti_2NH and TiN. It is noted that the addition of ammonia also leads to a decrease in the Si-O-Ti bands at 992 and 909 cm^{-1} which shows that there is some cleavage of the Si-O-Ti bond. This is more clearly seen in Figure 2.3a which is the difference spectrum of the B-step in cycle 1 using the A-step of cycle 1 as a reference. The removal of Si-O-Ti bonds is accompanied by the re-emergence of the Si-OH band at 3742 cm^{-1} . The intensity of this band is about 28% of the original silanols' intensity. Thus, we conclude that a secondary reaction occurs with ammonia in which a portion of the surface $(\text{SiO})_n\text{TiCl}_{4-n}$ ($n=1,2$) are cleaved and the Si-O group is hydrogenated by ammonia reforming isolated Si-OH groups. This behavior with ammonia is similar to the addition of water vapor which also led to a partial cleavage of the Si-O-Ti bond and reformation of Si-OH groups [45]. It is also found that the number of Si-OH groups returning decreases with each cycle. While 28% of the Si-OH groups reform at the end of cycle 1, 15% of the Si-OH groups regenerate after the second cycle. From the third to sixth cycles, no Si-OH regeneration was observed.

To recap, in the first half cycle, the isolated silanol groups have been removed from the surface, while covalent monodentate and bidentate $(\text{Si-O})_n\text{Ti-Cl}_{4-n}$ ($n=1,2$) species are formed. In the second half cycle, the main reaction occurs between ammonia

and the Ti-Cl_x groups leading to TiN terminated with $\text{Ti}_2\text{-NH}$ surface groups. There is a secondary reaction with the ammonia resulting in some cleavage of the $(\text{Si-O})_n\text{TiCl}_{4-n}$ groups at the Si-O-Ti bond and reformation of isolated Si-OH groups.

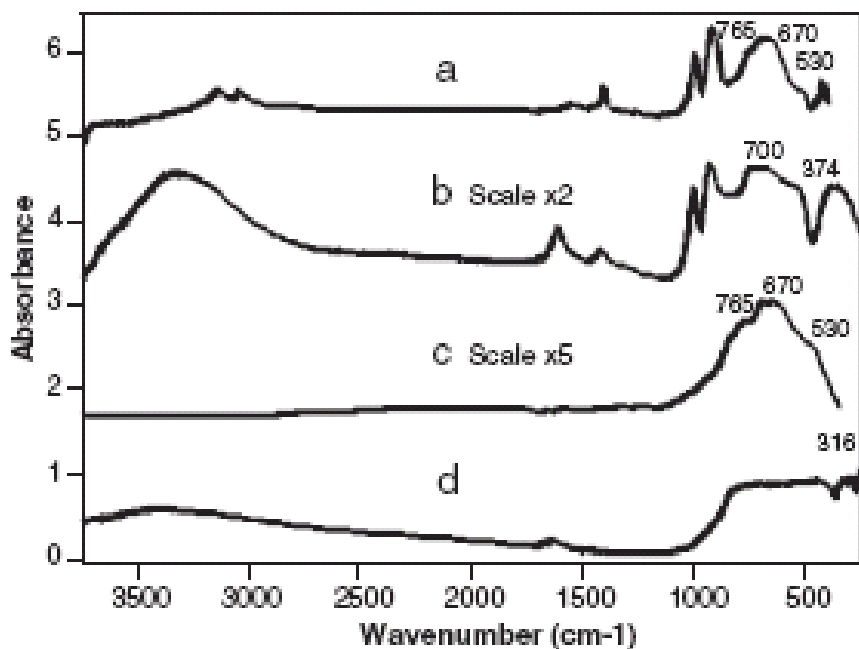


Figure 2.2 IR spectra of (a) the first exposure of NH_3 compared with (b) TiO_2 ALD on silica, (c) DRIFT IR spectra on TiN standard powder, and (d) Degussa P25 TiO_2 .

2.3.2 Cycle 2 and Higher

Figure 2.3b is the difference spectrum recorded for TiCl_4 addition in cycle 2. In this case the reference is the single beam spectrum after ammonia addition in the first cycle. In other words, this spectrum shows the difference in reaction of the TiCl_4 with the underlying layer produced at the end of cycle 1. The spectrum contains bands due to reaction with the TiN layer as well as bands due to reaction with exposed sites on the underlying silica. Reaction with the underlying silica is evidenced by the negative band at 3742 cm^{-1} along with positive Si-O-Ti bands at 992 and 909 cm^{-1} and Ti-Cl_x at 503 cm^{-1} . This shows that the Si-OH groups that reformed with the addition of ammonia

in cycle 1 again reacted with the TiCl_4 giving rise to $(\text{Si-O})_n\text{TiCl}_{4-n}$ (where $n=1,2$) groups. As mentioned earlier, this above reaction only occurs during the first three cycles where there is a transition from the silica to a TiN surface. With each cycle, the number of Si-OH groups reforming with addition of ammonia diminishes and does not appear after the third complete cycle.

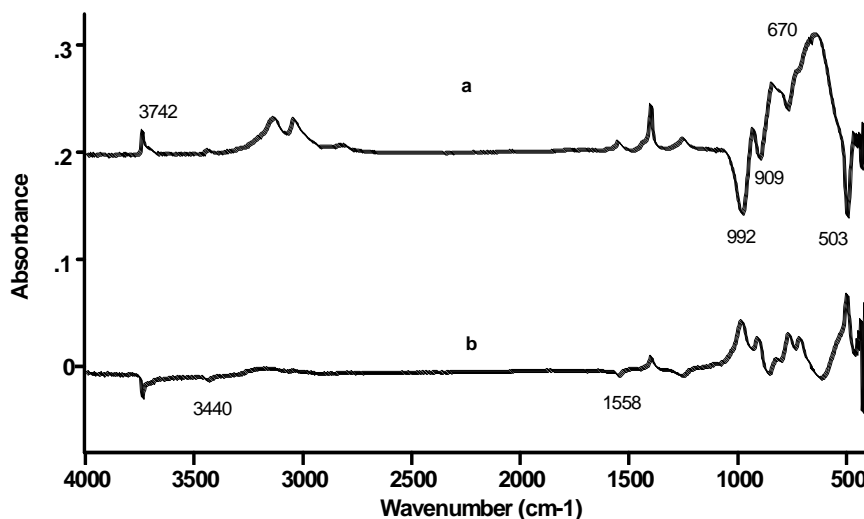


Figure 2.3 Difference IR spectrum of (a) the first NH_3 exposure using a reference spectrum of the first exposure of TiCl_4 (1c – 1b), and (b) the difference spectrum of the second TiCl_4 exposure using a reference of the first exposure to NH_3 .

There are several peaks in Figure 2.3b that indicate reaction of TiCl_4 with the underlying TiN surface. These changes appear in cycle 2 and occur each time in higher cycles. The negative bands at 3440 cm^{-1} and 1558 cm^{-1} show that the surface $\text{Ti}_2\text{-NH}$ groups react with incoming TiCl_4 molecules. While the Ti-Cl_x band at 503 cm^{-1} in Figure 2.3a is partially due to $(\text{SiO})_n\text{TiCl}_{4-n}$, the reaction of TiCl_4 with the Ti_2NH also produces a Ti-Cl_x band at 500 cm^{-1} . Comparison of the integrated peak areas of the Ti-Cl_x and -NH bands shows a consistent increase and decrease with each cycle. However, during a typical half-cycle, only 30-40% of the surface species are removed. An in situ mass

spectroscopy study by Juppo et al. further supports surface reactions at Ti-Cl_x and $-\text{NH}$ sites [63]. Using deuterated ammonia (ND_3), the formation of DCl as the only reaction byproduct after each half cycle was observed [63]. There is no increase in the TiN peak at 670 cm^{-1} and bands due to multiply bonded Ti-O bands, [139] at 767 and 715 cm^{-1} , again appear. In addition, NH_4Cl is formed as a byproduct as the bands at 3138 , 3046 , 2811 , and 1404 cm^{-1} increase in intensity.

Figure 2.4 contains the IR spectra recorded after the first and sixth ALD cycles for the A step and B step, respectively. As mentioned above, after the initial transition phase, the reaction of TiCl_4 in step A of each cycle involves a reaction with the $\text{Ti}_2\text{-NH}$ groups producing an adsorbed TiCl_x species. During step A, there is no change from the previous step in intensity of the TiN band at 670 cm^{-1} and only an approximate 5% change in intensity of the NH_4Cl bands. In step B, the addition of ammonia leads to a decrease in the Ti-Cl band around 500 cm^{-1} and this is accompanied by the reappearance of bands at 3436 and 1558 cm^{-1} due to Ti_2NH and an increase in intensity of the TiN band at 670 cm^{-1} . Comparing the A step spectra (2.4a and 2.4c) with the B step spectra (2.4b and 2.4d) indicates that NH_3 addition continues to change the shape of the peak centered at 670 cm^{-1} . NH_4Cl is primarily formed during step B of each cycle.

Figure 2.5 is a plot of the change in integrated peak area for bands representing mono- and bidentate Si-O-Ti , Si-OH , and TiN as a function of the number of ALD cycles. During the first two cycles we observe a non-linear growth in TiN along with changes in the Si-O-Ti bands. The decrease in intensity of the Si-O-Ti band shows that reformation of Si-OH groups occurs through cleavage by gaseous NH_3 of the monodentate SiOTiCl_3 and bidentate $(\text{SiO})_2\text{TiCl}_2$ species. This was also found with

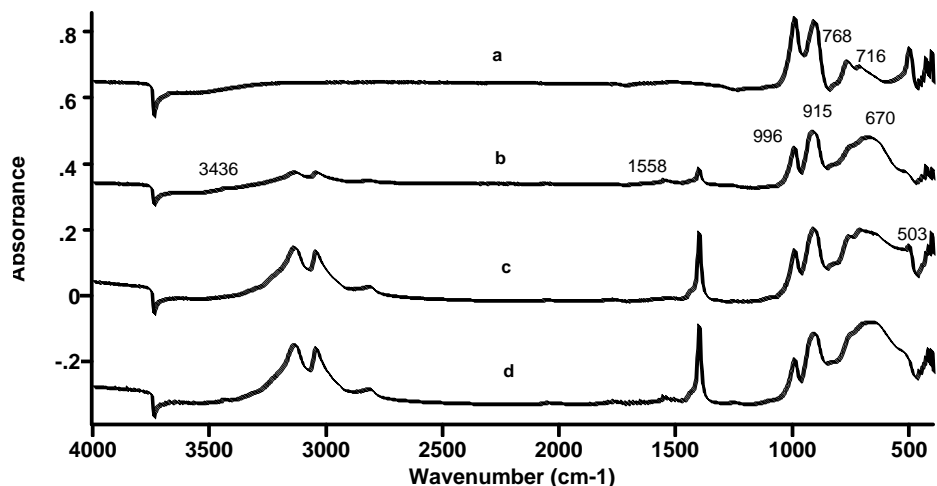


Figure 2.4 IR spectra of steps A (TiCl_4 addition) and B (NH_3 addition) in cycles 1 (a, b) and 6 (c, d), respectively, using the silica substrate as a reference.

addition of H_2O vapor instead of NH_3 [45]. After the transition cycles (2-3 cycles), growth of TiN bands is linear with each ALD cycle and there is little reaction with the underlying silica as evidenced by the almost constant intensity of the Si-O-Ti bands. The rapid rate of formation of Si-O-Ti bonds [45] and the low growth rate of TiN by ALD has been noted in the literature [8]. Three-dimensional growth has been observed at this temperature, thus leading to a relatively constant amount of the surface species even though TiN is accumulating [56]. Furthermore, adsorbed molecules prevent subsequent reactant molecules from close-packing resulting in the formation of intervals larger than required for a TiN molecule in the transient region of the film [83]. Additionally, the spectral evidence of incomplete removal of Cl and H ligands at 400°C , which supports the suggestion of Ritala [8], as well as reformation of surface silanols, demonstrates that the low growth rate may be related to incomplete surface reactions.

The results lead to a proposed mechanism consistent with the data for the creation of a TiN thin film. In this reaction, the TiCl_4 vapor reacts with the surface silanol groups and form TiCl_2 and TiCl_3 molecules [42] that are covalently bonded to the surface via Si-O-Ti bonds. HCl gas is formed as a by-product and purged from the reactor. Addition of NH_3 creates a bond with covalent and metallic properties [4] resulting in a Ti_2NH compound. Once the silica surface has been saturated with the Ti_2NH compound, it reoccurs on top of the preceding layer. All successive reactions can be illustrated by Figure 2.6.

2.4 Conclusions

The initial stages of titanium nitride atomic layer deposition on silica powder were investigated using *in situ* FTIR techniques. There is a transition between a silica and TiN-covered surface that requires about three ALD cycles. During the first complete cycle, Si-O-Ti bond formation is observed indicating that titanium atoms have been covalently attached to the silica surface through $(\text{SiO})_n\text{-TiCl}_{4-n}$ (where $n=1,2$). Reaction with NH_3 in step B leads to a reaction with the above species leading to Ti_2NH and TiN.

A secondary reaction occurs where the NH_3 cleaves the adsorbed species via the Si-O-Ti bond resulting in the reformation of Si-OH groups. After the first two to three cycles, the reaction proceeds through reaction of gaseous TiCl_4 with Ti_2NH to yield adsorbed Ti-Cl_x species, and the reaction of NH_3 in step B with this species to form TiN and Ti_2NH . Reappearance of Si-OH groups with the addition of NH_3 and incomplete surface reactions between Ti-Cl_x groups and $-\text{NH}$ groups help to explain the low TiN growth rate on silica surfaces.

IR Peak Areas vs. ALD Cycle

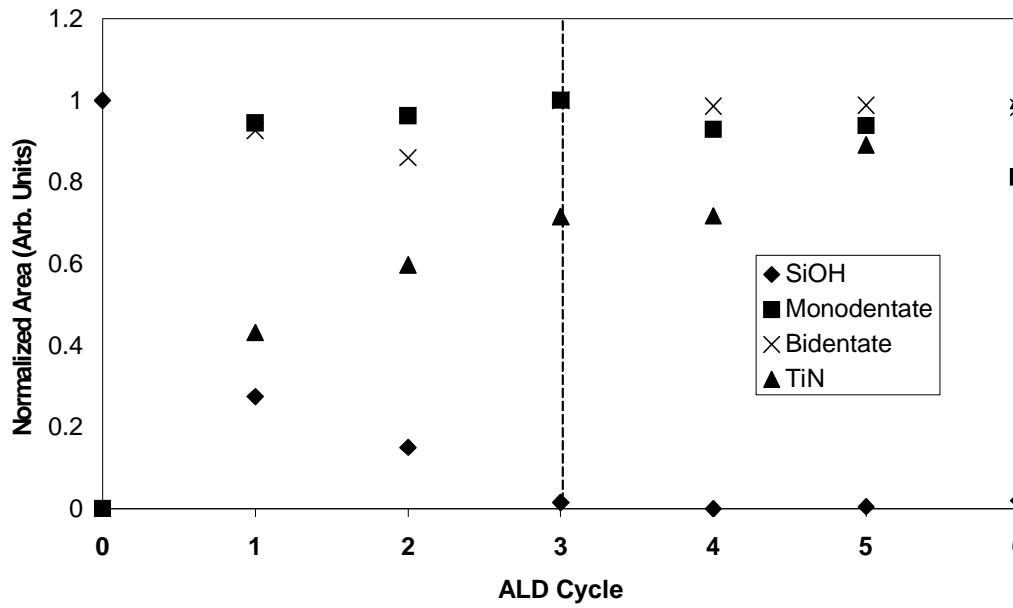


Figure 2.5 Comparison of normalized peak area vs. number of ALD cycles for various functional group bands.

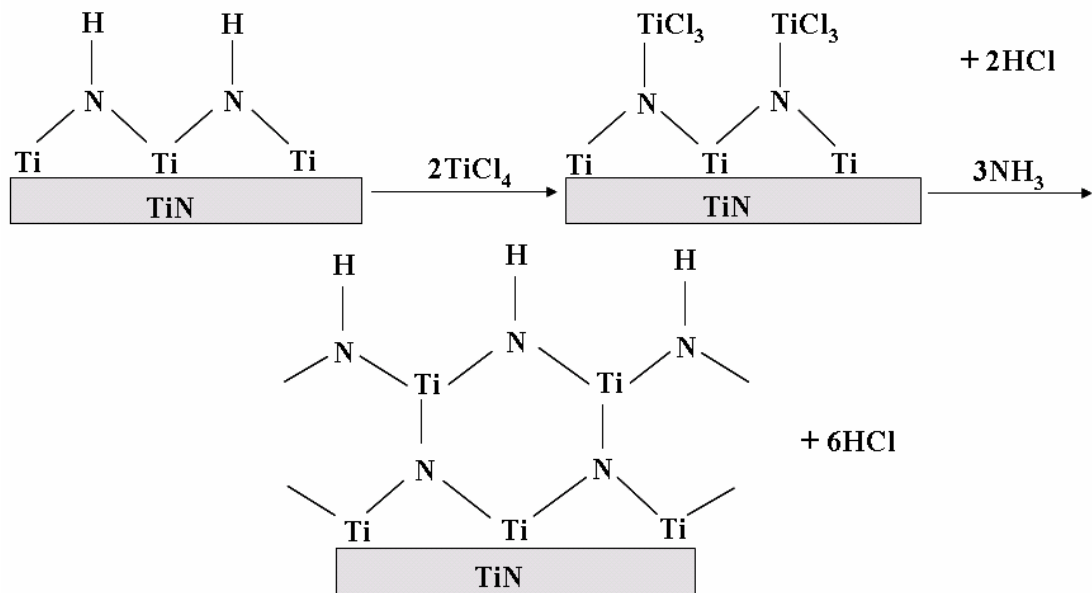


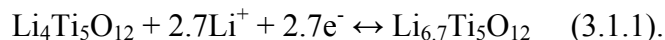
Figure 2.6 Proposed reaction scheme for TiN formation.

3 AN INFRARED STUDY OF THE SURFACE CHEMISTRY OF LITHIUM TITANATE SPINEL

3.1 Introduction

Li-ion battery anodes have been made out of Li, carbon-based materials, and Li alloys. An electrode, or Li-insertion compound, must conduct Li^+ ions and electrons as well as possess either a network or layered structure. Fabrication of anodes from nanoparticulate materials would lead to an increase of the surface area of the anode while decreasing anode volume. This has the potential to greatly enhance energy density. However, a disadvantage of high surface area materials is that the greater availability of reaction sites leads to deactivation of the active mass at a faster rate, and this shortens the life of the electrode [145]. Bulk changes to the nanoparticle-based anode may result as well [117]. Incorporation of a protective coating such as TiN could reduce this deactivation process [93] which, in turn, provides a means to improve Li-ion battery performance.

Lithium titanate spinel ($\text{Li}_4\text{Ti}_5\text{O}_{12}$, LTS) is available as a nanomaterial and has potential as a lithium ion battery electrode. Lithium titanate spinel is a “zero-strain” insertion material meaning that lithium ions can be inserted and extracted with minimal change to its lattice dimensions [146-151]. The anodic intercalation process, representing the charge cycle [112, 150, 152], is described in equation (1):



The material is highly reversible, demonstrating minimal capacity fade [112], and has a Li-insertion potential of 1.5 V which is above the reduction potential of most organic electrolytes. Thus, a solid electrolyte interphase (SEI) will not be formed on the particle

surface [112]. The low voltage potential of LTS allows for examination of any effects associated with fabrication of a TiN coating as this would occur without the interference of SEI formation.

Atomic layer deposition (ALD) can be an effective means for depositing a TiN coating on LTS. It was shown that uniform, conformal coatings of TiN could be achieved on SiO₂, Si (100) and soda lime glass using ALD [8, 47, 98]. The ALD reaction consists of a series of sequential, self-terminating surface half-reactions on a substrate followed by an inert gas purge [8, 38, 42, 47, 54]. ALD recently has been used to coat the surfaces of oxide powders with SiO₂ [48], TiN [93], and Al₂O₃ [55]. Recently, we fabricated TiN layers on LTS using ALD and showed increased specific capacity over various charge rates and an improved voltage profile [93]. However, it is essential to first understand the nature of the surface sites and surface chemistry of LTS in order to develop effective ALD methods for this material.

This study consists of an examination of the surface chemistry of LTS. Specifically, we use diffuse reflectance infrared Fourier transform (DRIFT) spectroscopy to monitor the dehydration and dehydroxylation behavior with heating in air and under vacuum conditions. In addition, chemical probes such as hexamethyldisilazane (HMDZ) and pyridine are used to identify reactive sites on the surface. HMDZ is a silanating agent [132] that reacts with surface hydroxyl groups at room temperature [132, 153]. Pyridine is a well known probe molecule used in IR studies for identifying Brønsted and Lewis acid sites [142, 154].

3.2 Experimental

The lithium titanate spinel powder, with a measured surface area (BET N₂) of 69 m²/g was obtained from Altair Nanomaterials, Inc. Pyridine and HMDZ (both from Aldrich) were used as received.

A Praying Mantis DRIFT apparatus equipped with an environmental reaction chamber (both from Harrick Scientific, Inc.) were used for in situ collection of IR spectra. In order to perform the experiments in vacuum, a high temperature (up to 600 °C) reaction chamber with a heated stage was used and connected to a standard vacuum line. KBr powder was used to record the reference spectrum and the sample consisted of approximately 5 wt.% LTS powder dispersed in KBr powder. The spectrum was recorded from 4000 to 500 cm⁻¹ at a resolution of 4 cm⁻¹ using an ABB FTLA 2000 FTIR spectrometer. Standard vacuum line techniques were used to deliver the HMDZ and pyridine to the LTS powder contained in the reaction chamber.

3.2.1 Dehydration/dehydroxylation

The LTS powder was heated, in air or vacuum, sequentially at 50, 100, 150, 200, 300, 400, and 500 °C. Infrared spectra were collected at each temperature. After heating at 500 °C, spectra were also collected when the powder cooled down to room temperature and again after exposure to the atmosphere over night (approximately 14 hours.)

3.2.2 Hexamethyldisilazane

The LTS powder was exposed to 600 mtorr HMDZ at the specified temperature under vacuum for approximately five minutes followed by evacuation of the excess reactant. A spectrum was collected during the gas exposure and after the system was

evacuated. A difference spectrum of the LTS powder was recorded using a reference spectrum of the powder under vacuum before addition of HMDZ. In a difference spectrum, positive bands represent bonds added to the surface, while negative bands represent bonds removed from the surface.

3.2.3 Pyridine

Excess pyridine (approximately 500 mtorr) was added to the LTS powder for five minutes, followed by evacuation at room temperature for ten minutes. Pyridine was also added to an LTS sample previously outgassed at 425 °C. In this case, the sample was heated to 425 °C for 120 minutes in air, then evacuated at 425 °C for 75 minutes followed by cooling to room temperature. A reference spectrum of the thermally treated sample was then collected. Excess pyridine was then added and spectra were collected during the pyridine exposure and after evacuating the cell.

3.3 Results

3.3.1 Heating in air

The spectra obtained for LTS recorded at ambient conditions and heated at various temperatures in air up to 150 °C is shown in Figure 3.1. The broad bands at 860 and 600 cm^{-1} are various bulk modes, and these bands do not change with heating in air or vacuum at temperatures up to 500 °C. The intensity of the bands due to bulk modes was used to compensate for sample-to-sample variation in the amount of LTS examined with DRIFT.

Several bands are observed in the hydroxyl spectral region (3800 cm^{-1} - 3000 cm^{-1}) and these bands change in intensity and position with heating in air. At room temperature, a small shoulder appears at 3690 cm^{-1} (Figure 3.1a) along with two broad peaks centered at 3440 and 3200 cm^{-1} . Heating the sample at temperatures up to $150\text{ }^{\circ}\text{C}$ results in the decrease in the band at 3440 cm^{-1} , and this is accompanied by a decrease in the band at 1638 cm^{-1} . The band at 1638 cm^{-1} is due to the bending mode of water and thus the band at 3440 cm^{-1} is assigned to the stretching mode of adsorbed water [155]. The removal of water sharpens and intensifies the band at 3690 cm^{-1} . This band is near 3694 cm^{-1} ,

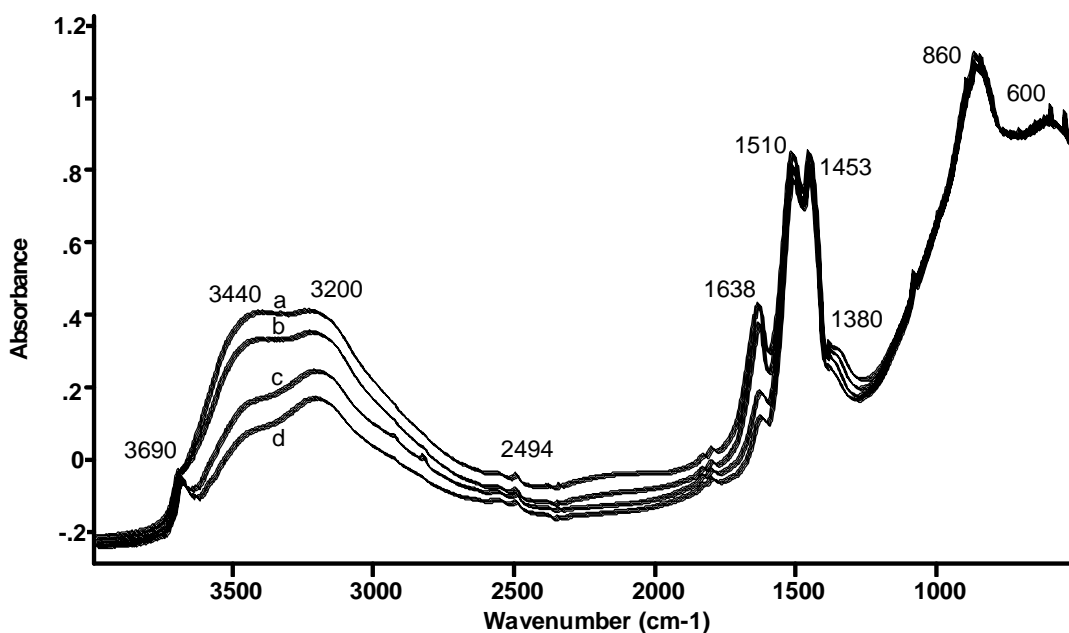


Figure 3.1 DRIFT spectra of LTS in air at (a) room temperature, (b) 50, (c) 100, and (d) $150\text{ }^{\circ}\text{C}$.

the frequency of the band due to isolated Ti-OH groups found on TiO_2 [156], and is assigned accordingly. An increase in intensity of the band due to isolated Ti-OH groups upon water removal is a common feature observed in oxides [67, 140, 157]. The isolated

hydroxyl peak has approximately the same intensity at 200 °C (Figure 3.2b) and 300 °C (Figure 3.2c) and reduces in intensity and shifts to lower frequencies with heating at progressively higher temperatures.

Heating the sample in air from 200 °C to 500 °C results in a reduction of the broad band at 3200 cm⁻¹. By 300 °C this band has disappeared (Figure 3.2c). This is similar to the behavior of hydrogen-bonded hydroxyl groups on other oxides and is assigned accordingly [67]. Heating oxides at temperatures between 150 and 400 °C is a dehydroxylation process resulting in the condensation of H-bonded groups producing coordinately unsaturated sites(cus)

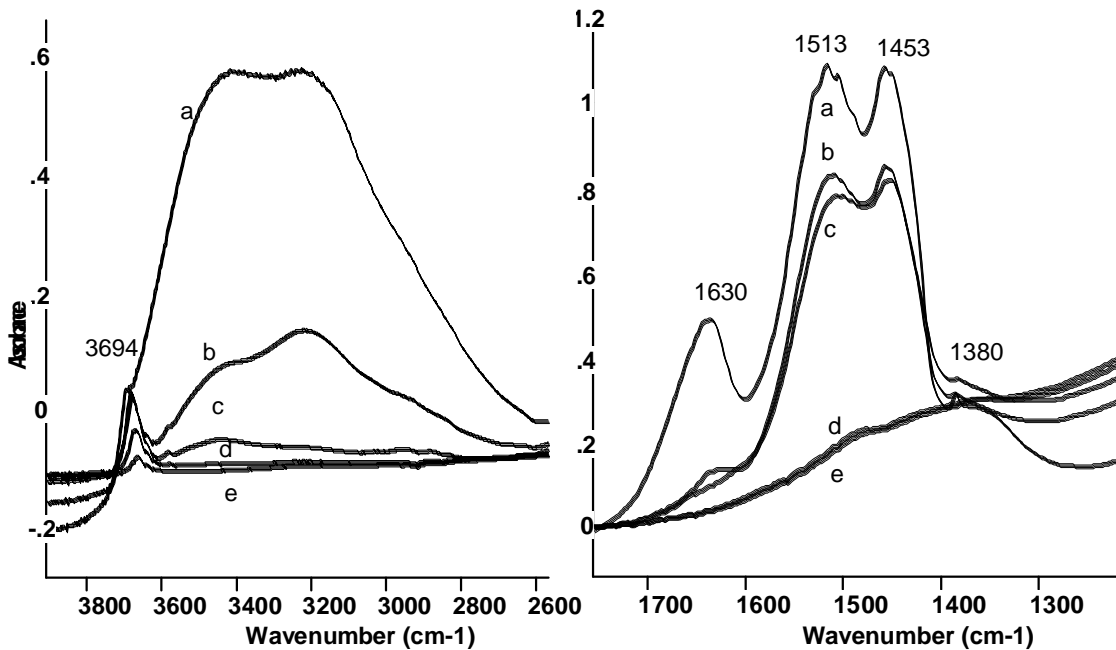
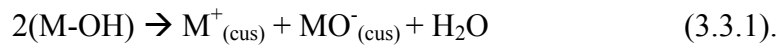


Figure 3.2 DRIFT spectra of LTS in air at (a) room temperature, (b) 200, (c) 300, (d) 400, and (e) 500 °C.

Additional strong, sharp peaks appear at 1513 and 1453 cm^{-1} with a shoulder at 1380 cm^{-1} . These bands are not removed by heating to 150 $^{\circ}\text{C}$ and from comparison to known compounds are assigned to carbonate ions [158]. Carbonates do form via the reaction of CO_2 on TiO_2 , but these bands are located at 1430 cm^{-1} (monodentate carbonate); 1580 cm^{-1} (bidentate carbonate); 1670, 1350 cm^{-1} (bicarbonate); and 1560, 1180 cm^{-1} (carboxylate anion) [156] and are much weaker than the bands observed in Figure 1. The carbonates on LTS are associated with the Li^+ cations as it is well known that Li_2O readily reacts with CO_2 to form lithium carbonate [159]. The carbonate peaks at 1513 and 1453 cm^{-1} disappeared after heating in air at 400 $^{\circ}\text{C}$ (see Figure 3.2.)

Figure 3.3 shows the initial spectrum of the LTS powder (Figure 3.3a), after heating in air to 500 $^{\circ}\text{C}$ followed by cooling to room temperature from 500 $^{\circ}\text{C}$ (Figure 3.3b), and after the sample was exposed to the atmosphere over night (Figure 3.3c). The spectrum obtained after heating to 500 $^{\circ}\text{C}$ and recorded after returning to room temperature is similar to the spectrum of the starting material. This indicates rehydration and reformation of carbonates occurs. The reappearance of carbonate peaks upon cooling in air shows that atmospheric CO_2 does interact with the powder to form surface carbonates. However, there is a difference in that the band due to H-bonded groups does not return to the same intensity in the spectrum of the starting material. After approximately one week in air, the H-bonded peak regained its original intensity, similar to the rehydroxylation of silica. On silica heated to 400 $^{\circ}\text{C}$, the H-bonded hydroxyl groups reform slowly over a period of one to two days [67].

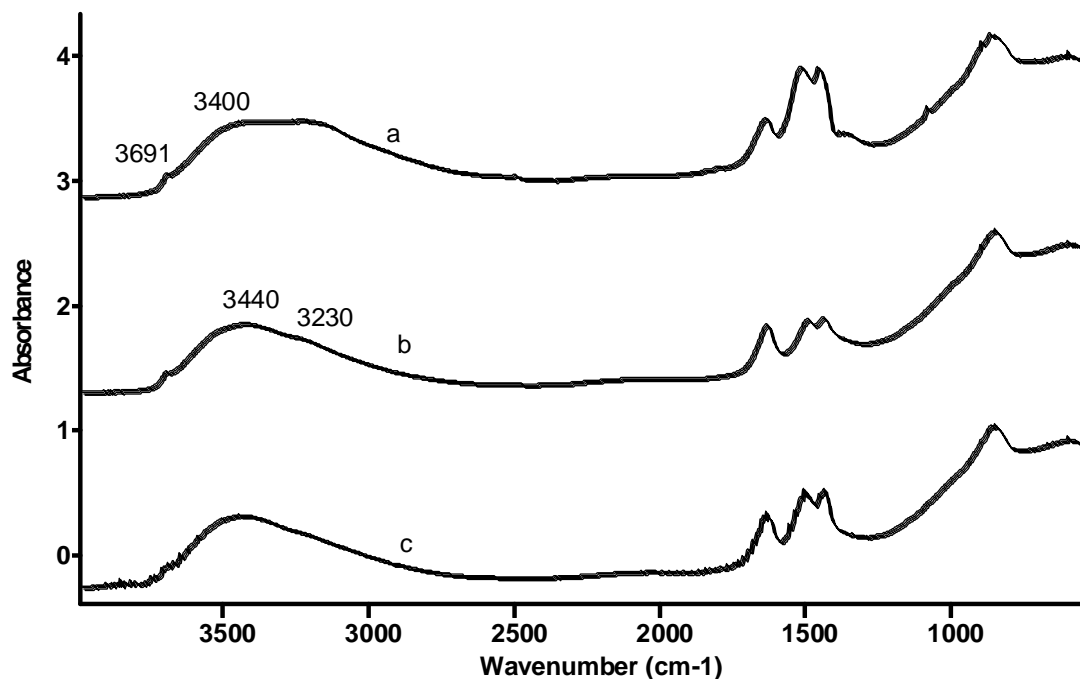


Figure 3.3 DRIFT spectra of LTS in air at (a) room temperature, followed by (b) heating to 500 °C for 30 minutes then recorded immediately after cooling to room temperature, and then (c) after leaving in air overnight.

3.3.2 Heating in vacuum

Figure 3.4 shows the spectra of the LTS powder in air and after evacuation at room temperature, followed by heating under vacuum at 50, 100, and 150 °C. The spectra of LTS evacuated at room temperature show a marked decrease in the adsorbed water bands at 3440 and 1620 cm^{-1} . The remaining water layer is removed by evacuation at 150 °C (Figure 3.4e). Removal of the water layer by evacuation at room temperature reveals the isolated TiOH band at 3690 cm^{-1} , and this band does not change in intensity with evacuation up to 150 °C. The carbonate overtone and combination modes at 2953, 2921, 2820, 2562 and 2494 cm^{-1} , along with the intense carbonate peaks at 1513 and 1453 cm^{-1} , do not change with evacuation at 150 °C.

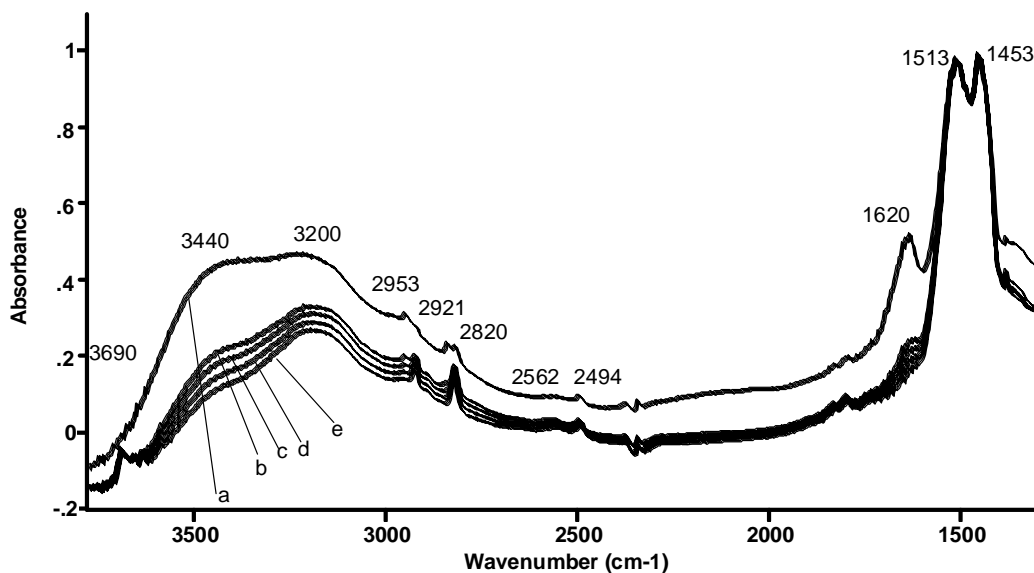


Figure 3.4 DRIFT spectra of LTS in (a) air followed by evacuation at (b) room temperature, (c) 50, (d) 100, and (e) 150 °C.

Upon heating the LTS from 200 °C (Figure 3.5a) to 500 °C (Figure 3.5d), the isolated Ti-OH group remains and shifts slightly from 3690 to 3680 cm^{-1} due to removal of the broad peak centered at 3200 cm^{-1} . Also, when evacuated at elevated temperatures, a peak at 3586 cm^{-1} appears in the area where $\text{LiOH}\cdot\text{H}_2\text{O}$ is found [158]. At lower temperatures, this band was barely observable as a shoulder in the larger band centered at 3200 cm^{-1} . The disappearance of the broad band at 3200 cm^{-1} due to hydrogen-bonded groups with increased temperature under vacuum is similar to that observed for heating in air. However, the carbonate ions exhibited a different behavior when the sample was heated in air from that seen in vacuum. Heating LTS under vacuum at 500 °C did not eliminate the bands due to carbonates. The carbonate modes at 1513 and 1453 cm^{-1} are still present at 99% of their original intensity when heated in vacuum at 500 °C (not shown).

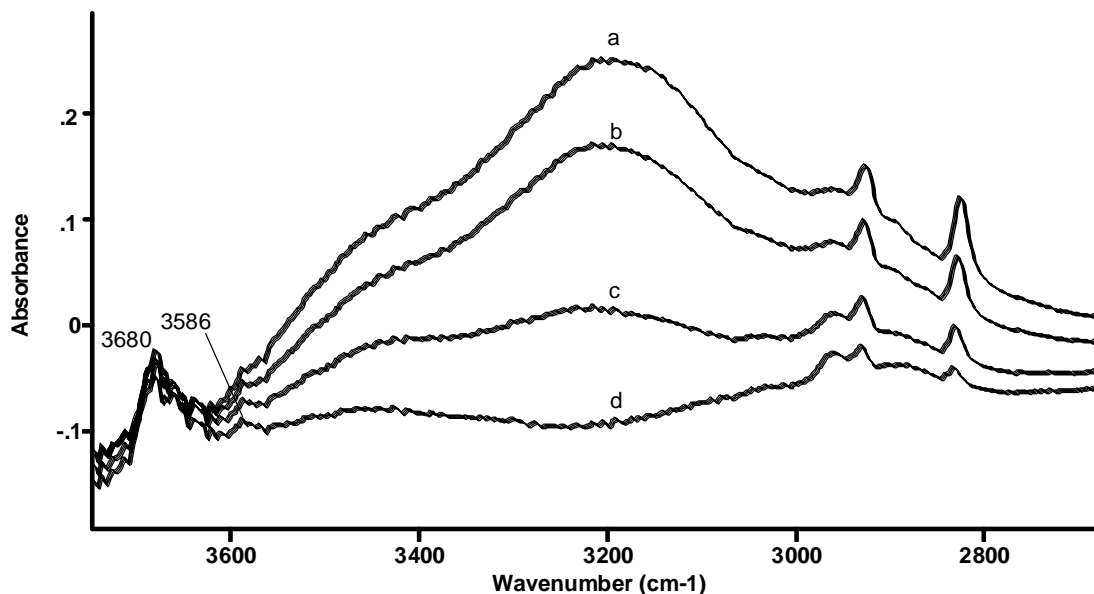
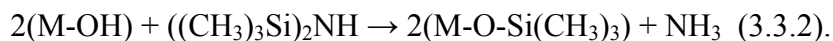


Figure 3.5 DRIFT spectra of LTS evacuated at (a) 200, (b) 300, (c) 400 and (d) 500 °C.

In contrast, heating LTS in air at 400 °C resulted in the removal of the bands due to carbonates (see Figure 3.2). This shows that the removal of carbonates occurs at 400 °C only in the presence of air. This was also observed for LiOH powders by Smyrl, et al. They found that the drying of LiOH powder containing Li₂CO₃ under vacuum at 400 °C did not remove the Li₂CO₃ [158].

3.3.3 Hexamethyldisilazane

HMDZ is a silanating agent commonly used as a gas-phase probe to study reactive sites on oxide surfaces [156, 160]. HMDZ reacts with surface hydroxyl groups according to



The IR spectra obtained for the reaction of LTS at room temperature with HMDZ is shown in Figure 3.6. The reference was recorded through the powder before addition of HMDZ. The negative band at 3688 cm^{-1} shows that a reaction has occurred with the isolated TiOH mode while the appearance of the band at 3635 cm^{-1} is attributed to weakly perturbed isolated TiOH groups due to van der Waals interactions between the surface MOH groups and SiCH₃ groups. Such a shift has been noted in IR studies of the reaction of HMDZ on oxides [161]. Positive bands at 2959 and 2900 cm^{-1} are CH₃ stretching modes, the strong peak at 1257 cm^{-1} is a SiCH₃ bending mode, and weak bands at 887 and 850 cm^{-1} represent CH₃ rocking modes. There is little, if any, change in the carbonate bands at 1513 and 1453 cm^{-1} showing that HMDZ does not displace the carbonate ions from the surface. The combined spectral data supports the reaction depicted in scheme 3.3.2.

Two bands in the M-O-Si spectral region are observed. The band at 960 cm^{-1} is near the Ti-O-Si frequency of 947 cm^{-1} reported for the reaction of HMDZ with TiO₂ and is assigned accordingly [156]. The second peak located at 1040 cm^{-1} is not observed in the reaction of HMDZ with TiO₂ [156]. The peak at 1040 cm^{-1} likely represents a Li-O-Si bond. A separate study was performed in which LiOH was exposed to HMDZ in the gas phase. This resulted in the appearance of a strong band around 1075 cm^{-1} . No other band in the HMDZ spectrum appears in this area. Thus the 1075 cm^{-1} band (and the 1040 cm^{-1} band on LTS) is attributed to a Li-O-Si mode.

3.3.4 Pyridine

Pyridine is a commonly used probe molecule for Lewis acidity of a metal oxide surface. Exposure of 500 mtorr pyridine for five minutes followed by evacuation to the LTS surface at room temperature yielded the spectrum shown in Figure 3.7. A strong band appears at 1594 cm^{-1} with smaller bands at 1575 , 1488 , and 1443 cm^{-1} when the sample is exposed to pyridine at room temperature (Figure 3.7a). Addition of pyridine vapor to a LTS sample heated to $425\text{ }^{\circ}\text{C}$ in air, placed under vacuum and cooled to room temperature gave peaks at the same frequencies although the band at 1443 cm^{-1} is relatively more intense than in the spectrum of pyridine adsorbed on the non-thermally treated powder (Figure 3.7b). With the exception of the 1594 cm^{-1} peak, the other bands in the spectrum have been observed for pyridine on the surface of other metal oxides and indicate the presence of coordinative bonds at Lewis acid sites [154, 155, 162].

Table 3.1 lists the IR bands for pyridine adsorbed on TiO_2 at room temperature and $150\text{ }^{\circ}\text{C}$ and from pyridine on LTS at room temperature. Spectra from Jones and Hockey and Kataoka and Dumesic both show a peak at 1606 cm^{-1} results from the reaction of pyridine on TiO_2 Lewis acid sites [155, 162]. Kataoka and Dumesic observe the growth of a peak at 1596 cm^{-1} when water vapor was added to the TiO_2 , and the band was assigned to hydrogen-bonded pyridine. In addition, the peak at 1606 cm^{-1} attributed to pyridine adsorption on Lewis acid sites decreased in intensity [162]. A band at 1593 cm^{-1} is also observed for molecular bonding between pyridine and aluminosilicate powder [142]. Therefore, the peak at 1594 cm^{-1} on LTS is assigned to hydrogen-bonded

pyridine. The existence of Brönsted acid sites is indicated by a band in the 1530 to 1550 cm^{-1} region which is assigned to an adsorbed pyridinium ion [154, 162]. This band is not observed in either spectrum in Figure 3.7.

Comparison of the relative intensity of the bands at 1594 cm^{-1} in Figures 3.7a and 3.7b, after adjusting for differing sample mass, shows that the peak at 1594 cm^{-1} in 3.7a is approximately twice as intense. Therefore, heat treating the powder to $425 \text{ }^\circ\text{C}$ reduces the number of hydrogen-bonded pyridine molecules, and this is accompanied by an increase in the number of pyridine molecules bound to Lewis acid sites. This is in agreement with the reaction depicted in scheme 2 in which the dehydroxylation of the surface leads to an increase in the number of Lewis acid/base sites.

Table 3.1 Comparison of Lewis acid sites by pyridine absorption bands on TiO_2 and $\text{Li}_4\text{Ti}_5\text{O}_{12}$ surfaces.

| TiO_2 (ambient) | TiO_2 (420 K) | $\text{Li}_4\text{Ti}_5\text{O}_{12}$ (ambient) | Assignment |
|--------------------------|------------------------|---|------------------------|
| 1640 | --- | --- | LPy [142, 155] |
| 1605 | 1606 | --- | LPy [142, 162] |
| --- | 1597 | 1594 | MPy [142, 162] |
| 1575 | 1576 | 1575 | LPy [142, 155, 162] |
| 1485 | 1493 | 1488 | LPy [142, 155, 162] |
| 1440 | 1446 | 1443 | LPy [142, 155, 162] |

LPy—Lewis acid surface site; MPy—molecularly adsorbed, hydrogen bonded to surface hydroxyls

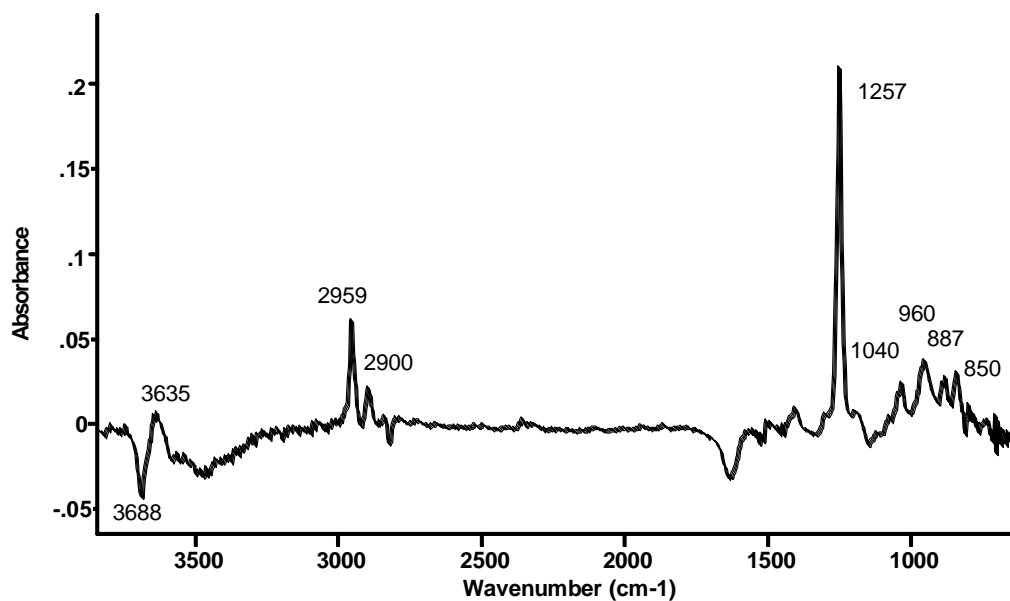


Figure 3.6 Difference spectra of an LTS sample evacuated at room temperature and then exposed to excess HMDZ vapor, followed by evacuation for 5 minutes.

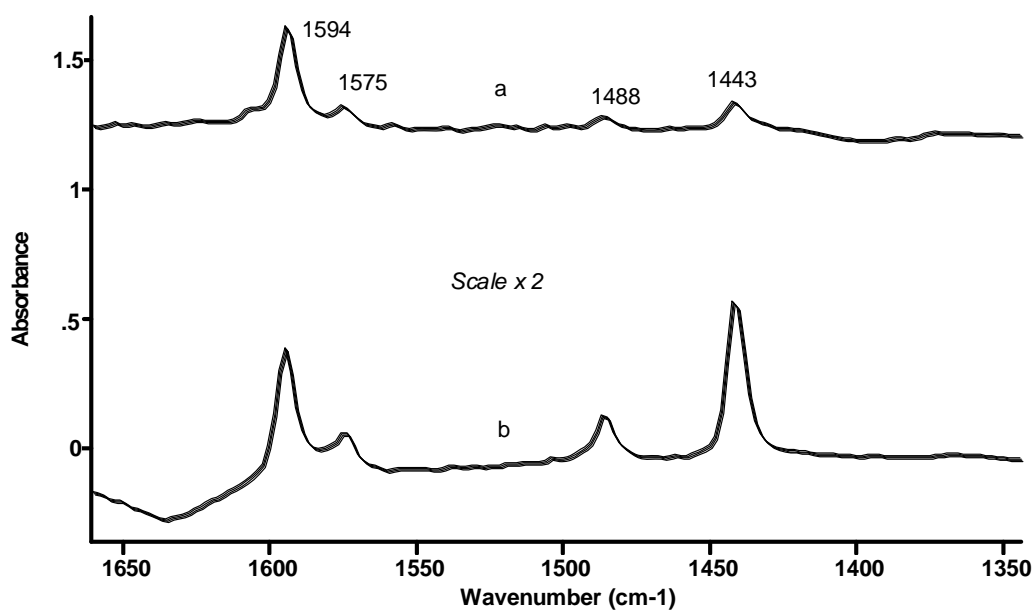


Figure 3.7 Difference spectra of 500 mtorr pyridine vapor added at room temperature to an LTS sample previously evacuated at (a) room temperature and (b) 425 °C.

3.4 Conclusion

The DRIFT spectra of LTS powder show that the surface contains molecularly adsorbed water, hydrogen-bonded TiOH groups, isolated TiOH and LiOH groups and surface carbonates. Dehydration and dehydroxylation of the surface occurred by heating in air or vacuum, and the adsorption of pyridine showed that the dehydroxylation was accompanied by an increase in the number of Lewis acid/base sites. The dehydration and dehydroxylation of the surface is similar to the behavior observed on TiO₂. However, the surface also contains LiOH groups as evidenced by the reaction with HMDZ with both TiOH and LiOH groups.

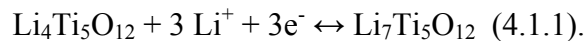
The presence of Li⁺ ions also led to the reaction with CO₂ to form carbonate ions on the surface. The carbonates are removed by heating in air at 400 °C but return when the material is cooled back to room temperature. The carbonates do not reform for samples heated in air and then evacuated. It is anticipated that LTS prepared in this same manner will exhibit similar reactions to ALD precursors as found for TiO₂.

4 SYNTHESIS AND CHARACTERIZATION OF ATOMIC LAYER DEPOSITED TITANIUM NITRIDE THIN FILMS ON LITHIUM TITANATE SPINEL POWDER AS A LITHIUM-ION BATTERY ANODE

4.1 Introduction

Desirable electrode materials for lithium-ion batteries (LIBs) are electronically conductive Li-insertion compounds with a structure that allows lithium mobility. Examples of LIB anodes include lithiated carbon materials and Li alloys. The most commonly distributed LIBs use graphite (or related carbonaceous materials) as anodes. While LIBs substantially reduce power cost, recharging LIBs at high rates remains a challenge. This limitation, to a large extent, is due to lithium metal plating on the surface of the carbon anode at high charging rates. This plating leads to capacity degradation and causes a safety hazard. The origin of lithium metal plating stems from the proximity of the anode potential to that of lithium metal. To avoid lithium plating, the anode charging potential must be less negative.

Lithium titanate spinel (LTS) is an emerging negative electrode material for high rate LIBs [146-150, 163-175]. Up to three Li ions can be intercalated reversibly per each LTS formula unit, as shown by Equation 4.1.1



When fully lithiated, LTS has a specific capacity of 167.5 A·h kg⁻¹ and an energy density of 270 W·h kg⁻¹ in a Li-metal cell. By comparison, the specific capacity of graphite ranges from 300 to 370 A·h kg⁻¹ with an energy density between 380 to 460 W·h kg⁻¹.

Among the advantages of LTS over graphite is its working potential. Since the potential difference between LTS and Li/Li^+ is greater than 1 V, neither a solid electrolyte interphase (SEI) nor a lithium metal will form on the electrode surface regardless of charge rate. Additionally, it may be more stable at elevated temperatures (75-80 °C) because the electrode does not react with the electrolyte components. Without the formation of a SEI, the electrode surface area can be increased through the use of nanoparticulate LTS.

Another advantage of LTS is that it is a “zero-strain” material meaning that lithium ions can be inserted and extracted with minimal change to its lattice dimensions [175]. The ability of a cell to maintain its lattice dimensions is a reliable predictor of its voltage and capacity stability while cycling.

While LTS has many properties that make it a promising alternative to carbonaceous anodes, it has the disadvantage of being a poor electrical conductor ($\sim 1 \times 10^{-7} \text{ S cm}^{-1}$ at 140 °C) [120]. Conductive diluents are included in the electrode composite to overcome this problem. Still, more interparticle electrical contact is necessary. We have investigated the modification of the LTS surface chemistry as a means to improve LIB performance. In particular, we have considered coating the particle surface with a layer of TiN.

TiN is a hard, refractory material [8, 11] and an excellent metallic-type conductor [8, 11, 26]. Atomic layer deposition (ALD) may be an effective means for depositing such a coating. It has been shown that uniform, conformal coatings could be achieved using ALD [8, 47, 98]. Atomic layer deposition recently has been used to coat the surfaces of powders with SiO_2 [48], TiN [93], and Al_2O_3 [55, 136]. The ALD reaction

consists of a series of sequential, self-terminating surface half-reactions on a substrate followed by an inert gas purge [8, 38, 42, 47, 54]. In the case of TiN, made from TiCl₄ and NH₃, the TiCl₄ chemisorbs on to the substrate and, after purging the excess precursor from the system, NH₃ then reacts with the Ti-Cl-terminated surface to form one theoretical monolayer. A detailed description of the reaction chemistry is given in [93]. Actually, only a fraction of a monolayer is formed. Repeated sequential doses of TiCl₄ and NH₃ lead to growth of a titanium nitride film on the nanoparticle.

4.2 Experimental

4.2.1 ALD Materials

The ALD reaction was performed using approximately 0.30 g of lithium titanate spinel powder (Altair Nanomaterials). The as-received nanopowder had a particle diameter of approximately 25 nm, and a measured Brunnauer-Emmett-Teller (N₂) surface area of 69 m² g⁻¹. Titanium (IV) chloride (Acros, 99.9%) was used as received. Anhydrous ammonia (Matheson Tri-Gas, 99.99%) was used as the reducing agent and nitrogen source.

4.2.2 ALD In Situ Methods

Methods and equipment used to perform the in situ ALD experiments and diffuse reflectance infrared Fourier transform (DRIFT) spectroscopy have been described previously [93]. We used these methods to characterize the surface chemistry of LTS and examine the initial TiN reaction chemistry.

4.2.3 ALD Ex Situ Methods

4.2.3.1 Reactor description

The deposition cell was a vertically mounted quartz tube with a porous frit centered axially within the tube to act as a support platform for the powder substrate while allowing the excess precursors to exit the deposition area. A muffle furnace was used to maintain the reaction temperature at 500 °C. The run and vent lines were electrically heated with heating tape to 250 °C to prevent condensation and formation of a $\text{TiCl}_4\cdot\text{NH}_3$ adduct through weak interactions between the precursors and their adhering to the transfer lines. The pressures upstream and downstream of the reactor were monitored with Baratron differential pressure gauges. The system was equipped with a mechanical vacuum pump and a liquid nitrogen trap. A schematic is provided in Figure 4.1.

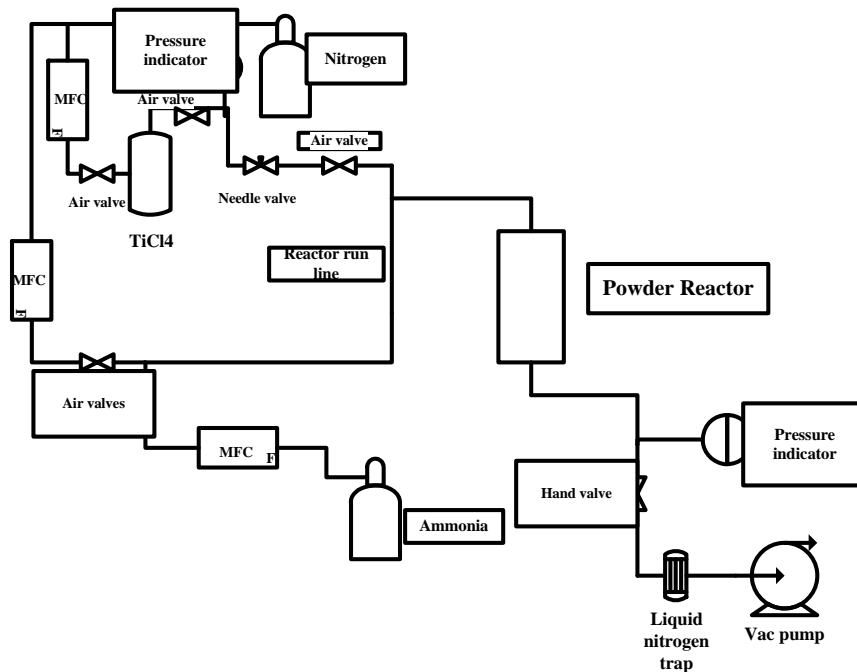


Figure 4.1 Schematic of home-built atomic layer deposition reactor.

4.2.3.2 Precursor delivery

The atomic layer deposition reactor consisted of one stainless steel bubbler to supply the TiCl_4 . Anhydrous ammonia was supplied by a tank, pressurized to about 2000 Torr. Air-actuated valves regulated precursor delivery via computer software. Titanium (IV) chloride flow was controlled by maintaining bubbler temperature at $0\text{ }^\circ\text{C}$ resulting in a vapor pressure of approximately 2.5 Torr. The substrate was exposed to 5×10^6 Langmuirs (10^{-6} Torr-seconds = 1 Langmuir, L) of TiCl_4 followed by a three-second evacuation and a two-second nitrogen purge for the first half-cycle. Ammonia flow was controlled by an MKS Instruments Type 247 mass flow controller with a flow rate of 20 standard $\text{cm}^3 \text{ s}^{-1}$ at approximately 2000 Torr. The substrate was exposed to 1.2×10^9 L of NH_3 followed by a three-second evacuation and a two-second purge.

4.2.3.3 Total nitrogen content test

Upon modification of an LTS sample by TiN ALD, 0.15 g of the sample was oxidized completely at $1350\text{ }^\circ\text{C}$. The combustion products, NO_x , were measured through the electrical conductivity of the resulting gas.

4.2.4 Coin Cell Testing

4.2.4.1 Coin cell materials

The electrode materials were tested in coin-type cells. The materials were prepared by coating aluminum or nickel foil with slurry consisting of either 80 % (by weight) uncoated or ALD TiN-coated LTS (active material), 10% carbon black (conductive diluent), and 10% PVDF (polyvinylidene fluoride) binder suspended in N-

methylpyrrolidone. The slurry was manually spread onto the foil with a Gardco Film Applicator (a.k.a. doctor blade) so the thickness of the coating corresponded to a capacity of 0.6-0.8 mA·h cm⁻².

4.2.4.2 Coin cell fabrication methods

After coating, the electrodes were calendered, dried under vacuum at 110 °C, and punched to the diameter of 1.3 cm. Lithium foil was used as a counter electrode. A 1-M solution of LiPF₆ dissolved in ethylene carbonate/dimethyl carbonate/diethyl carbonate (Ferro, Inc.) mixed 1:1:1 by volume was used as the electrolyte. This electrolyte is typical for lithium-ion cells. A Setella polyethylene separator, with a thickness of 20 μm, was used.

4.3 Results

Lithium titanate spinel powder modified by ALD was characterized with in situ and ex situ methods. Analysis with in situ DRIFT spectroscopy was performed to monitor changes to the LTS powder surface after each of the precursors reacted with the substrate and to verify the surface reaction. Modification of the LTS powder also was carried out in a home-built, automated ALD reactor so that a large number of ALD cycles could be deposited.

4.3.1 ALD with in situ DRIFT characterization

Lithium titanate spinel powder was examined with DRIFT spectroscopy to characterize surface groups and confirm the availability of attachment sites for TiCl₄, the first half-reaction in the formation of TiN by ALD. Spectra were collected before and after each surface exposure to TiCl₄. The availability of surface hydroxyl groups is a

crucial component in functionalizing surfaces and forming thin films. Past work has demonstrated that these hydroxyls are preferred binding sites for metal thin film precursors like TiCl_4 [26, 54, 88, 140]. At room temperature, the DRIFT spectrum (Figure 4.2a) revealed a small shoulder at 3690 cm^{-1} and a broad peak that stretched from approximately 3410 to 3220 cm^{-1} . These bands were due to isolated metal hydroxyls (M-OH), molecularly adsorbed water, and hydrogen-bonded hydroxyl groups, respectively. A group of absorption bands were observed between 1700 and 1300 cm^{-1} : a peak at 1640 cm^{-1} and a doublet at 1510 and 1460 cm^{-1} with a shoulder at 1350 cm^{-1} . The band at 1640 cm^{-1} represents surface-adsorbed water, while the other peaks were assigned to carbonate impurities, as Li_2O readily absorbs CO_2 [159]. The presence of surface hydroxyls on LTS powder indicated that reaction sites were available for TiCl_4 .

Figure 4.2b is a difference spectrum collected after the addition to the surface and evacuation of TiCl_4 vapor. The spectrum of LTS at reaction temperature is used as the reference. Positive bands represent an addition to the surface, while negative bands indicate that a surface group has been removed. Due to the limitations of the environmental chamber, the in situ reaction was performed at $425\text{ }^\circ\text{C}$. The negative band at 3675 cm^{-1} indicates that M-OH groups have shifted downfield because of higher temperatures and have been removed from the surface. Negative bands between 1640 and 1300 cm^{-1} also show that additional carbonate species have been removed as well. The positive band at 940 cm^{-1} represents a Ti-O bond to the surface. Hence, the initial step of reaction of TiCl_4 with the LTS was confirmed.

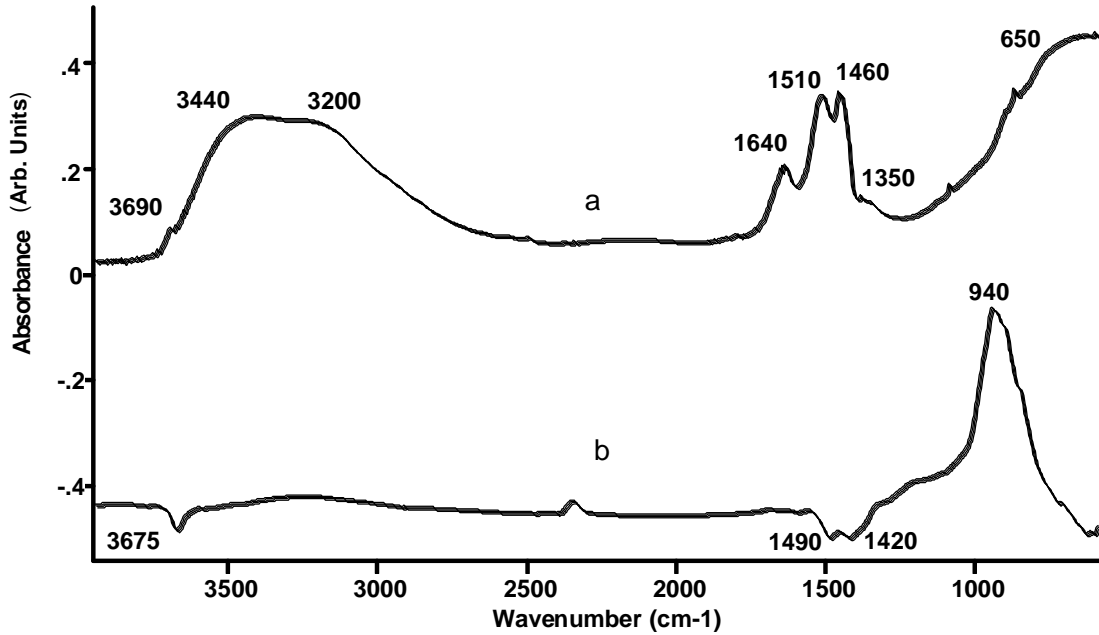


Figure 4.2 DRIFT spectrum of (a) LTS at room temperature in air and (b) DRIFT difference spectrum of LTS at 425 °C under vacuum after an addition of TiCl₄. The reference is LTS under vacuum at 425 °C.

4.3.2 ALD with ex situ characterization

In addition to the in situ DRIFT studies, TiN was synthesized on LTS powder for further characterization and evaluation as an anode for lithium or lithium-ion cells.

4.3.2.1 Total nitrogen content

The thickness of the TiN layer is difficult to determine directly because its surface is known to oxidize in air [4, 7, 23, 176-178]. We used the average content of nitrogen in the coated material as the measure of the deposited amount of nitride. A nitrogen content of 0.061% (by weight) was measured for the thin film synthesized by 200 ALD cycles at 500 °C.

4.3.2.2 TEM analysis

Atomic layer deposition has been shown to coat powders uniformly by other groups [48], and we used transmission electron microscopy (TEM) to verify the uniformity of our coatings. LTS powder, modified with 200 ALD cycles of TiN at 500°C, was examined with a TEM. Micrographs of unmodified and modified LTS particles are presented in Figure 4.3. The unmodified particles (Figure 4.3a) appear flat and plate-like. The micrographs of the modified particles show similarly-shaped flat, plate-like structures. However, there is a discernible halo of a different density than the rest of the particles (Figure 4.3b). While the coating appears uniform, it is difficult to discern whether the specimen shown in Figure 4.3b consists of several individual particles or an agglomeration formed by sintering. Determination of the film thickness by visual inspection of the TEM micrographs gives an average thickness of approximately 58 Å, or approximately 0.3 Å cycle⁻¹. Assuming the film is stoichiometric TiN, this is slightly greater than the growth per cycle (0.2 Å) for TiN on SiO₂ observed by Ritala et al. [8, 24] and similar to the growth per cycle (0.28 Å) for TiN on SiO₂ seen by Satta et al. [56]. The growth per cycle indicates that a non-continuous film is deposited during each cycle.

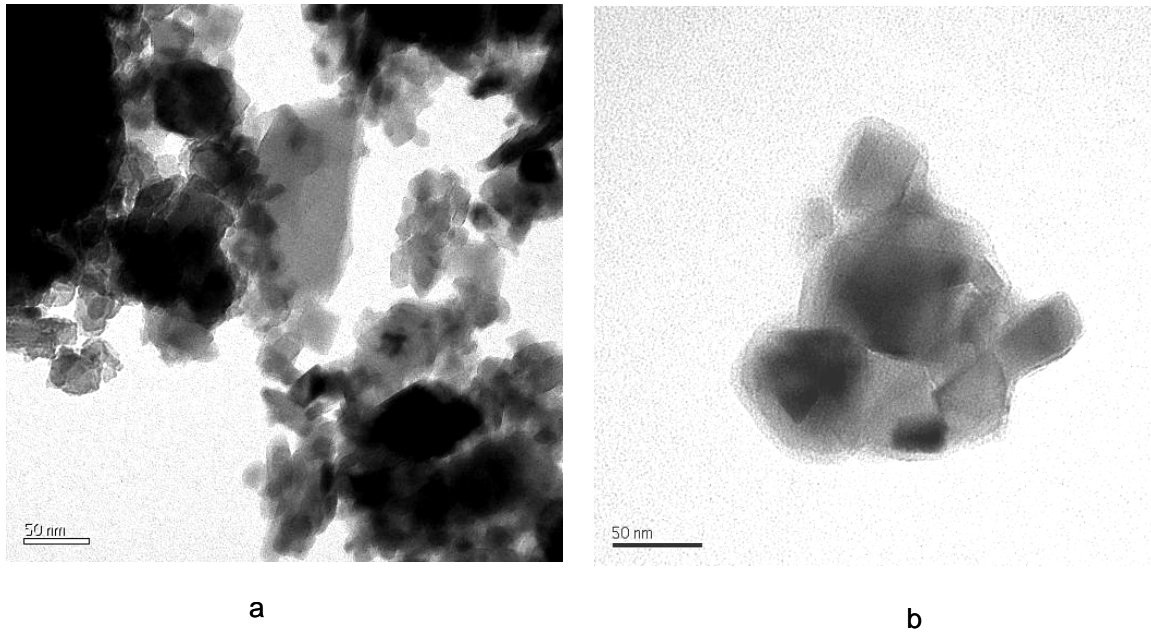


Figure 4.3 TEM micrographs of (a) unmodified LTS and (b) LTS modified with 200 cycles of TiN ALD at 500 °C.

4.3.3 Coin Cell Tests

Figures 4.4 and 4.5 represent the voltage profile and capacity, respectively, of the coin cells during cycling. A cell with LTS modified by TiN ALD was compared to a cell with unmodified LTS. The cells were cycled within 2.2 V and 1.4 V at 25 °C. The rate of the first cycle was $C/20$ (C is the expected capacity in mAh), followed by two cycles at $C/10$, three at $C/5$, and several more $C/10$ cycles. It is assumed that the product of the LTS reduction, the $\text{Li}_7\text{Ti}_5\text{O}_{12}$, appears as a new phase mechanically mixed with the original species [170]. Since the molar Gibbs energy of a two-phase system does not depend on the composition, the voltage of the $\text{Li}/\text{Li}_4\text{Ti}_5\text{O}_{12}$ cell should not vary noticeably during lithiation and de-lithiation at constant current, as has been observed in the literature [149, 150, 170, 171].

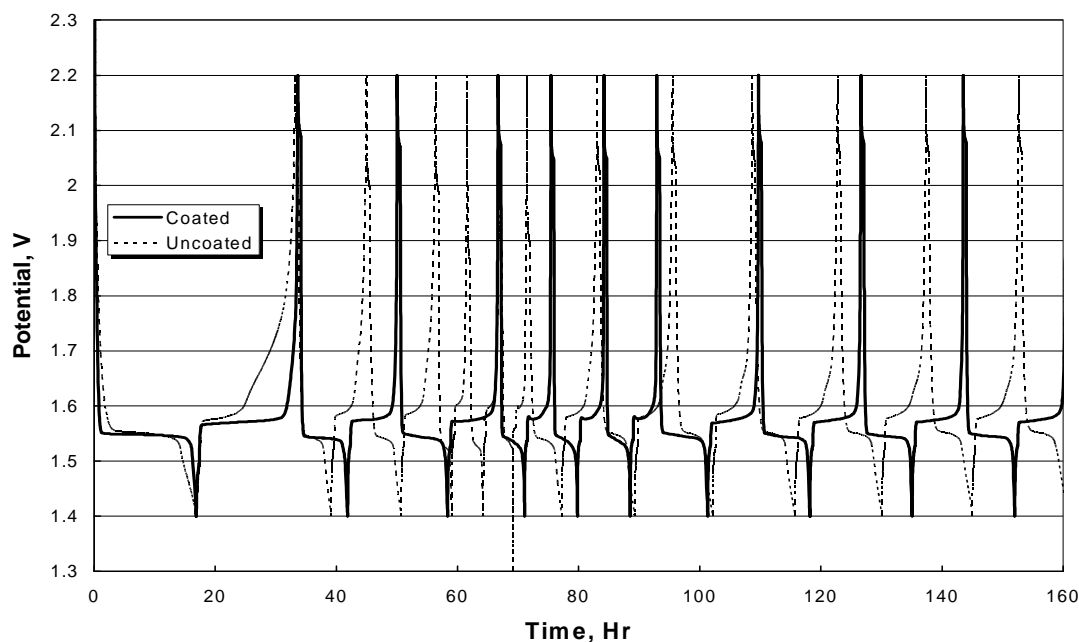


Figure 4.4 Cyclic voltammogram of unmodified LTS and LTS modified with 200 cycles of TiN ALD at 500 °C tested as coin-type cells in a lithium ion battery.

In Figure 4.4, the shape of the potential-time curve of the cell with unmodified LTS differs from that of the modified LTS. Whereas the discharging branch of the original material reveals a distinctive plateau corresponding to the formation of a two-phase product, the charging branch deviates from the plateau level when the electrode is approximately half-charged. The coulombic efficiency is about 80% of the theoretical maximum during the first cycle, and the electrode capacity decreases significantly during the first several cycles. We assume that the potential increase is due to the crystallite conductance decrease along with delithiation and weakening of the electrical contact between the particles. The same effect can be observed in [175]. The slow response of the material is attributed by the authors to poor interparticle electrical contact.

The substitution of the unmodified LTS electrode for LTS coated with TiN via ALD visibly improves the cell performance. Both charging and discharging branches are comprised of relatively long, flat plateaus appearing after a short transient period and followed by abrupt process termination due to a sharp increase (when charging) or decrease (when discharging) of the cell voltage.

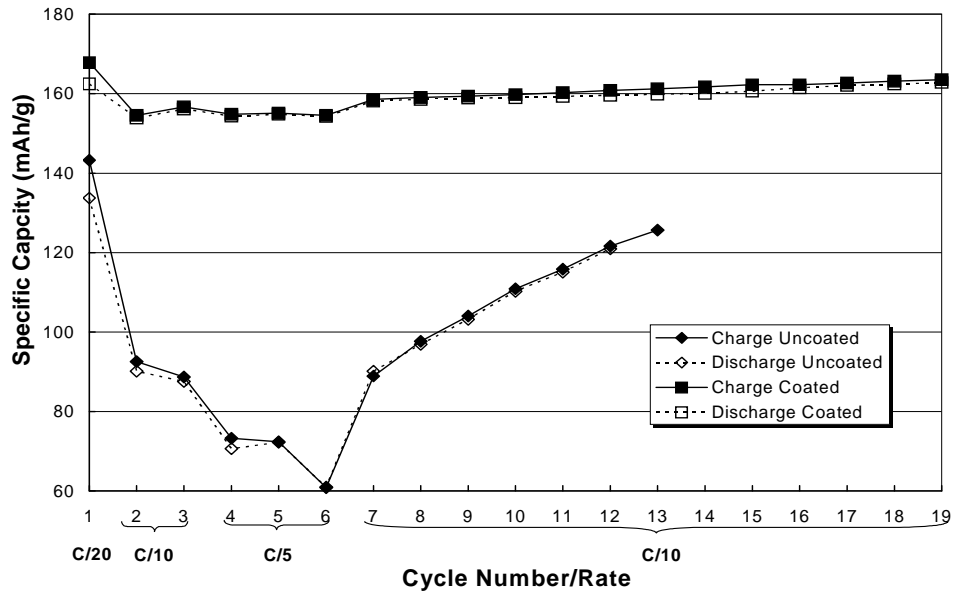


Figure 4.5 Measurement of specific capacity of unmodified LTS and LTS modified with 200 cycles of TiN ALD at 500 °C tested as coin-type cells in a lithium ion battery versus the number of charge/discharge cycles. The discharge rate is given below the cycle number on the x-axis.

The change in specific capacity of the unmodified and modified electrodes brought about by continued cycling and varying charge rates is shown in Figure 4.5. The specific charge capacity of the modified electrode nearly maintains its theoretical value over numerous charge/discharge cycles and at different charge rates. Typically, a faster charge rate will decrease charge capacity. However, this is witnessed to only a small extent with the TiN-coated LTS powder coin cell.

The unmodified LTS powder coin cell shows a drastic decrease in specific capacity with increasing charge rate. Ultimately, the cell reaches its lowest specific capacity after the third charge at $C/5$ (sixth overall). Upon decreasing the rate to $C/10$ during the seventh and eighth charge cycles, the specific capacity increases to values similar to those obtained during previous charges at $C/10$. At the ninth and tenth cycles and beyond, an increase in specific capacity occurs. Perhaps this can be attributed to a deformation of the LTS lattice, but otherwise this phenomenon is not readily explained.

4.4 Discussion

The capacity results indicate the TiN-coated LTS coin cell did not undergo typical capacity fade at higher currents and delivered a constant charge throughout the charging sequence. At higher currents, reduction of the anode occurs only on the outer surface that is coated with an insoluble compound that prevents access to reaction sites in the inner portions of the electrode [108].

It is not clear whether the capacity depends on the rate or if it varies due to macrostructural changes within the electrode upon cycling. Since neither the electrode component composition nor the conductive diluent selection has been optimized, the efficiency improvement in the unmodified electrode particles may be the result of improved interparticle contact while the modified particles have better electrical contact throughout cycling.

Possibilities for the improved performance of the modified LTS powder over the unmodified powder were identified. The first is the change in particle morphology that occurs at high temperature. Removal of electrically non-conducting carbonate species

may also be a contributing factor. The second reason for improved performance was the presence of the TiN thin film. Since the conductance of the LTS is low by nature [149, 150], the deposition of a conducting component on its surface may have improved electrical contact. Side reactions with the electrolyte and resistance to fouling by the electrolyte solvent because of the passivating layer may have been averted while preserving the bulk material for Li-ion intercalation.

4.5 Conclusion

Lithium titanate spinel powder was determined to have surface hydroxyl groups suitable for reaction with TiCl_4 to initiate the formation of TiN by ALD. Total nitrogen content testing identified nitrogen as a component of the ALD-modified LTS powder. A thin film was observed surrounding the LTS particles observed in a micrograph collected by TEM.

Coin cell testing indicated that the deposition of a TiN thin film on LTS enhanced LTS electrode performance, possibly through the removal of surface carbonate species and prevention of anode decomposition by the electrolyte. ALD-modified LTS powder produced a constant voltage and sharp process termination upon potential change while either charging or discharging. Cycling tests indicated that the ALD-modified LTS powder maintained a constant charge capacity, close to its theoretical capacity, at various cycling rates. Optimization of the composition of the electrode and the selection of an appropriate binder may enhance performance even further.

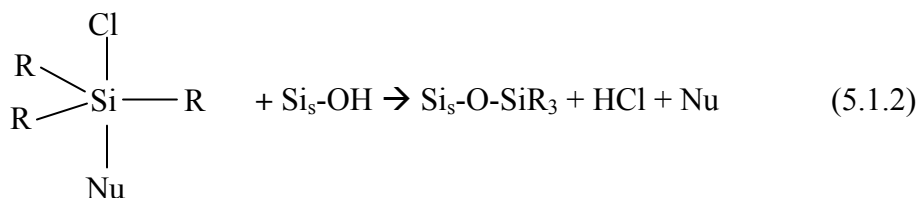
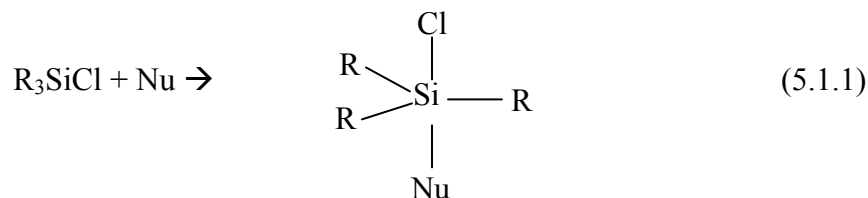
5 ATTACHMENT OF ORGANOCHLOROSILANES BY CATALYSIS OF NON-VOLATILE BASES IN SUPERCRITICAL CARBON DIOXIDE

5.1 Introduction

Beyond modifying silica with metal nitride films through vapor deposition, the attachment of organosilanes to silica is another way to alter the properties of a silica surface [144]. Functionalization of silica with organosilanes occurs through one of two methods. The first method requires that a volatile organosilane be used at temperatures greater than 300 °C for vapor-phase attachment to the substrate because the formation of $\text{Si}_s\text{-O-Si}$ (where the subscript “s” denotes a surface species) bonds between surface silanols and organopolychlorosilanes cannot occur at room temperature [132, 144]. Without trace amounts of adsorbed water at the solid/gas interface necessary for covalent bond formation, the organochlorosilane will physisorb onto a dehydrated silica surface without undergoing a condensation or polymerization reaction and form a weak bond through van der Waals forces. The second approach is to perform the reaction in solution. However, the organochlorosilane, after being hydrolyzed by trace amounts of water in the solution, polymerizes and adsorbs on the surface, again, only forming a weak bond through van der Waals forces [144].

The use of a nitrogen-containing base to catalyze the attachment of a silane to surface SiOH groups at room temperature has been used to solve this problem [144, 179-182]. Tripp and Hair present two different mechanisms for organochlorosilane attachment, both involving the formation of a silicon pentacoordinate intermediate [144].

The first mechanism results from the attachment of the catalyst to the organochlorosilane (Scheme 5.1.1). This leads to the lengthening of the SiCl bond and greater vulnerability to nucleophilic bonding with the oxygen atom in the Si_sOH (Scheme 5.1.2).



Another mechanism for base-catalyzed attachment of an organochlorosilane to Si_sOH groups is through the formation of a pentacoordinate intermediate with the Si_sOH group and the base[144]. In this mechanism, the direct bond between the nucleophilic base and the Si_sOH makes the Si-O bond more nucleophilic and able to bond with the approaching Si atom in the organochlorosilane (Figure 5.1).

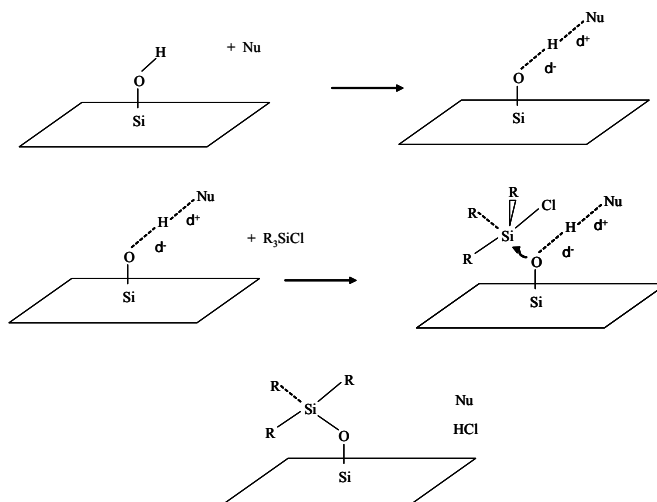


Figure 5.1 Illustration of the base-catalyzed attachment of an organochlorosilane to a surface SiOH group through formation of a pentacoordinate intermediate with the silanol.

A drawback of base-catalyzed reactions is the polymerization of the organochlorosilane caused by the presence of even the smallest amount of water. To prevent the undesired polymerization from happening, the base and organochlorosilane are added in separate steps. For this attachment to successfully occur without polymerization, the second mechanism is the more reasonable one[144]. Indeed, this mechanism is supported by Klaus and George as well[179].

An interesting application of this technique is the base-catalyzed ALD (bcALD) of SiO₂, with pyridine, in mesoporous membranes[180, 181]. Prior to bcALD, pore size modification was first conducted with chemical vapor deposition (CVD)[183] and traditional ALD methods[184]. Catalyzed ALD allows for lower reaction temperatures and reduced reactant exposure times [180, 181]. Furthermore, since the catalyst was larger than either of the ALD precursors (SiCl₄ and H₂O), deposition of SiO₂ into the pores was controlled by size exclusion. Once pyridine (the largest of the precursors) was no longer able to fit in the pores, the reaction ceased. The result was a material with a uniform pore diameter[180, 181].

Nitrogen-containing bases also have been used to catalyze the deposition of SiO₂ in sc-CO₂. In unpublished work, McCool and Tripp used triethylamine (TEA) to catalyze the ALD reaction of SiCl₄ and H₂O on fumed SiO₂[182]. Using ALD to synthesize thin films on powders is a challenge because it is difficult for the vapor to access the entire powder surface and its pores. Fluidization of the material has been noted in the past [135, 136]. Process scale-up to industry requirements also presents a challenge for ALD. Because of the exceptional diffusivity, low viscosity[128], and lack of surface tension[124, 127] in sc-CO₂, better surface coverage of the substrate may be attained.

Several industries already employ sc-CO₂ processes indicating that it can be applied on a large scale. Furthermore, since sc-CO₂ can functionalize the previously-inaccessible interparticle silanols (silanols hidden from the surface at the interface of two particles) [130], a more continuous film is obtainable. When using nitrogen-containing bases in sc-CO₂, tertiary bases must be used to avoid formation of carbamates [156].

The ability of sc-CO₂ to dissolve reactants negates the requirement that reactants have an appreciable vapor pressure and thus allows for the use of non-volatile precursors[127]. In this chapter, sc-CO₂ is used to solubilize a relatively large base (molecular diameter of approximately 11 Å) to catalyze the attachment of organochlorosilanes to a microporous substrate. The proof of principle is first demonstrated in solution phase on fumed silica.

5.2 Experimental

5.2.1 Solution-phase reaction

A ratio of 1 mg Aerosil A300 fumed silica (DeGussa) to 1 mL of toluene was stirred for one hour at room temperature. S-triazolo [4,3-a] quinoline (or sTQ, from Aldrich, Figure 5.2) was added to make a 0.001 M base solution and stirred for three hours. A Whatman drainage jar and funnel with a Millipore polymer membrane (RAWP 025 00, RA 1.2 µm, 25 mm) were used to filter and dry the solution over night. The modified silica which collected on the membrane was then removed and ground with a mortar and pestle. An IR spectrum was collected with an ABB FTLA FTIR spectrometer and an MCT detector on a CsI disk at a resolution of 4 cm⁻¹.

The remainder of the modified silica was added to toluene at the same ratio as above and stirred. Approximately 58 μL of octadecyldimethylchlorosilane (ODCS, 70% in toluene) from Gelest was added to create a 0.001 M solution and stirred for 30 minutes. The same filtering procedure was used to recover the silica from solution, and an IR spectrum of the modified silica was collected. The same procedure was carried out for two other bases: tributylamine (99%) and tri-*n*-octylamine (98%). Both were acquired from Acros Organics and used as received. Also, approximately 0.001 M ODCS was added to fumed silica in toluene without first adding the sTQ base to generate a basis for comparison of the effect of the base.

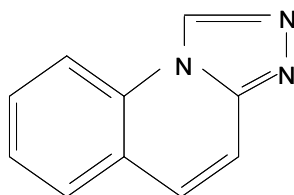


Figure 5.2 Molecular structure of s-triazolo [4,3-a] quinoline.

5.2.2 Supercritical reactor system

The supercritical CO_2 reactor consists of a cylinder of liquid CO_2 pumped from a siphon tank through a modified HPLC pump capable of pressurizing the CO_2 into the supercritical phase. The sc- CO_2 flow may then be directed by two three-way valves (High Pressure Equipment Co.) to either of two 10-mL precursor chambers (TharTech, Inc.), or through a bypass line (see Figure 5.3). A second set of three-way valves allows the sc- CO_2 to flow into a 100-mL reaction chamber (TharTech Inc.) or through another bypass line. The system is pressurized by a TharTech backpressure regulator downstream from the reaction chamber. Upon exiting the back pressure regulator, the sc- CO_2 is vented to atmosphere.

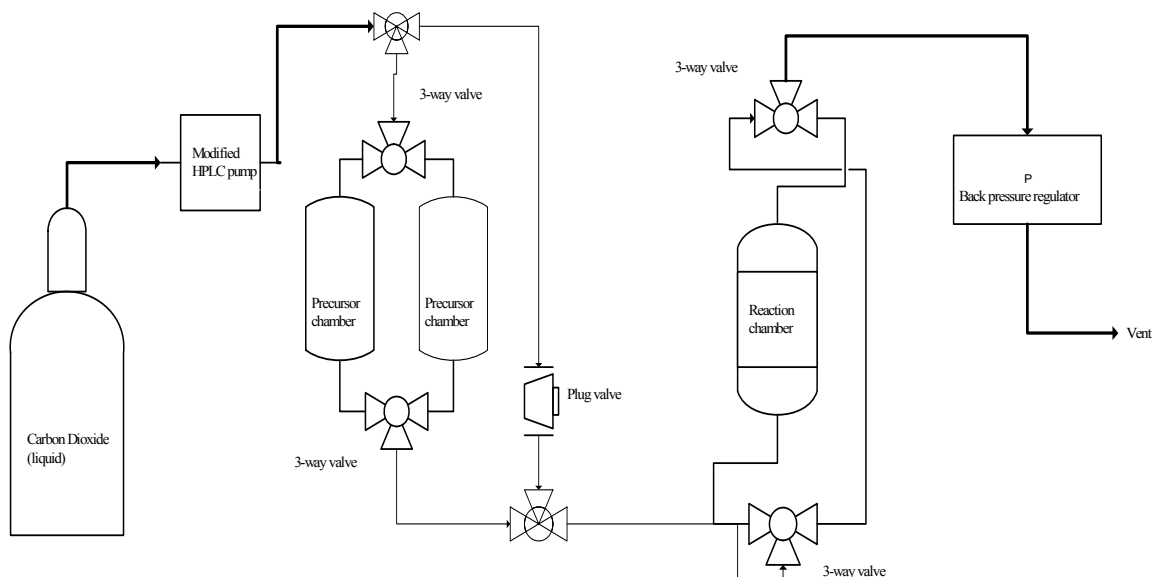


Figure 5.3 Schematic representation of the supercritical carbon dioxide reactor.

5.2.3 Supercritical CO₂ reaction

To attach the non volatile sTQ to A300 fumed silica in sc-CO₂, a solution of 0.01 M sTQ in toluene was added to a 5-mL glass vial, with the tapered top portion of the bottle cut off to increase interaction with the sc-CO₂, and loaded into the precursor chamber. A silicon wafer coated with mesoporous silica, described in detail by Ninness et al., [185], was cleaned, dried and loaded into the reaction chamber. The reaction chamber was pressurized to 170 bar with sc-CO₂. The precursor chamber was pressurized to 220 bar with sc-CO₂ and the dissolved sTQ for two hours. The external temperatures of both chambers were set to 70 °C. The 50-bar pressure differential acted as the driving force to transport the precursor between the precursor and reaction chambers. The pressure-driven precursor transfer occurred for 30 minutes followed by flushing sc-CO₂ through the precursor and reaction chambers at 170 bar for thirty minutes. At the end of this

exposure, the reaction chamber was flushed with sc-CO₂ at 170 bar to purge reaction byproducts. An IR silica spectrum was collected. This same procedure was also carried out using 68 mg of dry sTQ in the 5-mL glass vial instead of a 0.01 M sTQ solution.

5.3 Results and Discussion

5.3.1 Solution-phase reaction

5.3.1.1 Catalysis with s-Triazolo [4,3-a] Quinoline

The spectrum of A300 before and after reaction with sTQ in toluene is shown in Figure 5.4. In Figure 5.4a, the most prominent feature is the isolated hydroxyl peak at 3743 cm⁻¹. After the reaction of the base with the fumed silica, that same peak in Figure 5.4b, has drastically decreased in intensity. By calculating the ratio of the isolated hydroxyl peak area at 3743 cm⁻¹ and normalizing the peak area of the bulk Si-O-Si mode before and after reaction, it was determined that approximately 80% of the isolated hydroxyl groups hydrogen bonded. Additionally, a broad band centered at 3245 cm⁻¹ appears after the reaction (Figure 5.4b). This can be attributed to the formation of hydrogen bonding of surface hydroxyls caused by the perturbation of mixing the solution. This broad band obscures the aromatic stretching that would be observed in this region.

Bands are visible in the 1300-1700 cm⁻¹ region attributed to the addition of sTQ in Figure 5.4b. This region is expanded in Figure 5.5a. For comparison, the spectrum of sTQ is shown in Figure 5.5b (after baseline correction and smoothing). This region of the IR spectrum represents C=C, C-N and C=N bonding. The C=C and C=N stretching regions often overlap [131] and are represented by the peaks at 1619 and 1485 cm⁻¹ in Figure 5.5a and 1614 and 1480 cm⁻¹ in Figure 5.5b. A band at 1350 cm⁻¹ can be assigned to C-N stretching in Figure 5.5a and 1339 cm⁻¹ in Figure 5.5b. Other bands can be

assigned to various aromatic stretching modes. Examination of the spectra reveal a strong correspondence in the location of the peaks with the exception that the peaks are shifted upfield between 2 to 13 cm^{-1} in the spectrum of the sTQ attached to the A300 compared with that of sTQ.

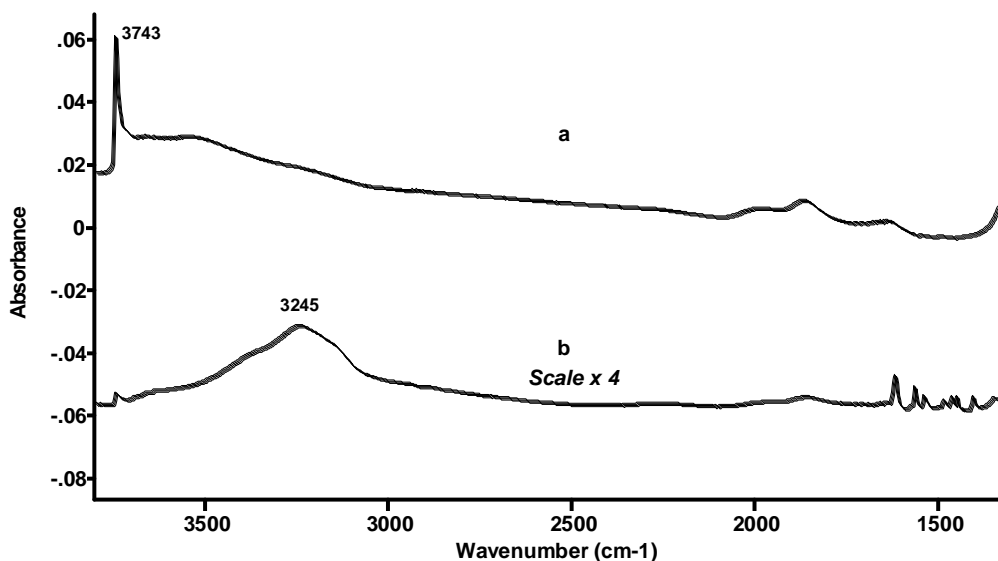


Figure 5.4 FTIR spectra of (a) unmodified A300 fumed silica and (b) fumed silica after modification with s-triazolo [4,3-a] quinoline (sTQ) in toluene at room temperature.

After collecting the IR spectrum of sTQ on fumed silica, the modified silica was stirred in toluene to catalyze the reaction with ODCS. After addition of ODCS and removal of the toluene solvent by suction filtration, an IR spectrum was collected (Figure 5.6). The intense peak at 3245 cm^{-1} attributed to hydrogen-bonded hydroxyls and first observed in Figure 5.6a is still present in Figure 5.6b. Also present are the hydrocarbon stretching modes. The weak band at 2960 cm^{-1} represents asymmetric stretching of the

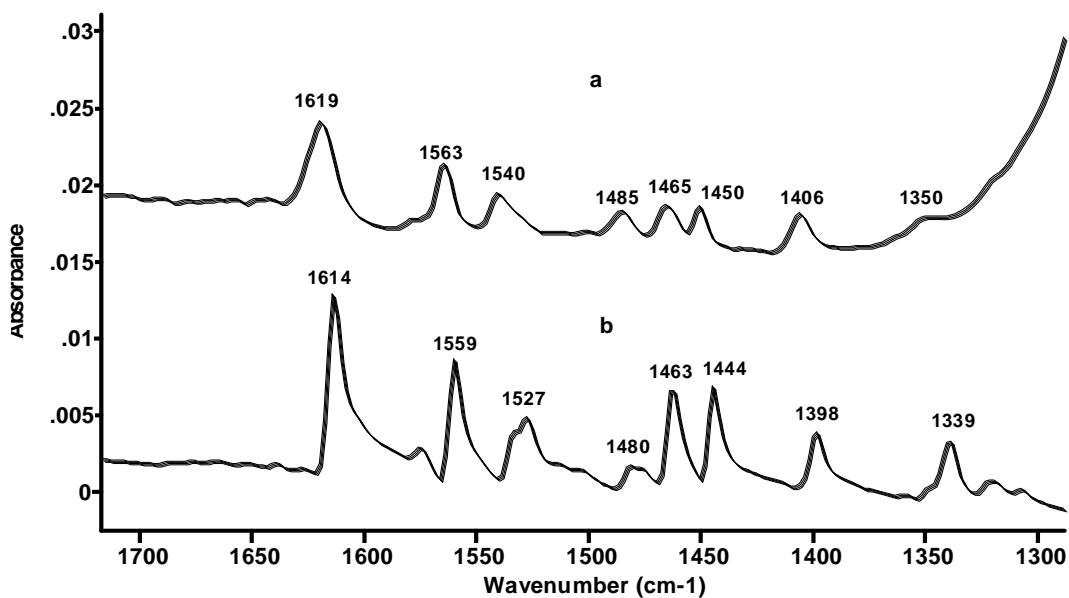


Figure 5.5 FTIR spectra of the 1300-1700 cm^{-1} region of (a) Figure 5.4b and (b) pure sTQ.

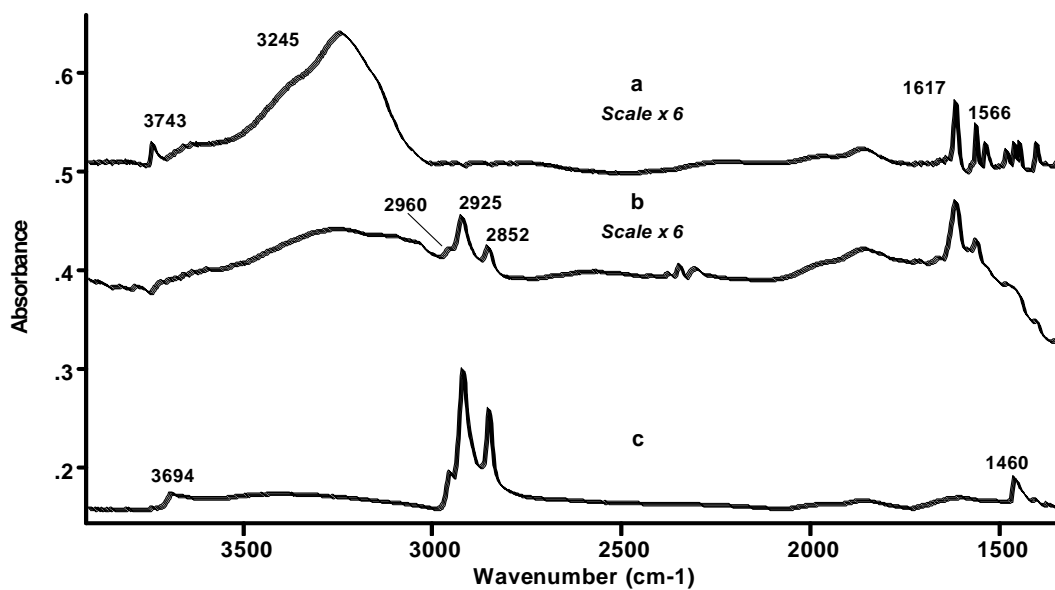


Figure 5.6 FTIR spectra of fumed silica with (a) 0.001 M sTQ, (b) sTQ-catalyzed reaction with 0.001 M ODCS, and (c) 0.001 M ODCS reacted directly with silica without a catalyst in toluene.

CH₃ group while the peaks at 2925 and 2852 cm⁻¹ are assignable to CH₂ asymmetric and symmetric stretching, respectively. The symmetric CH₃ stretch, usually located around 2872 cm⁻¹ is obscured by the more intense band at 2925 cm⁻¹.

Examining the spectral region between 1500 and 1700 cm⁻¹ in Figure 5.6b shows that bands attributed to aromatic C=C and C=N stretching are still present. The presence of these bands indicates that base catalysis of the fumed silica with ODCS was not complete. Rogue water in the solution may have caused the organochlorosilane to hydrolyze and merely physisorb onto the surface as well.

To determine if ODCS can chemisorb onto the fumed silica surface without the prior addition of a base catalyst, a 0.001M solution of ODCS in toluene with silica was prepared. The resulting IR spectrum is shown in Figure 5.6c. Most notable in Figure 5.6c is the shift of the isolated SiOH peak from 3743 to 3694 cm⁻¹. This shift is caused by the van der Waals interactions between toluene and isolated SiOH groups. Furthermore, the appearance of this peak indicates that the ODCS did not react directly with the surface, but physisorbed instead in accordance with the findings of past similar research [186, 187]. The alkyl peaks between 2850 and 3000 cm⁻¹ are more intense than those in the catalyzed reaction in Figure 5.6b because the presence of sTQ partially sterically hindered adsorption of ODCS onto the silica surface. Finally, the 1460 cm⁻¹ peak in Figure 5.6c is assigned to CH₂ stretching.

5.3.1.2 Catalysis with Tributylamine

Tributylamine (TBA) also was examined as a base catalyst. McCool and Tripp have studied triethylamine (TEA) as a base catalyst soluble in $sc\text{-CO}_2$ [182]. Because both bases have a similar structure, the performance of TBA would be expected to be similar to that of TEA. The principal difference is that TBA has a lower vapor pressure. Addition, filtration, and drying of a 0.001 M solution of TBA to fumed silica in toluene resulted in the IR spectrum seen in Figure 5.7a. The peaks at 2966 cm^{-1} and 2877 cm^{-1} can be assigned to CH_3 asymmetric and symmetric stretching, respectively. The alkyl peak at 2935 cm^{-1} is attributed to CH_2 stretching. Downfield, the peaks at 1468 and 1377 cm^{-1} are assigned to CH_2 and CH_3 bending, respectively. As stated earlier, the broad peaks between 1600 and 2000 cm^{-1} are SiO_2 overtone and combination modes.

Peak assignments for ODCS and TBA are quite similar as can be seen in Figure 5.7b. However, the CH_2 asymmetric and symmetric stretches (2935 and 2851 cm^{-1}) are considerably more intense because ODCS contains more CH_2 groups than TBA. Alkyl bending and C-N modes are found in the same region of the IR spectrum, so it is difficult to determine the effectiveness of the catalytic reaction. One piece of evidence to determine if the reaction indeed took place is the appearance of a band around 1250 cm^{-1} attributed to Si- CH_3 stretching. Unfortunately, this band is obscured by the intense SiOSi bulk mode around 1100 cm^{-1} . However, the bands at 2725 , 2634 , and 2528 cm^{-1} are likely due to TBA:HCl salt formation arising from the reaction of the base with HCl byproduct from ODCS thus providing evidence of chemisorption on the base-terminated silica surface.

5.3.1.3 Catalysis with Tri-n-octylamine

Finally, tri-n-octylamine (TOA) was considered as a base catalyst for the attachment of ODCS to fumed silica. Like TBA, it is structurally similar to TEA only varying in the number of $-\text{CH}_2$ groups. Because TOA has a heavier molecular weight than TEA and TBA, it is also less volatile. The IR spectrum collected after the addition, filtration and drying of fumed silica mixed with a 0.001 M solution of TOA is shown in Figure 5.8a. The base did not react with all isolated silanols based on the appearance of the peaks at 3739 cm^{-1} and 3690 cm^{-1} , attributed to isolated silanols and silanols perturbed by toluene, respectively. The broad band at 3245 cm^{-1} is assigned to hydrogen-bonded hydroxyl groups as seen in previous spectra in this section. Asymmetric CH_3 stretching is observed by the peak at 2957 cm^{-1} . The complimentary symmetric stretch, usually observed at 2875 cm^{-1} is hidden by the peak at 2855 cm^{-1} . Asymmetric and symmetric CH_2 peaks appear at 2925 and 2855 cm^{-1} , respectively. A CH_2 bending mode is visible at 1465 cm^{-1} . The higher ratio of CH_2 groups to CH_3 groups in TOA compared to TBA (Figure 5.7a) leads to relatively more intense CH_2 stretching and bending peaks. Comparing the ratio of the peak area of the isolated silanols with SiOSi bulk modes of the catalyzed reaction with those of unmodified silica shows that approximately half of the silanols formed a covalent bond with the TOA.

Addition of 0.001 M ODCS to the catalyzed fumed silica was carried out in the same manner as described for the other bases. An IR spectrum was collected (Figure 5.8b). The isolated silanols at 3739 cm^{-1} and the toluene-perturbed silanols are no longer present as seen in Figure 5.8a. Instead, an intense, broad band is now visible at 3245 cm^{-1}

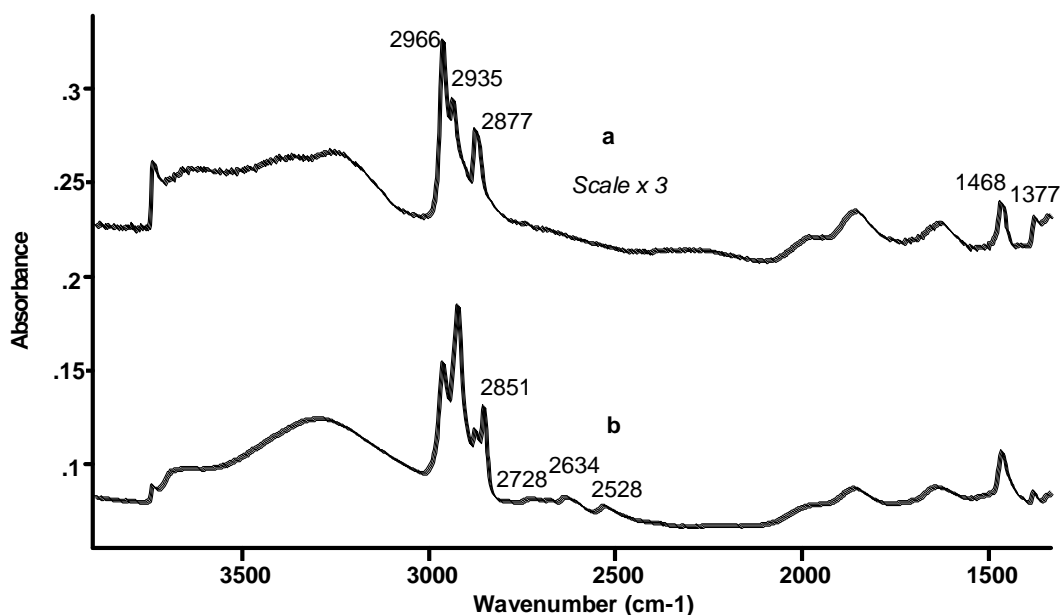


Figure 5.7 FTIR spectrum of (a) fumed silica reacted with 0.001 M TBA solution in toluene and (b) TBA catalyzed reaction of 0.001 M ODCS solution in toluene on fumed silica.

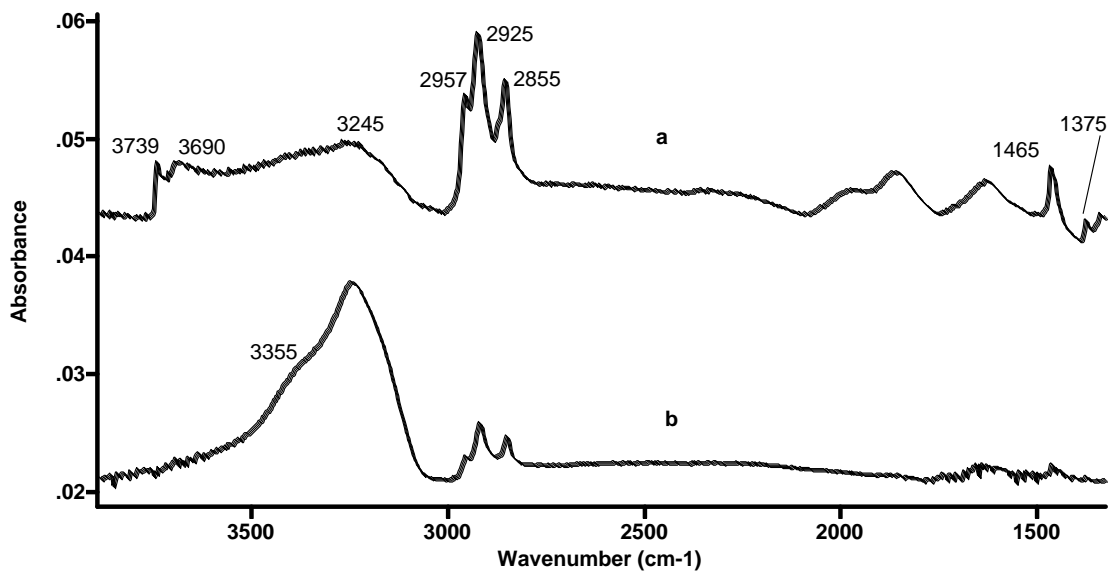


Figure 5.8 FTIR spectrum of (a) fumed silica after reaction with 0.001 M TOA solution and (b) TOA-catalyzed reaction with fumed silica and 0.001 M ODCS solution.

with a shoulder at 3355 cm^{-1} . In earlier figures, the band in this area was attributed to hydrogen-bonded hydroxyl groups, but the cause of this shift, resulting in the disappearance of all isolated silanols, is unexplained. Since ODCS contains only one chlorine atom, it could not have polymerized in solution. If the ODCS had physisorbed on the fumed silica and catalyst, isolated silanols should be present in the spectrum around 3740 cm^{-1} . Furthermore, the CH_3 and CH_2 stretching modes are ambiguous because of the large number of CH_2 groups relative to CH_3 in both the base catalyst and the organochlorosilane. Determination whether the ODCS chemisorbed on to the silica through a catalyzed nucleophilic reaction is difficult. As mentioned with the TBA catalyst, the SiCH_3 stretch is obscured by the broad SiOSi bulk modes. The bulky nature of the TOA molecule may cause steric hindrances leading to incomplete surface reactions with the silica and eventually to ineffective catalysis of the reaction with fumed silica and ODCS.

5.3.2 Supercritical CO_2 reaction

Studying the spectra collected from the attachment of sTQ to the silica-coated silicon wafer revealed no apparent reaction occurred between the base and the substrate. None of the characteristic aromatic hydrocarbon stretching bands above 3000 cm^{-1} were seen, nor were $\text{C}=\text{C}$, $\text{C}=\text{N}$ and $\text{C}-\text{N}$ stretching modes visible between 1300 and 1700 cm^{-1} . Furthermore, there was no apparent change to the isolated SiOH peak intensity at 3738 cm^{-1} indicating no covalent bonding of the base to the substrate. After the 0.01 M solution of sTQ in toluene was used as the precursor in the reaction, sTQ particles were seen on the bottom of the 5-mL glass vial. Prior to the reaction, the base was completely dissolved in the toluene. Upon completion of the reaction with the dry base,

approximately 1.4 mg was unaccounted for, though a small amount of solid matter was found in the bottom of the precursor chamber. Again, the IR spectrum showed no indication that the base chemisorbed onto the Si wafer. This finding leads to the assertion that the base, though soluble in toluene, is not soluble in sc-CO₂.

5.3.3 Future work

The results detailed above indicate that the attachment of sTQ to fumed silica in sc-CO₂ was not successful under the prescribed conditions. However, this does not mean that the reaction itself is infeasible. Fluorinated precursors have received a considerable amount of use in chemical fluid deposition[125-127] because of their solubility in sc-CO₂. Therefore, the fluorination of aromatic CH groups may enhance the solubility of sTQ. Fluorination of aromatic rings can occur through electrophilic aromatic substitution with molecular fluorine[188].

Sarbu et al., report on the use of poly(ether-carbonate) copolymers as surfactants and building blocks of CO₂-soluble amphiphiles in place of fluorinated materials. The resulting copolymer has a greater solubility than either of the individual monomers. The copolymer consists of two polymers. Propylene oxide (M₁) monomers add flexibility to the copolymer and have a low cohesive energy density to minimize solute-solute interactions. A carbonyl group (M₂), in the form of CO₂, acts as a Lewis base and forms carbonates which aid in dissolution of the copolymer in sc-CO₂. [189].

Besides making adjustments to the chemistry of this reaction, some changes to the experimental equipment may improve the effectiveness of the procedure. Upon pressurizing the precursor chamber, there is no further mixing of the precursor with the sc-CO₂. Dissolution of the precursor may be enhanced by additional mixing or

recirculation of the solvent. Unfortunately, this would require that an additional pump be added to the system to drive the recirculation. Alternatively, an additional recirculation loop could be added to the precursor chamber with a valve added to bleed a slight amount of solvent out to create a pressure drop and continue sc-CO₂ through the chamber. Finally, Thar Technologies, the manufacturer of the chambers, produces reaction chambers that are equipped with magnetic stirrers. This may be the simplest approach to improved mixing in the precursor chamber.

5.4 Conclusions

The IR spectra collected from the solution-phase reactions indicate that sTQ and TBA can catalyze the reaction with fumed silica and ODCS. Aromatic ring signatures and/or alkane bending modes, however, were still present on the silica surface after addition of the ODCS meaning that not all available, catalyzed surface sites underwent reaction. Use of TOA as a catalyst in the solution resulted in a significant shift or perturbation of hydroxyl groups and inconclusive spectral evidence of whether or not catalyzed attachment of ODCS occurred.

When sTQ was used in a reaction with sc-CO₂ as a solvent, no attachment of the base to the silica surface was evident. The sTQ, neither dissolved in toluene nor as a neat powder, was transported to the silica. Possible reasons are that the base is insoluble in sc-CO₂ and that the base may not be adequately mixed with the sc-CO₂ solvent. Several suggestions to address these issues have been provided.

6 CONCLUSIONS

The research conducted for this thesis describes the characterization and modification of semi-metal oxide and metal oxide powders by atomic layer deposition (ALD) and base-catalyzed reactions. A performance evaluation of the atomic layer deposition-coated metal-oxide powders was carried out and the results analyzed.

The first component of this research was to use ALD to deposit titanium nitride on a powder and to elucidate the growth mechanism for the initial stages of titanium nitride atomic layer deposition on silica powder using in situ FTIR techniques. There is a transition between a silica and TiN-covered surface that does not exhibit the linear relationship between film thickness and number of deposited cycles typically observed with ALD. In step A of the deposition, spectral evidence demonstrated the formation of covalent bonds between the SiO₂ surface and TiCl_x. Exposure of the TiCl_x-terminated surface to NH₃ in step B leads to a reaction with the above species leading to Ti₂NH and TiN.

A side reaction was observed during TiN growth. The reformation of SiOH surface groups occurred during step B when the Si-O-Ti bond was cleaved by NH₃. After the third cycle, and subsequent complete monolayer coverage of the surface, this no longer happened. Beyond this stage, though, the reaction proceeds through reaction of gaseous TiCl₄ with Ti₂NH to yield adsorbed Ti-Cl_x species, and the reaction of NH₃ in step B with this species to form TiN and Ti₂NH. Another contributor to the transition between the silica surface and bulk TiN is the incomplete reaction of NH₃ with surface TiCl_x groups.

Because of the attention lithium titanate spinel has received as a lithium-ion battery anode, it was considered as a candidate for surface modification via ALD, specifically TiN ALD. Little information was available about the surface characteristics of LTS, so DRIFT spectroscopy was used to examine this metal oxide nanopowder.

The DRIFT spectra of LTS powder show that molecularly adsorbed water, hydrogen-bonded TiOH groups, isolated TiOH and LiOH groups and surface carbonates reside on its surface. The presence of isolated hydroxyls means that LTS can be modified by ALD. It is anticipated that LTS prepared in this same manner will exhibit similar reactions to ALD precursors as found for TiO₂.

Dehydration and dehydroxylation characteristics resemble those of other metal oxide powders. Probe molecules gave insight to the Lewis acidity of the surface and the molecules involved in covalent bonding. The affinity with which Li⁺ ions bind with CO₂ to form carbonates also had an effect on the surface chemistry of LTS.

Having determined that LTS was suitable for ALD, a DRIFT in situ reaction to synthesize TiN coatings by ALD confirmed the changes to the LTS surface. Total nitrogen content testing and TEM micrographs provided further evidence of thin film formation.

Coin cell testing using the modified LTS indicated that the deposition of a TiN thin film on LTS enhanced LTS electrode performance, possibly through the removal of surface carbonate species and prevention of anode decomposition by the electrolyte. The voltage profiles and specific capacity of the LTS powder during charge/discharge cycling indicated that the ALD-modified LTS powder was superior to that of the unmodified LTS powder.

Finally, it was determined that a nonvolatile base, sTQ, is capable of attaching an organochlorosilane to fumed silica in solution, though not in sc-CO₂. Apparently, the low solubility of the base in sc-CO₂ was the determining factor. Despite this setback, the use of supercritical fluids for deposition of nonvolatile reactants still holds great promise. Tributylamine, a base with a low vapor pressure, catalyzed the attachment of an organochlorosilane to fumed silica as well and may have a higher solubility in sc-CO₂ although it was tested in sc-CO₂ in this thesis. Tri-n-octylamine was examined as well but produced ambiguous results. Suggestions for modifying the process are offered to further stimulate progress in this area.

REFERENCES

- [1] H.-E. Cheng and Y.-W. Wen, *Surface and Coatings Technology* **2004**, *179*, 103-109.
- [2] H. De Baynast, A. Bouteville and J.-C. Remy, *Chemical Vapor Deposition* **2000**, *6*, 115-119.
- [3] C. H. Winter, J. W. Proscia, A. L. Rheingold and T. S. Lewkebandara, *Inorganic Chemistry* **1994**, *33*, 1227-1229.
- [4] H. G. Tompkins, *Journal of Applied Physics* **1991**, *70*, 3876-3880.
- [5] J. N. Musher and R. G. Gordon, *Journal of the Electrochemical Society* **1996**, *143*, 736-744.
- [6] N. C. Saha and H. G. Tompkins, *Journal of Applied Physics* **1992**, *72*, 3072-3079.
- [7] L. E. Griffiths, A. R. Mount, C. R. Pulham, M. R. Lee, H. Kondoh and T. Ohta, *Chemical Communications (Cambridge, United Kingdom)* **2001**, 579-580.
- [8] M. Ritala, M. Leskelae, E. Rauhala and P. Haussalo, *Journal of the Electrochemical Society* **1995**, *142*, 2731-2737.
- [9] A. Berry, R. Mowery, N. H. Turner, L. Seitzman, D. Dunn and H. Ladouceur, *Thin Solid Films* **1998**, *323*, 10-17.
- [10] S. Y. Umanskii, K. P. Novoselov, A. K. Minushev, M. Siodmiak, G. Frenking and A. A. Korkin, *Journal of Computational Chemistry* **2001**, *22*, 1366-1376.
- [11] C. J. Carmalt, A. H. Cowley, R. D. Culp, R. A. Jones, Y. M. Sun, B. Fitts, S. Whaley and H. W. Roesky, *Inorganic Chemistry* **1997**, *36*, 3108-3112.
- [12] K. Jun, I.-T. Im and Y. Shimogaki, *Japanese Journal of Applied Physics, Part 1: Regular Papers, Short Notes & Review Papers* **2004**, *43*, 1619-1624.
- [13] A. Sherman, *Journal of the Electrochemical Society* **1990**, *137*, 1892-1897.

- [14] M. Leskela and M. Ritala, *Angewandte Chemie, International Edition* **2003**, *42*, 5548-5554.
- [15] F. Greer, D. Fraser, J. W. Coburn and D. B. Graves, *Journal of Vacuum Science & Technology, A: Vacuum, Surfaces, and Films* **2003**, *21*, 96-105.
- [16] S. Ishihara and M. Hanabusa, *Journal of Applied Physics* **1998**, *84*, 596-599.
- [17] M. Juppo, P. Alen, M. Ritala and M. Leskela, *Chemical Vapor Deposition* **2001**, *7*, 211-217.
- [18] M. Juppo, P. Alen, M. Ritala, T. Sajavaara, J. Keinonen and M. Leskela, *Electrochemical and Solid-State Letters* **2002**, *5*, C4-C6.
- [19] J. W. Klaus, S. J. Ferro and S. M. George, *Thin Solid Films* **2000**, *360*, 145-153.
- [20] J. W. Klaus, S. J. Ferro and S. M. George, *Journal of the Electrochemical Society* **2000**, *147*, 1175-1181.
- [21] J.-S. Min, H.-S. Park and S.-W. Kang, *Applied Physics Letters* **1999**, *75*, 1521-1523.
- [22] Y. Mochizuki, Y. Okamoto, A. Ishitani, K. Hirose and T. Takada, *Japanese Journal of Applied Physics, Part 2: Letters* **1995**, *34*, L326-L329.
- [23] H. G. Tompkins, *Journal of Applied Physics* **1992**, *71*, 980-983.
- [24] M. Ritala, T. Asikainen, M. Leskela, J. Jokinen, R. Lappalainen, M. Utriainen, L. Niinisto and E. Ristolainen, *Applied Surface Science* **1997**, *120*, 199-212.
- [25] L. E. Toth in *Transition Metal Carbides and Nitrides, Vol. 7* Academic, New York, **1971**.
- [26] J. W. Elam, M. Schuisky, J. D. Ferguson and S. M. George, *Thin Solid Films* **2003**, *436*, 145-156.

- [27] K. E. Elers, V. Saanila, W. M. Li, P. J. Soininen, J. T. Kostamo, S. Haukka, J. Juhanoja and W. F. A. Besling, *Thin Solid Films* **2003**, 434, 94-99.
- [28] V. Panic, A. Dekanski, V. B. Miskovic-Stankovic, B. Nikolic and S. Milonjic, *Materials and Manufacturing Processes* **2005**, 20, 89-103.
- [29] V. Panic, A. Dekanski, G. Wang, M. Fedoroff, S. Milonjic and B. Nikolic, *Journal of Colloid and Interface Science* **2003**, 263, 68-73.
- [30] X. Chen and J. Mazumder, *Physical Review B: Condensed Matter* **1995**, 52, 5947-5952.
- [31] M. Grujicic and S. G. Lai, *Journal of Materials Science* **2001**, 36, 2937-2953.
- [32] A. M. Shevyakov, G. N. Kuznetsova and V. B. Aleskovskii, *Khim. Vysokotemp. Mater., Tr. Vses. Soveshch., 2nd* **1965**, 149-55, 149-155.
- [33] M. Ritala, M. Leskelae, E. Nykaenen, P. Soininen and L. Niinistoe, *Thin Solid Films* **1993**, 225, 288-295.
- [34] S. I. Kol'tsov and V. B. Aleskovskii, *Zhurnal Prikladnoi Fiziki* **1967**, 40, 907.
- [35] E. L. Lakomaa, A. Root and T. Suntola, *Applied Surface Science* **1996**, 107, 107-115.
- [36] T. Tanaka, T. Nakajima and K. Yamashita, *Thin Solid Films* **2002**, 409, 51-57.
- [37] C. E. Morosanu in *Thin Films by Chemical Vapour Deposition, Vol. 7* Elsevier, **1990**, p. 718.
- [38] M. Juppo, M. Ritala and M. Leskela, *Journal of the Electrochemical Society* **2000**, 147, 3377-3381.
- [39] F. Pintchovski and E. Travis, *Materials Research Society Symposium Proceedings* **1992**, 260, 777-786.

- [40] D.-G. Park, K.-Y. Lim, H.-J. Cho, T.-H. Cha, I.-S. Yeo, J.-S. Roh and J. W. Park, *Applied Physics Letters* **2002**, *80*, 2514-2516.
- [41] S. Haukka, E. L. Lakomaa and T. Suntola, *Thin Solid Films* **1993**, *225*, 280-283.
- [42] E. L. Lakomaa, S. Haukka and T. Suntola, *Applied Surface Science* **1992**, *60-61*, 742-748.
- [43] S. M. George, A. W. Ott and J. W. Klaus, *Journal of Physical Chemistry* **1996**, *100*, 13121-13131.
- [44] R. L. Puurunen, *Journal of Applied Physics* **2005**, *97*, 121301/121301-121301/121352.
- [45] W. Gu and C. P. Tripp, *Langmuir* **2005**, *21*, 211-216.
- [46] E. Langereis, S. B. S. Heil, M. C. M. van de Sanden and W. M. M. Kessels, *Journal of Applied Physics* **2006**, *100*, 023534/023531-023534/023510.
- [47] A. W. Ott, J. W. Klaus, J. M. Johnson and S. M. George, *Thin Solid Films* **1997**, *292*, 135-144.
- [48] J. D. Ferguson, A. W. Weimer and S. M. George, *Chemistry of Materials* **2000**, *12*, 3472-3480.
- [49] Y. J. Lee and S.-W. Kang, *Journal of Vacuum Science & Technology, A: Vacuum, Surfaces, and Films* **2003**, *21*, L13-L15.
- [50] J.-W. Lim, H.-S. Park and S.-W. Kang, *Journal of Applied Physics* **2000**, *88*, 6327-6331.
- [51] J.-S. Min, J.-S. Park, H.-S. Park and S.-W. Kang, *Journal of the Electrochemical Society* **2000**, *147*, 3868-3872.

- [52] K.-E. Elers, M. Ritala, M. Leskelae and E. Rauhala, *Applied Surface Science* **1994**, 82/83, 468-474.
- [53] S. Haukka, E. L. Lakomaa, O. Jylha, J. Vilhunen and S. Hornytkyj, *Langmuir* **1993**, 9, 3497-3506.
- [54] S. Haukka, E. L. Lakomaa and A. Root, *Journal of Physical Chemistry* **1993**, 97, 5085-5094.
- [55] B. Min, J. S. Lee, J. W. Hwang, K. H. Keem, M. I. Kang, K. Cho, M. Y. Sung, S. Kim, M. S. Lee, S. O. Park and J. T. Moon, *Journal of Crystal Growth* **2003**, 252, 565-569.
- [56] A. Satta, J. Schuhmacher, C. M. Whelan, W. Vandervorst, S. H. Brongersma, G. P. Beyer, K. Maex, A. Vantomme, M. M. Viitanen, H. H. Brongersma and W. F. A. Besling, *Journal of Applied Physics* **2002**, 92, 7641-7646.
- [57] A. Satta, A. Vantomme, J. Schuhmacher, C. M. Whelan, V. Sutcliffe and K. Maex, *Applied Physics Letters* **2004**, 84, 4571-4573.
- [58] P. Tagtstrom, P. Martensson, U. Jansson and J. O. Carlsson, *Journal of the Electrochemical Society* **1999**, 146, 3139-3143.
- [59] H. Tiznado and F. Zaera, *Journal of Physical Chemistry B* **2006**, 110, 13491-13498.
- [60] J. W. Klaus, S. J. Ferro and S. M. George, *Applied Surface Science* **2000**, 162-163, 479-491.
- [61] H. Kim and S. M. Rosnagel, *Thin Solid Films* **2003**, 441, 311-316.
- [62] J. Uhm and H. Jeon, *Japanese Journal of Applied Physics, Part 1: Regular Papers, Short Notes & Review Papers* **2001**, 40, 4657-4660.
- [63] M. Juppo, A. Rahtu and M. Ritala, *Chemistry of Materials* **2002**, 14, 281-287.

- [64] M. Ylilammi, *Thin Solid Films* **1996**, 279, 124-130.
- [65] P. Atkins, *Physical Chemistry*, W. H. Freeman and Company, New York, **1994**, p. 1031.
- [66] G. F. Froment and K. B. Bischoff, *Chemical Reactor Analysis And Design*, John Wiley & Sons, New York, **1990**, p. 664.
- [67] B. A. Morrow in *Surface Groups on Oxides, Vol. 57* (Ed. J. L. G. Fierro), Elsevier, Amsterdam, **1990**, p. 384.
- [68] R. L. Puurunen, A. Root, S. Haukka, E. I. Iiskola, M. Lindblad and A. O. I. Krause, *Journal of Physical Chemistry B* **2000**, 104, 6599-6609.
- [69] I. V. Babich, Y. V. Plyuto, P. Van Der Voort and E. F. Vansant, *Journal of Colloid and Interface Science* **1997**, 189, 144-150.
- [70] R. L. Puurunen, M. Lindblad, A. Root and A. O. I. Krause, *Physical Chemistry Chemical Physics* **2001**, 3, 1093-1102.
- [71] R. L. Puurunen, A. Root, P. Sarv, M. M. Viitanen, H. H. Brongersma, M. Lindblad and A. O. I. Krause, *Chemistry of Materials* **2002**, 14, 720-729.
- [72] M. Ritala, M. Leskela, L. Niinisto and P. Haussalo, *Chemistry of Materials* **1993**, 5, 1174-1181.
- [73] M. Ritala, M. Leskela and E. Rauhala, *Chemistry of Materials* **1994**, 6, 556-561.
- [74] S. A. Morozov, A. A. Malkov and A. A. Malygin, *Russian Journal of Applied Chemistry (Translation of Zhurnal Prikladnoi Khimii)* **2003**, 76, 7-11.
- [75] H. Siimon and J. Aarik, *Journal of Physics D: Applied Physics* **1997**, 30, 1725-1728.
- [76] R. L. Puurunen, *Chemical Vapor Deposition* **2003**, 9, 327-332.

- [77] R. L. Puurunen, S. M. K. Airaksinen and A. O. I. Krause, *Journal of Catalysis* **2003**, *213*, 281-290.
- [78] N. V. Dolgushev, A. A. Malkov, A. A. Malygin, S. A. Suvorov, A. V. Shchukarev, A. V. Beljaev and V. A. Bykov, *Thin Solid Films* **1997**, *293*, 91-95.
- [79] H.-K. Kim, T.-Y. Seong, J. H. Lim, Y.-W. Ok, W. I. Cho, Y. H. Shin and Y. S. Yoon, *Journal of Vacuum Science & Technology, B: Microelectronics and Nanometer Structures* **2002**, *20*, 1827-1832.
- [80] J. W. Elam and S. M. George, *Chemistry of Materials* **2003**, *15*, 1020-1028.
- [81] M. L. Green, M. Y. Ho, B. Busch, G. D. Wilk, T. Sorsch, T. Conard, B. Brijs, W. Vandervorst, P. I. Raisanen, D. Muller, M. Bude and J. Grazul, *Journal of Applied Physics* **2002**, *92*, 7168-7174.
- [82] R. L. Puurunen, *Journal of Applied Physics* **2004**, *95*, 4777-4786.
- [83] J.-W. Lim, H.-S. Park and S.-W. Kang, *Journal of the Electrochemical Society* **2001**, *148*, C403-C408.
- [84] J.-W. Lim, J.-S. Park and S.-W. Kang, *Journal of Applied Physics* **2000**, *87*, 4632-4634.
- [85] R. L. Puurunen and W. Vandervorst, *Journal of Applied Physics* **2004**, *96*, 7686-7695.
- [86] R. L. Puurunen, W. Vandervorst, W. F. A. Besling, O. Richard, H. Bender, T. Conard, C. Zhao, A. Delabie, M. Caymax, S. De Gendt, M. Heyns, M. M. Viitanen, M. de Ridder, H. H. Brongersma, Y. Tamminga, T. Dao, T. de Win, M. Verheijen, M. Kaiser and M. Tuominen, *Journal of Applied Physics* **2004**, *96*, 4878-4889.

- [87] J. D. Ferguson, A. W. Weimer and S. M. George, *Applied Surface Science* **2000**, 162-163, 280-292.
- [88] B. J. Ninness, D. W. Bousfield and C. P. Tripp, *Colloids and Surfaces, A: Physicochemical and Engineering Aspects* **2003**, 214, 195-204.
- [89] G. Oya, M. Yoshida and Y. Sawada, *Applied Physics Letters* **1987**, 51, 1143-1145.
- [90] T.-P. Lee, C. Jang, B. Haselden, M. Dong, S. Park, L. Bartholomew, H. Chatham and Y. Senzaki, *Journal of Vacuum Science & Technology, B: Microelectronics and Nanometer Structures--Processing, Measurement, and Phenomena* **2004**, 22, 2295-2298.
- [91] S. K. Kim and C. S. Hwang, *Journal of Applied Physics* **2004**, 96, 2323-2329.
- [92] J. B. Kim, D. R. Kwon, K. Chakrabarti, C. Lee, K. Y. Oh and J. H. Lee, *Journal of Applied Physics* **2002**, 92, 6739-6742.
- [93] M. Q. Snyder, B. A. McCool, J. DiCarlo, C. P. Tripp and W. J. DeSisto, *Thin Solid Films* **2006**, 514, 97-102.
- [94] J. D. Ferguson, A. W. Weimer and S. M. George, *Thin Solid Films* **2002**, 413, 16-25.
- [95] D. M. Hausmann, E. Kim, J. Becker and R. G. Gordon, *Chemistry of Materials* **2002**, 14, 4350-4358.
- [96] K.-E. Elers, V. Saanila, P. J. Soininen, W.-M. Li, J. T. Kostamo, S. Haukka, J. Juhanoja and W. F. A. Besling, *Chemical Vapor Deposition* **2002**, 8, 149-153.
- [97] J. Kim, H. Hong, K. Oh and C. Lee, *Applied Surface Science* **2003**, 210, 231-239.
- [98] J.-S. Min, Y.-W. Son, W.-G. Kang, S.-S. Chun and S.-W. Kang, *Japanese Journal of Applied Physics, Part 1: Regular Papers, Short Notes & Review Papers* **1998**, 37, 4999-5004.

- [99] R. L. Puurunen, A. Root, P. Sarv, S. Haukka, E. I. Iiskola, M. Lindblad and A. O. I. Krause, *Applied Surface Science* **2000**, *165*, 193-202.
- [100] J. W. Elam, C. E. Nelson, R. K. Grubbs and S. M. George, *Thin Solid Films* **2001**, *386*, 41-52.
- [101] J. W. Klaus, O. Sneh and S. M. George, *Science (Washington, D. C.)* **1997**, *278*, 1934-1936.
- [102] M. Q. Snyder, S. A. Trebukhova, B. Ravdel, M. C. Wheeler, J. DiCarlo, C. P. Tripp and W. J. DeSisto, *Journal of Power Sources* **2007**, *165*, 379-385.
- [103] S. M. Bedair, M. A. Tischler, T. Katsuyama and N. A. El-Masry, *Applied Physics Letters* **1985**, *47*, 51-53.
- [104] J. Nishizawa, H. Abe and T. Kurabayashi, *Journal of the Electrochemical Society* **1985**, *132*, 1197-1200.
- [105] S. Haukka, E. L. Lakomaa and T. Suntola, *Studies in Surface Science and Catalysis* **1999**, *120A*, 715-750.
- [106] M. V. Kuznetsov, Y. F. Zhuravlev and V. A. Gubanov, *Journal of Electron Spectroscopy and Related Phenomena* **1992**, *58*, 169-176.
- [107] W. van Schalkwijk and B. Scrosati in *Introduction, Vol.* Eds.: W. van Schalkwijk and B. Scrosati), Kluwer Academic/Plenum Publishers, New York, **2002**, p. 513.
- [108] K. Lahiri, A. Raghunathan, S. Dey and D. Panigrahi, *International Conference on VLSI Design/ASP-DAC (Bangalore, India)* **2002**, pp. 261-267.
- [109] S. Dearborn in *Power Management in Portable Applications: Charging Lithium-Ion/Lithium-Polymer Batteries, Vol.* Microchip Technologies, Inc., **2004**, pp. 1-16.

- [110] M. Schindler in *Proper handling helps make the most of Li-ion batteries*, Vol. EDN, **1996**.
- [111] Panasonic in *Overview of Lithium Ion Batteries*, Vol. 2005 **2000**.
- [112] K. M. Abraham in *A Critical Review of the Characterization Studies of Altair's $\text{Li}_4\text{Ti}_5\text{O}_{12}$ Materials for Li-Ion Batteries*, Vol. E-KEM Sciences, **2001**, p. 14.
- [113] M. Herstedt in *Towards Safer Lithium-Ion Batteries*, Vol. Uppsala University, Uppsala, Sweden, **2003**, p. 52.
- [114] E. Peled and H. Yamin, *Israel Journal of Chemistry* **1979**, *18*, 131-135.
- [115] E. Peled in *Anode-Electrolyte Interface*, Vol. (Ed. J. O. Besenhard), Wiley-VCH, Weinheim, **1999**, pp. 419-458.
- [116] Z. Ogumi and M. Inaba in *Carbon Anodes*, Vol. Eds.: W. van Schalkwijk and B. Scrosati), Kluwer Academic/Plenum Publishers, New York, **2002**, pp. 79-99.
- [117] D. Aurbach in *The Role Of Surface Films On Electrodes In Li-Ion Batteries*, Vol. Eds.: W. van Schalkwijk and B. Scrosati), Kluwer Academic/Plenum Publishers, New York, **2002**, pp. 7-77.
- [118] J. O. Besenhard, M. Winter, J. Yang and W. Biberacher, *Journal of Power Sources* **1995**, *54*, 228-231.
- [119] M. Winter, G. H. Wrodnigg, J. O. Besenhard, W. Biberacher and P. Novak, *Journal of the Electrochemical Society* **2000**, *147*, 2427-2431.
- [120] I. A. Leonidov, O. N. Leonidova, L. A. Perelyaeva, R. F. Samigullina, S. A. Kovyazina and M. V. Patrakeev, *Physics of the Solid State (Translation of Fizika Tverdogo Tela (Sankt-Peterburg))* **2003**, *45*, 2183-2188.

- [121] T. Umeno, K. Fukuda, H. Wang, N. Dimov, T. Iwao and M. Yoshio, *Chemistry Letters* **2001**, 1186-1187.
- [122] T. Hasegawa, S. R. Mukai, Y. Shirato and H. Tamon, *Carbon* **2004**, *42*, 2573-2579.
- [123] S. Morooka, K. Kusakabe, A. Kobata and Y. Kato, *Journal of Chemical Engineering of Japan* **1988**, *21*, 41-46.
- [124] J. J. Watkins, J. M. Blackburn and T. J. McCarthy, *Chemistry of Materials* **1999**, *11*, 213-215.
- [125] T. Gougousi, D. Barua, E. D. Young and G. N. Parsons, *Chemistry of Materials* **2005**, *17*, 5093-5100.
- [126] N. E. Fernandes, S. M. Fisher, J. C. Poshusta, D. G. Vlachos, M. Tsapatsis and J. J. Watkins, *Chemistry of Materials* **2001**, *13*, 2023-2031.
- [127] J. M. Blackburn, D. P. Long and J. J. Watkins, *Chemistry of Materials* **2000**, *12*, 2625-2631.
- [128] M. A. McHugh and V. J. Krukonis, *Supercritical Fluid Extraction*, Butterworth-Heinemann, Boston, **1994**, p. 512.
- [129] C. P. Tripp and J. R. Combes, *Langmuir* **1998**, *14*, 7348-7352.
- [130] B. McCool and C. P. Tripp, *Journal of Physical Chemistry* **2005**, ACS ASAP.
- [131] D. L. Pavia, G. M. Lampman and G. S. Kriz, *Introduction to Spectroscopy*, Harcourt Brace College Publishers, New York, **1996**, p. 511.
- [132] J. R. Combes, L. D. White and C. P. Tripp, *Langmuir* **1999**, *15*, 7870-7875.
- [133] M. Lindblad, S. Haukka, A. Kytoekivi, E.-L. Lakomaa, A. Rautiainen and T. Suntola, *Applied Surface Science* **1997**, *121/122*, 286-291.

- [134] L. A. Sergeeva, I. P. Kalinkin and V. B. Aleskovskii, *Izvestiya Leningradskogo Elektrotekhnicheskogo Instituta imeni V. I. Ul'yanova* **1966**, No. 57, 103-111.
- [135] J. R. Wank, S. M. George and A. W. Weimer, *Powder Technology* **2001**, 121, 195-204.
- [136] J. R. Wank, S. M. George and A. W. Weimer, *Journal of the American Ceramic Society* **2004**, 87, 762-765.
- [137] J. B. Peri, *Journal of Physical Chemistry* **1966**, 70, 2937-2945.
- [138] C. P. Tripp and M. L. Hair, *Langmuir* **1991**, 7, 923-927.
- [139] D. T. Molapo in *Vol. University of Ottawa, Ottawa*, **1998**.
- [140] J. P. Blitz, *Colloids and Surfaces* **1992**, 63, 11-19.
- [141] I. D. Chapman and M. L. Hair, *Transactions of the Faraday Society* **1965**, 61, 1507-1510.
- [142] A. V. Kiselev and V. I. Lygin, *Infrared Spectra of Surface Compounds*, John Wiley & Sons, Inc., Jerusalem, **1975**, p. 384.
- [143] S. D. Hamann, *Australian Journal of Chemistry* **1978**, 31, 919-921.
- [144] C. P. Tripp and M. L. Hair, *Journal of Physical Chemistry* **1993**, 97, 5693-5698.
- [145] A. S. Arico, P. Bruce, B. Scrosati, J.-M. Tarascon and W. van Schalkwijk, *Nature Materials* **2005**, 4, 366-377.
- [146] E. Ferg, R. J. Gummow, A. de Kock and M. M. Thackeray, *Journal of the Electrochemical Society* **1994**, 141, L147-L150.
- [147] J. Jiang, J. Chen and J. R. Dahn, *Journal of the Electrochemical Society* **2004**, 151, A2082-A2087.

- [148] L. Kavan, J. Prochazka, T. M. Spitler, M. Kalbac, M. Zikalova, T. Drezen and M. Gratzel, *Journal of the Electrochemical Society* **2003**, *150*, A1000-A1007.
- [149] T. Ohzuku, A. Ueda and N. Yamamoto, *Journal of the Electrochemical Society* **1995**, *142*, 1431-1435.
- [150] D. Peramunage and K. M. Abraham, *Journal of the Electrochemical Society* **1998**, *145*, 2609-2615.
- [151] E. M. Sorensen, S. J. Barry, H.-K. Jung, J. R. Rondinelli, J. T. Vaughey and K. R. Poeppelmeier, *Chemistry of Materials* **2006**, *18*, 482-489.
- [152] L. Aldon, P. Kubiak, M. Womes, J. C. Jumas, J. Olivier-Fourcade, J. L. Tirado, J. I. Corredor and C. Perez Vicente, *Chemistry of Materials* **2004**, *16*, 5721-5725.
- [153] J. K. Cox and C. P. Tripp, *Applied Spectroscopy* **2000**, *54*, 144-147.
- [154] S. M. Kanan, Z. Lu, J. K. Cox, G. Bernhardt and C. P. Tripp, *Langmuir* **2002**, *18*, 1707-1712.
- [155] P. Jones and J. A. Hockey, *Transactions of the Faraday Society* **1971**, *67*, 2669-2678.
- [156] W. Gu and C. P. Tripp, *Langmuir* **2006**, *22*, 5748-5752.
- [157] S. P. Zhdanov, L. S. Kosheleva and T. I. Titova, *Langmuir* **1987**, *3*, 960-967.
- [158] N. R. Smyrl, E. L. Fuller, Jr. and G. L. Powell, *Applied Spectroscopy* **1983**, *37*, 38-44.
- [159] H. A. Mosqueda, C. Vazquez, P. Bosch and H. Pfeiffer, *Chemistry of Materials* **2006**, *18*, 2307-2310.
- [160] M. L. Hair and W. Hertl, *Journal of Physical Chemistry* **1971**, *75*, 2181-2185.
- [161] C. P. Tripp and M. L. Hair, *Langmuir* **1994**, *10*, 4031-4038.

- [162] T. Kataoka and J. A. Dumesic, *Journal of Catalysis* **1988**, *112*, 66-79.
- [163] J. L. Allen, J. Wolfenstine and T. R. Jow, *42nd Power Source Conference* (Philadelphia, Pennsylvania) **2006**.
- [164] L. Cheng, H.-J. Liu, J.-J. Zhang, H.-M. Xiong and Y.-Y. Xia, *Journal of the Electrochemical Society* **2006**, *153*, A1472-A1477.
- [165] J. Christensen, V. Srinivasan and J. Newman, *Journal of the Electrochemical Society* **2006**, *153*, A560-A565.
- [166] A. Du Pasquier, A. Laforgue and P. Simon, *Journal of Power Sources* **2004**, *125*, 95-102.
- [167] K. Nakahara, R. Nakajima, T. Matsushima and H. Majima, *Journal of Power Sources* **2003**, *117*, 131-136.
- [168] A. Du Pasquier, A. Laforgue, P. Simon, G. G. Amatucci and J.-F. Fauvarque, *Journal of the Electrochemical Society* **2002**, *149*, A302-A306.
- [169] K. Zaghbi, M. Simoneau, M. Armand and M. Gauthier, *Journal of Power Sources* **1999**, *81-82*, 300-305.
- [170] S. Scharner, W. Weppner and P. Schmid-Beurmann, *Journal of the Electrochemical Society* **1999**, *146*, 857-861.
- [171] D. Peramunage and K. M. Abraham, *Journal of the Electrochemical Society* **1998**, *145*, 2615-2622.
- [172] A. Deschanvres, B. Raveau and Z. Sekkal, *Materials Research Bulletin* **1971**, *6*, 699-704.
- [173] N. V. Porotnikov, N. G. Chaban and K. I. Petrov, *Izvestiya Akademii Nauk SSSR, Neorganicheskie Materialy* **1982**, *18*, 1066-1067.

- [174] K. M. Colbow, J. R. Dahn and R. R. Haering, *Journal of Power Sources* **1989**, 26, 397-402.
- [175] L. Kavan and M. Gratzel, *Electrochemical and Solid-State Letters* **2002**, 5, A39-A42.
- [176] A. Tarniowy, R. Mania and M. Rekas, *Thin Solid Films* **1997**, 311, 93-100.
- [177] S. Kaskel, K. Schlichte, G. Chaplais and M. Khanna, *Journal of Materials Chemistry* **2003**, 13, 1496-1499.
- [178] F. Esaka, K. Furuya, H. Shimada, M. Imamura, N. Matsubayashi, H. Sato, A. Nishijima, A. Kawana, H. Ichimura and T. Kikuchi, *Journal of Vacuum Science & Technology, A: Vacuum, Surfaces, and Films* **1997**, 15, 2521-2528.
- [179] J. W. Klaus and S. M. George, *Surface Science* **2000**, 447, 81-90.
- [180] B. A. McCool and W. J. DeSisto, *Chemical Vapor Deposition* **2004**, 10, 190-194.
- [181] B. A. McCool and W. J. DeSisto, *Industrial & Engineering Chemistry Research* **2004**, 43, 2478-2484.
- [182] B. A. McCool and C. P. Tripp, (*In press*) **2005**.
- [183] C. A. Cooper and Y. S. Lin, *Journal of Membrane Science* **2002**, 195, 35-50.
- [184] M. A. Cameron, I. P. Gartland, J. A. Smith, S. F. Diaz and S. M. George, *Langmuir* **2000**, 16, 7435-7444.
- [185] B. J. Ninness, L. D. Doucette, B. McCool and C. P. Tripp, *2006 International Symposium on Spectral Sensing Research-Water and Frontiers* **2006**, pp. 80-91.
- [186] C. P. Tripp and M. L. Hair, *Langmuir* **1995**, 11, 1215-1219.
- [187] C. P. Tripp and M. L. Hair, *Langmuir* **1992**, 8, 1120-1126.

[188] J. McMurry, *Organic Chemistry*, Brooks/Cole Publishing Company, Boston, **1996**, p. 1243.

[189] T. Sarbu, T. Styranec and E. J. Beckman, *Nature (London)* **2000**, *405*, 165-168.

ACKNOWLEDGMENTS

The author wishes to acknowledge support from Yardney Technical Products, Inc., U.S. Army Grant DAFG 60-03-C-00733 and NSF grant CHE-0346124 for financial support of this research.

Additionally, the author would like to thank Boris Ravdel and Svetlana Trebukhova for performing the Li-ion coin cell tests, Bruce Hoskins for performing the total nitrogen tests and Kelly Edwards for collecting TEM images of the nanopowders used in this research.

TABLE OF CONTENTS

| | |
|---|------|
| ACKNOWLEDGMENTS..... | ii |
| LIST OF TABLES..... | vii |
| LIST OF FIGURES..... | viii |
| | |
| 1 INTRODUCTION | 1 |
| 1.1 TITANIUM NITRIDE | 2 |
| 1.2 THIN FILM DEPOSITION METHODS..... | 3 |
| 1.2.1 Chemical Vapor Deposition..... | 3 |
| 1.2.2 Atomic Layer Deposition..... | 4 |
| 1.2.2.1 The ALD Process..... | 4 |
| 1.2.2.2 ALD Thin Film Growth..... | 6 |
| 1.2.2.3 ALD Precursors | 12 |
| 1.2.2.4 TiN ALD..... | 14 |
| 1.3 LITHIUM-ION BATTERIES..... | 16 |
| 1.4 SUPERCRITICAL CARBON DIOXIDE AS A SOLVENT..... | 22 |
| 1.5 INFRARED SPECTROSCOPY | 23 |
| 1.6 OUTLINE OF THIS DISSERTATION | 26 |
| | |
| 2 AN INFRARED STUDY OF THE SURFACE CHEMISTRY OF TITANIUM NITRIDE ATOMIC LAYER DEPOSITION ON SILICA FROM TITANIUM TETRACHLORIDE AND AMMONIA..... | 29 |
| 2.1 INTRODUCTION | 29 |
| 2.2 EXPERIMENTAL METHODS..... | 32 |

| | | |
|-------|---|----|
| 2.3 | RESULTS AND DISCUSSION | 33 |
| 2.3.1 | Cycle 1 | 33 |
| 2.3.2 | Cycle 2 and Higher | 38 |
| 2.4 | CONCLUSIONS | 42 |
| 3 | AN INFRARED STUDY OF THE SURFACE CHEMISTRY OF LITHIUM TITANATE SPINEL | 44 |
| 3.1 | INTRODUCTION | 44 |
| 3.2 | EXPERIMENTAL | 46 |
| 3.2.1 | Dehydration/dehydroxylation | 46 |
| 3.2.2 | Hexamethyldisilazane | 46 |
| 3.2.3 | Pyridine | 47 |
| 3.3 | RESULTS | 47 |
| 3.3.1 | Heating in air | 47 |
| 3.3.2 | Heating in vacuum | 51 |
| 3.3.3 | Hexamethyldisilazane | 53 |
| 3.3.4 | Pyridine | 55 |
| 3.4 | CONCLUSION | 58 |
| 4 | SYNTHESIS AND CHARACTERIZATION OF ATOMIC LAYER DEPOSITED TITANIUM NITRIDE THIN FILMS ON LITHIUM TITANATE SPINEL POWDER AS A LITHIUM-ION BATTERY ANODE | 59 |
| 4.1 | INTRODUCTION | 59 |
| 4.2 | EXPERIMENTAL | 61 |
| 4.2.1 | ALD Materials | 61 |

| | | |
|---------|---|----|
| 4.2.2 | ALD In Situ Methods..... | 61 |
| 4.2.3 | ALD Ex Situ Methods | 62 |
| 4.2.3.1 | Reactor description | 62 |
| 4.2.3.2 | Precursor delivery | 63 |
| 4.2.3.3 | Total nitrogen content test | 63 |
| 4.2.4 | Coin Cell Testing | 63 |
| 4.2.4.1 | Coin cell materials | 63 |
| 4.2.4.2 | Coin cell fabrication methods | 64 |
| 4.3 | RESULTS | 64 |
| 4.3.1 | ALD with in situ DRIFT characterization | 64 |
| 4.3.2 | ALD with ex situ characterization | 66 |
| 4.3.2.1 | Total nitrogen content | 66 |
| 4.3.2.2 | TEM analysis | 67 |
| 4.3.3 | Coin Cell Tests..... | 68 |
| 4.4 | DISCUSSION | 71 |
| 4.5 | CONCLUSION..... | 72 |
| 5 | ATTACHMENT OF ORGANOCHLOROSILANES BY CATALYSIS OF NON- VOLATILE BASES IN SUPERCRITICAL CARBON DIOXIDE..... | 73 |
| 5.1 | INTRODUCTION..... | 73 |
| 5.2 | EXPERIMENTAL | 76 |
| 5.2.1 | Solution-phase reaction..... | 76 |
| 5.2.2 | Supercritical reactor system..... | 77 |
| 5.2.3 | Supercritical CO ₂ reaction | 78 |

| | | |
|---------|--|-----|
| 5.3 | RESULTS AND DISCUSSION..... | 79 |
| 5.3.1 | Solution-phase reaction..... | 79 |
| 5.3.1.1 | Catalysis with s-Triazolo [4,3-a] Quinoline..... | 79 |
| 5.3.1.2 | Catalysis with Tributylamine..... | 83 |
| 5.3.1.3 | Catalysis with Tri-n-octylamine | 84 |
| 5.3.2 | Supercritical CO ₂ reaction | 86 |
| 5.3.3 | Future work..... | 87 |
| 5.4 | CONCLUSIONS..... | 88 |
| 6 | CONCLUSIONS..... | 89 |
| | REFERENCES | 92 |
| | BIOGRAPHY OF THE AUTHOR..... | 108 |

LIST OF TABLES

| | |
|--|----|
| Table 3.1 Comparison of Lewis acid sites by pyridine absorption bands on TiO ₂ and Li ₄ Ti ₅ O ₁₂ surfaces..... | 56 |
|--|----|

LIST OF FIGURES

| | | |
|------------|---|----|
| Figure 1.1 | Mechanisms of ALD chemisorption on a surface by (a) ligand exchange between a precursor, ML_n and a surface group Za (hydroxyl, $-OH^*$), producing $-Z-ML_{n-1}^*$ and aL ; (b) dissociation forming $-Z-ML_{n-1}^*$ and M^+-L^* ; and (c) association of ML_n onto the surface to form $-Z-ML_n^*$ | 8 |
| Figure 1.2 | Three theoretical models of monolayer formation are (a) Model I which is based on the size of the reactant, ML_n , (b) Model II, determined by the size and geometry of the chemisorbed reactant, ML_z , and (c) Model III, which assumes a close-packed monolayer of ligands. Figure taken from Puurunen [42]..... | 10 |
| Figure 1.3 | The effect of ALD growth per cycle illustrated by three different growth models: (a) linear growth, (b) substrate-enhanced growth and substrate inhibited growth, which is further divided into (c) Type I growth and (d) Type II growth. Figure taken from Puurunen [42]..... | 11 |
| Figure 1.4 | Energy density for a variety of battery metals and the first year of their commercial deployment ^[105] | 16 |
| Figure 1.5 | Schematic of a Li-ion battery. Arrows within the figure indicate Li-ion discharge..... | 18 |
| Figure 1.6 | Solvent intercalation in a graphene anode ^[113] | 19 |
| Figure 1.7 | Schematic of an FTIR spectrometer..... | 26 |

| | |
|---|----|
| Figure 2.1 Thin film IR spectra of (a) silica substrate, (b) Cycle 1 first exposure of TiCl_4 , and (c) first exposure of NH_3 | 34 |
| Figure 2.2 IR spectra of (a) the first exposure of NH_3 compared with (b) TiO_2 ALD on silica, (c) DRIFT IR spectra on TiN standard powder, and (d) Degussa P25 TiO_2 | 38 |
| Figure 2.3 Difference IR spectrum of (a) the first NH_3 exposure using a reference spectrum of the first exposure of TiCl_4 ($1c - 1b$), and (b) the difference spectrum of the second TiCl_4 exposure using a reference of the first exposure to NH_3 | 39 |
| Figure 2.4 IR spectra of steps A (TiCl_4 addition) and B (NH_3 addition) in cycles 1 (a, b) and 6 (c, d), respectively, using the silica substrate as a reference..... | 41 |
| Figure 2.5 Comparison of normalized peak area vs. number of ALD cycles for various functional group bands..... | 43 |
| Figure 2.6 Proposed reaction scheme for TiN formation. | 43 |
| Figure 3.1 DRIFT spectra of LTS in air at (a) room temperature, (b) 50, (c) 100, and (d) 150 °C. | 48 |
| Figure 3.2 DRIFT spectra of LTS in air at (a) room temperature, (b) 200, (c) 300, (d) 400, and (e) 500 °C..... | 49 |
| Figure 3.3 DRIFT spectra of LTS in air at (a) room temperature, followed by (b) heating to 500 °C for 30 minutes then recorded immediately after cooling to room temperature, and then (c) after leaving in air overnight. | 51 |

| | |
|--|----|
| Figure 3.4 DRIFT spectra of LTS in (a) air followed by evacuation at (b) room temperature, (c) 50, (d) 100, and (e) 150 °C. | 52 |
| Figure 3.5 DRIFT spectra of LTS evacuated at (a) 200, (b) 300, (c) 400 and (d) 500 °C. | 53 |
| Figure 3.6 Difference spectra of an LTS sample evacuated at room temperature and then exposed to excess HMDZ vapor, followed by evacuation for 5 minutes. | 57 |
| Figure 3.7 Difference spectra of 500 mtorr pyridine vapor added at room temperature to an LTS sample previously evacuated at (a) room temperature and (b) 425 °C. | 57 |
| Figure 4.1 Schematic of home-built atomic layer deposition reactor. | 62 |
| Figure 4.2 DRIFT spectrum of (a) LTS at room temperature in air and (b) DRIFT difference spectrum of LTS at 425 °C under vacuum after an addition of TiCl ₄ . The reference is LTS under vacuum at 425 °C. | 66 |
| Figure 4.3 TEM micrographs of (a) unmodified LTS and (b) LTS modified with 200 cycles of TiN ALD at 500 °C. | 68 |
| Figure 4.4 Cyclic voltammogram of unmodified LTS and LTS modified with 200 cycles of TiN ALD at 500 °C tested as coin-type cells in a lithium ion battery. | 69 |

| | |
|--|----|
| Figure 4.5 Measurement of specific capacity of unmodified LTS and LTS modified with 200 cycles of TiN ALD at 500 °C tested as coin-type cells in a lithium ion battery versus the number of charge/discharge cycles. The discharge rate is given below the cycle number on the x-axis..... | 70 |
| Figure 5.1 Illustration of the base-catalyzed attachment of an organochlorosilane to a surface SiOH group through formation of a pentacoordinate intermediate with the silanol. | 74 |
| Figure 5.2 Diagram of s-triazolo [4,3-a] quinoline..... | 77 |
| Figure 5.3 Schematic representation of the supercritical carbon dioxide reactor. | 78 |
| Figure 5.4 FTIR spectra of (a) unmodified A300 fumed silica and (b) fumed silica after modification with s-triazolo [4,3-a] quinoline (sTQ) in toluene at room temperature. | 80 |
| Figure 5.5 FTIR spectra of the 1300-1700 cm ⁻¹ region of (a) Figure 5.4b and (b) pure sTQ..... | 81 |
| Figure 5.6 FTIR spectra of fumed silica with (a) 0.001 M sTQ, (b) sTQ-catalyzed reaction with 0.001 M ODCS, and (c) 0.001 M ODCS reacted directly with silica without a catalyst in toluene. | 81 |
| Figure 5.7 FTIR spectrum of (a) fumed silica reacted with 0.001 M TBA solution in toluene and (b) TBA catalyzed reaction of 0.001 M ODCS solution in toluene on fumed silica. | 85 |

Figure 5.8 FTIR spectrum of (a) fumed silica after reaction with 0.001 M TOA
solution and (b) TOA-catalyzed reaction with fumed silica and
0.001 M ODCS solution.85

BIOGRAPHY OF THE AUTHOR

Mark Snyder was born in Buffalo, New York, on December 12, 1975, and was raised in Marietta, Georgia. He graduated from Sprayberry High School in 1994. He attended the Georgia Institute of Technology where he received a B.S. degree in Chemistry in 1998. In 2001, he received a M.S. degree in Pulp and Paper Science and Technology from the Institute of Paper Science and Technology. Upon graduation he worked for two years at International Paper's Riverdale Mill in Selma, Alabama. He enrolled in the Chemical Engineering graduate program at the The University of Maine in 2003.

After receiving his degree, Mark will be joining Hollingsworth & Vose Co., an engineered paper and nonwovens manufacturer to begin his career as a research engineer. Mark is a candidate for the Doctor of Philosophy degree in Chemical Engineering from The University of Maine in May, 2007.